Modelling the impacts of tropical cyclones on coral cover across the Great Barrier Reef

Holly Ayesha Smith

Master of Science (by Research)

University of York

Department of Environment and Geography

December 2024

Abstract

Tropical cyclones (TCs) are major acute stressors on coral reefs and significantly contribute to coral decline, with increasing frequency and intensity due to climate change posing further challenges for the Great Barrier Reef (GBR). This project models multiple TCs over the GBR to assess coral reef damage using bed shear stress (BSS) as a proxy and evaluates future impacts of sea level rise (SLR) through simulations based on IPCC AR6 SSP projections (SSP1-1.9 and SSP2-4.5). Using Thetis, a flow solver for simulating coastal flows, BSS impacts were analysed in tide-only and tide-and-wind (cyclonic) environments. Statistical analysis showed significant trends in algae ($\tau = 0.19$, $p < 0.001$) and “Other” (e.g. sponges, tunicates and abiotics) ($\tau = -0.22$, $p < 0.001$), with algae cover increasing as BSS intensified, while other benthic decreased, suggesting physical damage or dislodgement creates space for algal growth. No significant changes in hard or soft coral cover in response to BSS were found. Simulations altering bathymetry based on the SLR projections revealed that the response of BSS to SLR varies across reefs, with deeper reefs experiencing stronger cyclonic BSS than shallower ones due to differences in wave energy. Coral species also respond differently to hydrodynamic forces, indicating the importance of species-specific analysis. These findings highlight the difficulty of generalizing results across the GBR due to variations in bathymetry, coral species, and environmental conditions. A reef-specific approach is necessary to accurately predict how individual reefs will respond to TCs and SLR in the future.

Declaration

I declare that this thesis is a presentation of original work and I am the sole author. This work has not previously been presented for a degree or other qualification at this University or elsewhere. All sources within this piece of work are acknowledged as references.

Holly Ayesha Smith
December 2024

Acknowledgements

I wish to acknowledge the Australian Government Bureau of Meteorology, the Australian Institute of Marine Science and the Thetis Project for making the data and models used within this study free and easy access. I also thank the projection authors for developing and making the sea-level rise projections available, multiple funding agencies for supporting the development of the projections, and the NASA Sea Level Change Team for developing and hosting the IPCC AR6 Sea Level Projection Tool. I would like to thank my family and friends, in particular my partner and my parents, for their continued support during my degree. I would also like to thank the Environmental Modelling Research Group for their support and help during our regular meetings. This research would not have been possible without my supervisors, Jon Hill and Fiona Hibbert, whose guided support and encouragement helped develop many key skills which were used in completing this research and writing this report.

Contents

Abstract 1
Declaration 2
Acknowledgements 3
List of Figures and Tables 6
Chapter 1 | Introduction and Literature Review 11
1.1 | Tropical Cyclones and Coral Reefs 11
1.2 | Coral Reefs in the Great Barrier Reef 14
1.3 | Threats to Coral Reef Ecosystems in the Great Barrier Reef 18
1.4 | Wave Dynamics and Bed Shear Stress 24
1.5 | Impacts of Climate Change and Sea Level Rise 27
1.6 | Modelling Tropical Cyclones on Coral Reefs 34
1.7 | Aims and Objectives 37
Chapter 2 | Numerically Modelling Tropical Cyclones 39
2.1 | Introduction 39
2.2 | Methodology 40
2.2.1 | Site Description 40
2.2.2 | Tropical Cyclones 41
2.2.3 | Model Framework and Set-up 48
2.2.4 | Generating a Mesh and Constructing the Model 49
2.2.4 | Model Analysis 55
2.3 | Results 55
2.3.1 | Tide-Only Model Validation 55
2.3.2 | Tide and Wind Model Validation 58
2.4 | Discussion 62
2.4.1 | Observed Tide Gauge Data 62
2.4.2 | Thetis vs ROMS 62
2.4.3 | Thetis Tide and Wind Model Limitations 64
2.5 | Conclusions 68
Chapter 3 | Impacts of Tropical Cyclones on Coral Reefs 69
3.1 | Introduction 69
3.2.1 | Coral Reef Data 69
3.2.2 | Numerical Model Data 72
3.2.3 | Statistical Testing 72
3.3 | Results 72
3.3.1 | Results of Simulations 72
3.3.2 | Shapiro-Wilk Normality Test 79

3.3.3 | Absolute Change in Benthic Cover......81
3.3.4 | Relative Change in Coral Cover......83
***3.4 | Discussion*......85**
3.4.1 | Interpretation of Results......85
3.4.2 | Methodological Insights......87
3.4.3 | Other Ecological Disturbances and Implications......93
3.4.4 | Coral Reef Recovery Patterns and Future Management Implications......95
***3.5 | Conclusions*......97**
Chapter 4 | Uncertainty for the Future: Sea Level Rise......98
***4.1 | Introduction*......98**
***4.2 | Methodology*......99**
4.2.1 | Shared Socio-Economic Pathways......99
4.2.2 | Bathymetry......100
4.2.3 | Model Set-Up......101
4.2.4 | Numerical Model Data......103
4.2.5 | Statistical Analysis......103
***4.3 | Results*......103**
4.3.1 | Depth......103
4.3.2 | Maximum Bed Shear Stress......107
4.3.3 | Tidal vs Cyclonic Bed Shear Stress Change in Magnitude......109
4.3.4 | Relationship between depth and bed shear stress......111
***4.4 | Discussion*......114**
4.4.1 | Implications of Sea-Level Rise on Coral Reefs......114
***4.5 | Conclusions*......115**
Chapter 5 | Conclusions......116
Bibliography......118
Appendices......128

List of Figures and Tables

Figure 1 *The location of the study area along the Australian east coast (A) and the locations of the 15 coral reefs studied in this research along the GBR (highlighted in green) (B). The boundary of the simulation area is denoted by the black line (landward) and red line (forced)....................15*

Figure 2 *Idealised variation of coral community forms and diversity from sums of stresses across a simple reef section and coral form responses to environmental stresses (Chappell 1980)....................17*

Figure 3 *Summary of the results from the AIMS GBR long-term monitoring program coral reef condition report for the 2022-2023 period demonstrating the hard coral cover, crowns-of-thorns starfish outbreaks and in-water bleaching prevalence status and trends for the northern, central and southern GBR (AIMS 2023)....................18*

Figure 4 *Summary of the results from the AIMS GBR long-term monitoring program coral reef condition report for the 2023-2024 period demonstrating the hard coral cover, crowns-of-thorns starfish outbreaks, in-water bleaching prevalence and aerial bleaching severity status and trends for the northern, central and southern GBR (AIMS 2024a)..........19*

Figure 5 *Schematic of a typical cross section of the GBR matrix, (a) a plan view; and (b) the profile view (Gallop et al. 2014)....................25*

Figure 6 *Annual anthropogenic emissions over the 2015–2100 period showing the emissions trajectories for carbon dioxide from all sectors (GtCO2/yr) (Masson-Delmotte et al. 2021)....................29*

Table 1 *Changes in global surface temperature, which are assessed based on multiple lines of evidence, for selected 20-year time periods and the five illustrative emissions scenarios considered. Temperature differences relative to the average global surface temperature of the period 1850–1900 are reported in °C. This includes the revised assessment of observed historical warming for the AR5 reference period 1986–2005, which in AR6 is higher by 0.08 [–0.01 to +0.12] °C than in AR5 (Masson-Delmotte et al. 2021)....................30*

Figure 7 *Global projected sea level change for SSP scenarios resulting from processes in whose projection there is medium confidence. Shaded ranges show the 17th-83rd percentile ranges. Projections are relative to a 1995-2014 baseline (NASA 2024)....................31*

Figure 8 *Locations of the eight tide gauges depicted by the small white circles studied in this chapter for model validation. The model mesh domain is depicted by the black and red lines, with the black line representing the landward boundary and the red line indicating the forced boundary....................40*

Table 2 *The key information of each TC in this research, including the name, start and end dates, the maximum category (based on the Saffir-Simpson scale), the maximum wind speed and wind gust and the lowest central pressure (BOM 2024)....................42*

Figure 9 *Tracks of the four TCs studied in this project - A: TC Dylan, B: TC Edna, C: TC Hadi, and D: TC Ita - across the GBR. The model mesh domain is depicted by the black and red lines, with the black line representing the landward boundary and the red line indicating the forced boundary. Small white triangles denote tide gauge locations across the GBR..... 43*

Figure 10 *Images of the ERA5 reanalysis data during TC Dylan on the 29/01/2014 at 00:00 (A, C and E) and the 30/01/2014 at 12:00 (B, D, F). A and B show the U10 Component of Wind (m/s), C and D show the V10 component of wind (m/s) and E and F show the Surface Pressure (Pa)....................44*

Figure 11 *Images of the ERA5 reanalysis data during TC Edna on the 03/02/2014 at 06:00 (A, C and E) and the 05/02/2014 at 18:00 (B, D, F). A and B show the U10 Component of Wind (m/s), C and D show the V10 component of wind (m/s) and E and F show the Surface Pressure (Pa). The model domain is outlined in black...45*

Figure 12 *Images of the ERA5 reanalysis data during TC Hadi on the 08/03/2014 at 06:00 (A, C and E) and the 12/03/2014 at 00:00 (B, D, F). A and B show the U10 Component of Wind (m/s), C and D show the V10 component of wind (m/s) and E and F show the Surface Pressure (Pa).. 46*

Figure 13 *Images of the ERA5 reanalysis data during TC Ita on the 10/04/2014 at 12:00 (A, C and E) and the 13/04/2014 at 18:00 (B, D, F). A and B show the U10 Component of Wind (m/s), C and D show the V10 component of wind (m/s) and E and F show the Surface Pressure (Pa).. 47*

Figure 14 *Tidal model validation for 0 m coastal contour model (A) and 10 m coastal contour model (B) showing four tidal constituents (semi-diurnal M2 and S2 and diurnal K1 and O1) with the black line representing the expected tides and the blue points representing the model output values... 51*

Table 3 *The models used in this project, including the model ID, the configuration of the model (simulating tides only or tides and wind), the tropical cyclone they were simulating, total model runtime, the spin-up duration, and the start/end dates for each model............... 53*

Figure 15 *The 10-m contour mesh with the contour depicted by the blue and red lines, with the blue line representing the landward contour and the red line indicating the forced boundary. A: the entire mesh domain; B: a section of the mesh showing the coastline; C: a section of the mesh showing the forced boundary within the Pacific Ocean......................... 54*

Table 4 *Tidal constituent validation statistics for the T_Val Thetis simulation for four major tidal constituents (M2, S2, K1 and O1)... 55*

Figure 16 *T_Val model validation: (A) a map showing the location of four tidal gauges across different sections of the GBR coastline; (B, C, D, E) tidal gauge data comparison between AusTides data and modelled water elevation from Thetis at Pelican Island, Cairns, Bowen and Breaksea Split, respectively.. 57*

Table 5 *Comparison of the W4_I modelled maximum water elevation from the Thetis tide and wind model simulation and the observed maximum water elevation from the BOM publication (Greenslade et al. 2018) at six locations. The difference and percentage difference (Eq. 11) between the modelled and observed maximum water elevation has also been calculated.. 58*

Table 6 *Comparison of the W4_I modelled maximum water elevation from the Thetis tide and wind model simulation and the ROMS modelled maximum water elevation from the BOM publication (Greenslade et al. 2018) at six locations. The difference and percentage difference (Eq. 11) between the modelled and observed maximum water elevation has also been calculated.. 59*

Figure 17 *A comparison of the water elevation modelled by Thetis for the W4_I simulation (red), the water elevation modelled by ROMS (blue) (Greenslade et al. 2018) and the observed de-tided tide gauge data (black) (Greenslade et al. 2018) between the 10th April 2014 and the 14th April 2014 at six locations across the GBR... 60*

Table 7 *Comparison of W4_I modelled peak water elevation times from the Thetis tide and wind model simulation, observed peak times, and ROMS modelled peak times (Greenslade et al. 2018) at six locations. Differences between Thetis modelled and observed peak times, Thetis modelled and ROMS modelled peak times and ROMS modelled and observed peak times, have also been calculated.. 61*

Table 8 *Comparison of the model set-ups for both Thetis and ROMS (Greenslade et al. 2018).. 63*

Figure 18 *Comparison of surge residual between Thetis model results, CS3X hindcast results, and British Oceanographic Data Centre tide gauges, for 5th-7th December 2013 (Warder et al. 2020)*.. 65

Table 9 *Values of the Manning's drag and viscosity used for the test simulations as well as the forcing used for each model (L&Y - Large and Yeager, 2009; Pond - Large and Pond, 1981; Smith - Smith and Banke, 1975). (Hill 2024)*...66

Figure 19 *Results of the test simulations described in Table 9. Note: Model 5 (green) storm surge model stopped after 14th April 2014 and only shows a tidal signal towards the end of the model. (Hill 2024)*.. 67

Figure 20 *The white points indicate the coral reefs within the model boundary that are used within this research. The model mesh domain is delineated by the black and red lines, signifying the landward boundary and forced boundary, respectively*.................................... 71

Figure 21 *Locations of the coral reefs Dunk North (B), Pine (E), Daydream (D) and Palms West (C) along the GBR for the graphs shown in Figures 16, 17, 18 and 19, respectively*... 73

Figure 22 *Graphs showing the bed shear stress, water elevation and water velocity modelled for the T1_D simulation period (A), and the W1_D simulation period (B) for each location across Dunk North reef*..74

Figure 23 *Graphs showing the bed shear stress, water elevation and water velocity modelled for the T2_E simulation period (A), and the W2_E simulation period (B) for each location across Pine reef*...75

Figure 24 *Graphs showing the bed shear stress, water elevation and water velocity modelled for the T3_H simulation period (A), and the W3_H simulation period (B) for each location across Daydream reef*... 76

Figure 25 *Graphs showing the bed shear stress, water elevation and water velocity modelled for the T4_I simulation period (A), and the W4_I simulation period (B) for each location across Palms West reef*..77

Table 10 *Results of the Shapiro-Wilk Normality test for absolute change and relative change in benthic cover for algae, hard coral, soft coral and other (NS – not significant (p > 0.05); * - significant to p 0.05; ** - significant to p 0.01; *** - significant to p 0.001)*..........................79

Figure 26 *Q-Q plots showing the results of the Shapiro-Wilk normality test for the four benthic categories for absolute and relative benthic change. Each plot represents the distribution of the variable comparing the observed (sample) data against a theoretical normal distribution. Deviations from the red line indicate variations from normality. Corresponding W-values and significance levels for the normality tests are presented in Table 10, respectively, with Algae - A and*...80

Table 11 *Results of the Kendall Tau's statistical analysis between the absolute change in benthic cover (for algae, hard coral, soft coral and other), and both the maximum bed shear stress modelled at each reef during each simulation (W1_D, W2_E, W3_H, W4_I) and the change in bed shear stress magnitude modelled at each reef during each simulation. (NS – not significant (p > 0.05); * - significant to p 0.05; ** - significant to p 0.01; *** - significant to p 0.001)*.. 81

Figure 27 *Graphs showing the relationship between the absolute change in benthic cover (for algae, hard coral, soft coral and other benthic) and both the maximum bed shear stress and change in bed shear stress magnitude with Loess curves added to visualise trends in the data. Each plot corresponds to the statistical analysis results presented in Table 11, respectively, with Algae - A and E, Hard Coral - B and F, Soft Coral - C and G, Other - D and H, and Maximum Bed Shear Stress - A-D and Change in Bed Shear Stress Magnitude - E-H.* 82

Table 12 *Results of the Kendall Tau's statistical analysis between the relative change in benthic cover (for algae, hard coral, soft coral and other), and both the maximum bed shear stress modelled at each reef during each simulation (W1_D, W2_E, W3_H, W4_I) and the change in bed shear stress magnitude modelled at each reef during each simulation. (NS – not significant (p > 0.05); * - significant to p 0.05; ** - significant to p 0.01; *** - significant to p 0.001)*............ 83

Figure 28 *Graphs showing the relationship between the relative change in benthic cover (for algae, hard coral, soft coral and other benthic) and both the maximum bed shear stress and change in bed shear stress magnitude with Loess curves added to visualise trends in the data. Each plot corresponds to the statistical analysis results presented in Table 12, respectively, with Algae - A and E, Hard Coral - B and F, Soft Coral - C and G, Other - D and H, and Maximum Bed Shear Stress - A-D and Change in Bed Shear Stress Magnitude - E-H*............ 84

Figure 29 *Percentage cover of hard coral life-forms on four reefs from before TC Rona (Jan-99) to 1-2 months after the TC (Mar-99) to 11-12 months after Cyclone Rona (Jan-00) (Cheal et al. 2002)*............ 89

Table 13 *Results of the Kendall Tau's statistical analysis between the absolute change in benthic cover for all species of algae found across all reefs, and both the maximum bed shear stress modelled at each reef during each simulation (W1_D, W2_E, W3_H, W4_I) and the change in bed shear stress magnitude modelled at each reef during each simulation. (NS – not significant (p > 0.05); * - significant to p 0.05; ** - significant to p 0.01; *** - significant to p 0.001)*............ 90

Table 14 *Results of the Kendall Tau's statistical analysis between the absolute change in benthic cover for all species of hard coral found across all reefs, and both the maximum bed shear stress modelled at each reef during each simulation (W1_D, W2_E, W3_H, W4_I) and the change in bed shear stress magnitude modelled at each reef during each simulation. (NS – not significant (p > 0.05); * - significant to p 0.05; ** - significant to p 0.01; *** - significant to p 0.001)*............ 91

Table 15 *Results of the Kendall Tau's statistical analysis between the absolute change in benthic cover for all species of soft coral found across all reefs, and both the maximum bed shear stress modelled at each reef during each simulation (W1_D, W2_E, W3_H, W4_I) and the change in bed shear stress magnitude modelled at each reef during each simulation. (NS – not significant (p > 0.05); * - significant to p 0.05; ** - significant to p 0.01; *** - significant to p 0.001)*............ 92

Figure 30 *Projected sea level change for Bowen for scenario SSP1-1.9 and SSP2-4.5 Shaded ranges show the 17th-83rd percentile ranges. Projections are relative to a 1995-2014 baseline (NASA 2024)*............ 100

Figure 31 *Raster file from QGIS showing the variable level of sea-level change since the AR6 reference period for the SSP1-1.9 scenario*............ 101

Table 16 *The models used for the future sea level rise scenarios, including the model ID, the configuration of the model (simulating tides only or tides and wind), the tropical cyclone they were simulating, total model runtime, the spin-up duration, and the start/end dates for each model. For the model ID, 119 denotes the SSP1-1.9 scenario and 245 denotes the SSP2-4.5 scenario*............ 102

Table 17 *The depth of a point at each coral reef across 2 scenarios: current-day bathymetry (W4_I) and varied bathymetry using SSP1-1.9 sea level projections (W4I_119), with the change in depth calculated between each scenario*............ 104

Table 18 *The depth of a point at each coral reef across 2 scenarios: current-day bathymetry (W4_I) and varied bathymetry using SSP2-4.5 sea level projections (W4I_245), with the change in depth calculated between each scenario*............ 105

Figure 32 *Maps showing the depth measured at each coral reef used within this study under different bathymetric scenarios - (A) Current bathymetry; (B) varied bathymetry for SSP1-1.9 sea level projection; and (C) varied bathymetry for SSP2-4.5 sea level............................ 106*

projection...106

Figure 33 *Both the left and right figures are heatmaps showing the maximum bed shear stress (colour and value) extracted from each model (x axis) during the simulation*

period.. 108

Figure 34 *Heatmap showing the change in bed shear stress magnitude calculated between the extracted maximum bed shear stress from the tide-only models (T4_I, T4I_119 and T4I_245) and the corresponding tide and wind models (W4_I, W4I_119 and W4I_245) for each scenario.. 110*

Table 19 *Results of the Shapiro-Wilk Normality test for maximum bed shear stress and change in bed shear stress magnitude (NS – not significant (p > 0.05); * - significant to p 0.05; ** - significant to p 0.01; *** - significant to p 0.001).. 111*

Table 20 *Results of the Kendall Tau's statistical analysis between the reef depth and the modelled maximum bed shear stress and change in bed shear stress magnitude at each reef for each scenario (current-day bathymetry; varied bathymetry for SSP1-1.9 sea level projection; and varied bathymetry for SSP2-4.5 sea level projection) (NS – not significant (p > 0.05); * - significant to p 0.05; ** - significant to p 0.01; *** - significant to p 0.001)....... 111*

Figure 35 *Graphs showing the relationship between the reef depth and (A) the maximum bed shear stress and (B) the change in bed shear stress magnitude modelled at each reef during each scenario with Loess curves added to visualise trends in the data...................113*

Chapter 1 | Introduction and Literature Review

1.1 | Tropical Cyclones and Coral Reefs

The Australian Bureau of Meteorology defines a tropical cyclone (TC) as a large-scale, non-frontal, cyclonic low-pressure system originating in tropical regions (McBride and Keenan 1982). This system is marked by 10-minute mean winds reaching at least 17.5 m/s, categorised as gale force, with the highest wind speeds concentrated at the cyclone's centre (Puotinen, 2004).

The impact of an individual TC on coral reef communities is contingent upon factors such as its strength (measured by maximum wind speed in m/s), duration (the duration of extreme conditions near reefs in hours), spatial extent (size, gauged as the distance from the track to where wind speed drops to gale force at 17 m/s), and translation speed (the forward motion speed of the TC in m/s) (Puotinen et al. 2020). The probability of significant damage is heightened when a TC has considerable strength (maximum wind speeds >33 m/s), endures for an extended period (sustaining gale force winds near reefs for at least 12 hours), exhibits substantial size (size >300 km), and progresses slowly (translation speed <5 m/s) across numerous reefs (Cheal et al. 2017). Puotinen (2007) identified that, for three recent cyclones in the Great Barrier Reef (GBR), maximum wind speed was the most accurate predictor of total damage in one instance, while storm duration proved to be the superior predictor in the other two cyclones. This suggests that both intensity and duration of a TC are crucial determinants of the extent of damage. TCs generate various kinds of damage to coral reefs through mechanical destruction, changes in sedimentation, an increase in turbidity and the lowering of salinity (Harmelin-Vivien 1994).

The occurrence of a TC has frequently been reported to cause immediate mechanical destruction to reef habitats, because of extreme winds, waves and swells (Cheal et al. 2002). The extent of physical wave damage to coral reef communities caused by TCs varies, ranging from the breakage of colony tips and branches to the dislodgement and removal of entire colonies, and in some cases, the removal of portions of the reef structure itself (Puotinen et al. 2016). In March 2003, TC Erica, classified as a category five storm, crossed New Caledonia in the subtropical region of the South Pacific (Guillemot, Chabanet, and Le Pape 2010). The cyclone had average wind speeds of 59.7 m/s and gusts reaching up to 87.5 m/s, leading to significant changes in coral reef habitat characteristics between 2002 and 2003 (Guillemot et al. 2010). The mechanical degradation of reef habitats following the cyclone was marked by a reduction in dead corals present on barrier reefs located near pass (less than 3 km from the nearest pass) and an increase in coral debris and blocks on barrier reefs located far from pass (more than 3 km from the nearest pass) (Guillemot et al. 2010). The direct mechanical effects of TC Erica appeared to have resulted in significant alterations of the 3D-structure of reef habitats on barrier reefs, especially on barrier reefs far from pass which showed significant modification of live hard coral composition (Guillemot et al. 2010).

The displacement of ordinarily stable sediments is the net impact of exceptionally energetic conditions, with surface sediment up to 30 cm thick potentially being removed from some regions and accumulated in others, burying and killing benthic creatures, including corals (Hubbard et al. 1991). Heavy rains caused by cyclonic activity on islands and the mainland can result in turbid waters migrating seawards to coral reefs, potentially limiting coral colony growth since water turbidity reduces the quantity of light reaching reefs (Harmelin-Vivien 1994). In the Coral Coast region of southwest Viti Levu Island, Fiji, the relatively undisturbed Votua rainforest catchment was investigated as a result of nearby watersheds undergoing logging and cultivation, posing a risk of elevated sedimentation to nearby coral reefs (Ram and Terry 2016). The South Pacific wet season experiences periodic tropical cyclones, with approximately 10–12 cyclones passing through Fiji waters per decade (Ram and Terry 2016). Some of these cyclones bring heavy precipitation and lead to significant river floods (Kostaschuk, Terry, and Raj 2001). Previous research indicates that floods generated by cyclones can transport exceptionally high concentrations of suspended sediment in Fiji rivers (Kostaschuk, Terry, and Raj 2003; Terry, Garimella, and Kostaschuk 2002), thereby posing a threat of increased sedimentation and therefore increased turbid waters to adjacent coral reefs.

Significant quantities of sediments, nutrients, and pesticides are introduced into the ocean during river flood events, exerting considerable impacts on vulnerable marine ecosystems, particularly inshore coral reefs (Fabricius et al. 2005). Although much emphasis has been placed on these ‘pollutants’, low salinity, as a result of river discharge, also provides an additional stressor to reefs (Faxneld, Jörgensen, and Tedengren 2010). This low salinity condition can be exacerbated by TCs, which contribute to reduced seawater salinity through intense rainfall and increased river flows onto nearby reefs (Lough 2008). Few studies have examined salinity thresholds for corals; however, freshwater discharge to inshore marine environments such as the GBR have become more variable with more 'very wet' and 'very dry' extremes occurring in recent decades (Lough 2007). These 'very wet' extreme events result in widespread coral mortality (Huang et al. 2014). Reduced seawater salinity plumes (as low as 28 ppt) can persist for up to seven weeks on the GBR (Berkelmans and Oliver 1999). While corals may endure moderate exposure and eventually recover from such events (Jokiel et al. 1993), exposure to very low-salinity seawater leads to coral bleaching and eventual death (Kerswell and Jones 2003). Coral bleaching has been described as a sublethal response of corals involving loss of endosymbiotic dinoflagellate microalgae from the coral tissues and/or loss of the pigments of the algae (Fitt et al. 2001). The impact of these events became highly apparent on the GBR after extensive flooding in Queensland during the extreme summer monsoon of 2010–11, linked to a major La Niña event (Lough, Lewis, and Cantin 2015). More than 33 m^3 of water flowed from the Fitzroy River between December 2010 and March 2011, creating a substantial freshwater plume in the southern GBR lagoon (Tan et al. 2012). During this period, significant mortality of scleractinian (hard) corals on Great Keppel Island reef, situated less than 50 km from the river mouth, was documented, as well as 100% mortality observed among 60 tagged colonies of *Acropora millepora* (Tan et al. 2012).

1.2 | Coral Reefs in the Great Barrier Reef

The GBR is the world's largest coral reef ecosystem and a UNESCO World Heritage Area, containing ~3,000 individual coral reefs within an area of 345,000 km^2 (De'ath et al. 2012) (*Figure 1*). Reefs along the GBR have been classified as the world's least threatened as a result of strong legal protection and their distance from human population centres, with reefs generally lying more than 30 km offshore (with the exception of the Cairns region, where fringing reefs line much of the coast) (Burke et al. 2011). However, the GBR is not immune to the general degradation of reef condition, particularly in the mid to southern sections and in-shore habitats (Graham et al. 2014). This raises substantial concern as the GBR supports an annual revenue of ~AU$5.5 billion through tourism and fisheries, as well as providing a wide range of ecosystem goods and services (Stoeckl et al. 2011).

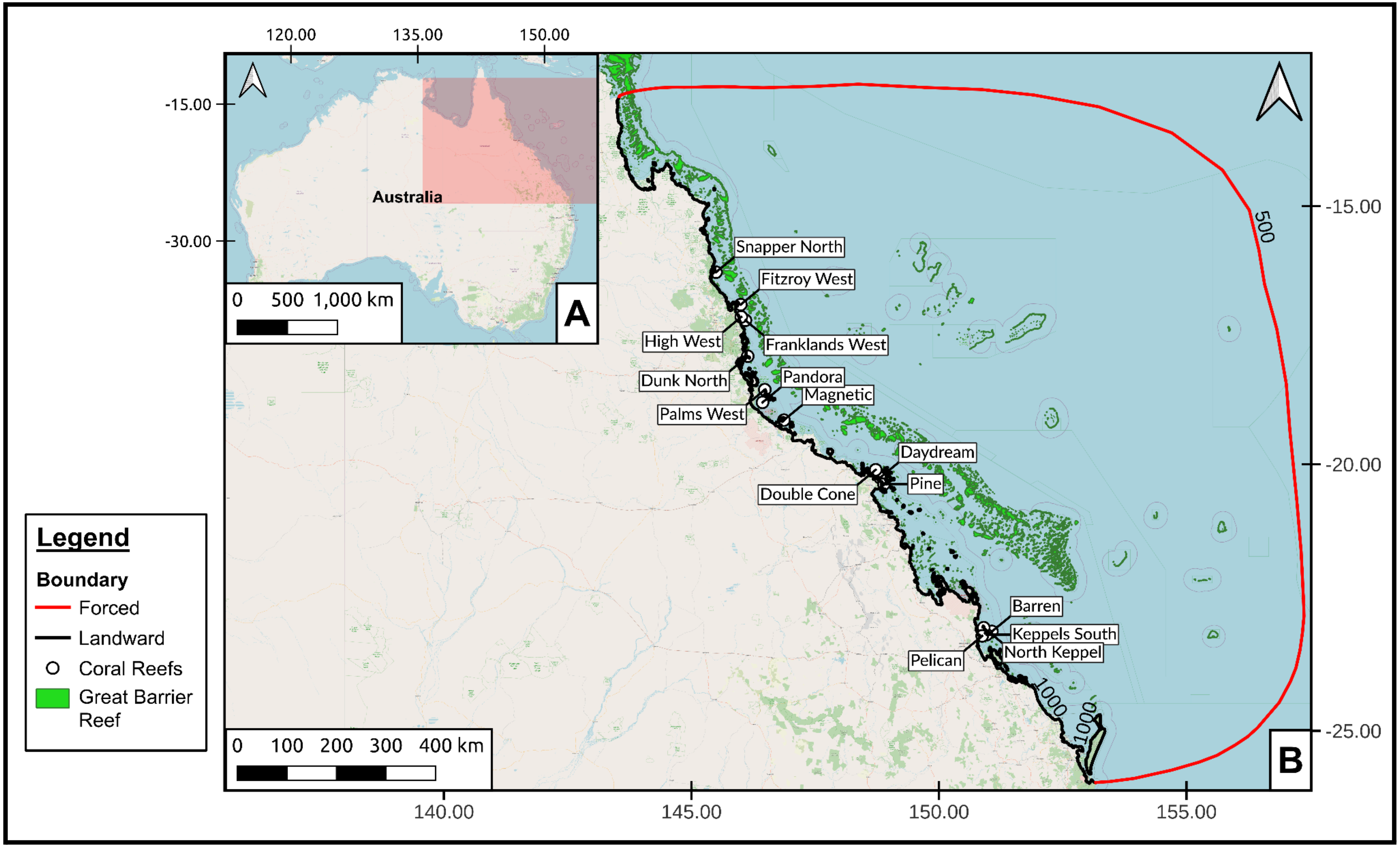

Figure 1 *The location of the study area along the Australian east coast* ***(A)*** *and the locations of the 15 coral reefs studied in this research along the GBR (highlighted in green)* ***(B)****. The boundary of the simulation area is denoted by the black line (landward) and red line (forced).*

Coral assemblages at any particular site, at any given time, are the result of a combination of large-scale biogeographical processes, local-scale environmental conditions, and stochastic disturbances. Large-scale processes include habitat availability and regional species diversity (Bellwood and Hughes 2001). Local-scale conditions encompass wave exposure, light irradiance and turbidity (Done 1982). Stochastic disturbances, which vary in temporal scales, consist of TCs, disease outbreaks, predation, bleaching and anthropogenic impacts (Roberts et al. 2015). The vulnerability of coral reefs to these stochastic disturbances, in particular TCs, is as a result of the robustness and fragility of the reef, which varies according to location, coral community type and successional stage of coral development (Fabricius et al. 2008).

Outer-shelf reefs are more exposed to prevailing south-easterly waves than inshore reefs (which are sheltered by outer reefs); however, the offshore reef framework is substantially stronger than that of inshore reefs (Fabricius et al. 2008). This is as a result of the offshore reefs coral skeleton density being much higher as they are consolidated by crustose coralline algae and calcium carbonate precipitation (Lough and Barnes 2000); whereas, inshore coral skeletons have lower skeletal density and weaker reef substrata (more loosely assembled and poorly cemented) as a result of greater internal bioerosion and fewer crustose coralline algae (Perry and Smithers 2006).

The community type at individual coral reefs is another predictor of a coral reefs vulnerability to disturbances. Coral growth form responds to several factors including light, hydrodynamic stress, sediment flux effect and subaerial exposure as outlined in *Figure 2* (Chappell 1980). The shape of reef corals is affected by light levels and by wave stress, leading to the zonation of coral form associations with exposure and depth (*Figure 2)* (Chappell 1980). It is proposed that coral growth, like diversity, is limited by the same four stress factors, with growth decreasing as overall stress increases, until any factor becomes limiting (Chappell 1980). In shallow, wave-exposed outer-reef crests, solid, low streamlined coral frameworks develop, consisting mainly of *Acropora* with ridged growth forms, complemented by low and compact branching colonies of light skeletal structure (Fabricius et al. 2008). Table corals (known for their broad and horizontal growth) and taller branching forms, including *Acropora* and *Pocillopora*, only become common below the reach of storm waves or in sheltered back-reef margins of outer reefs, and on fronts, flanks, or backs of inner reefs (Fabricius et al. 2008).

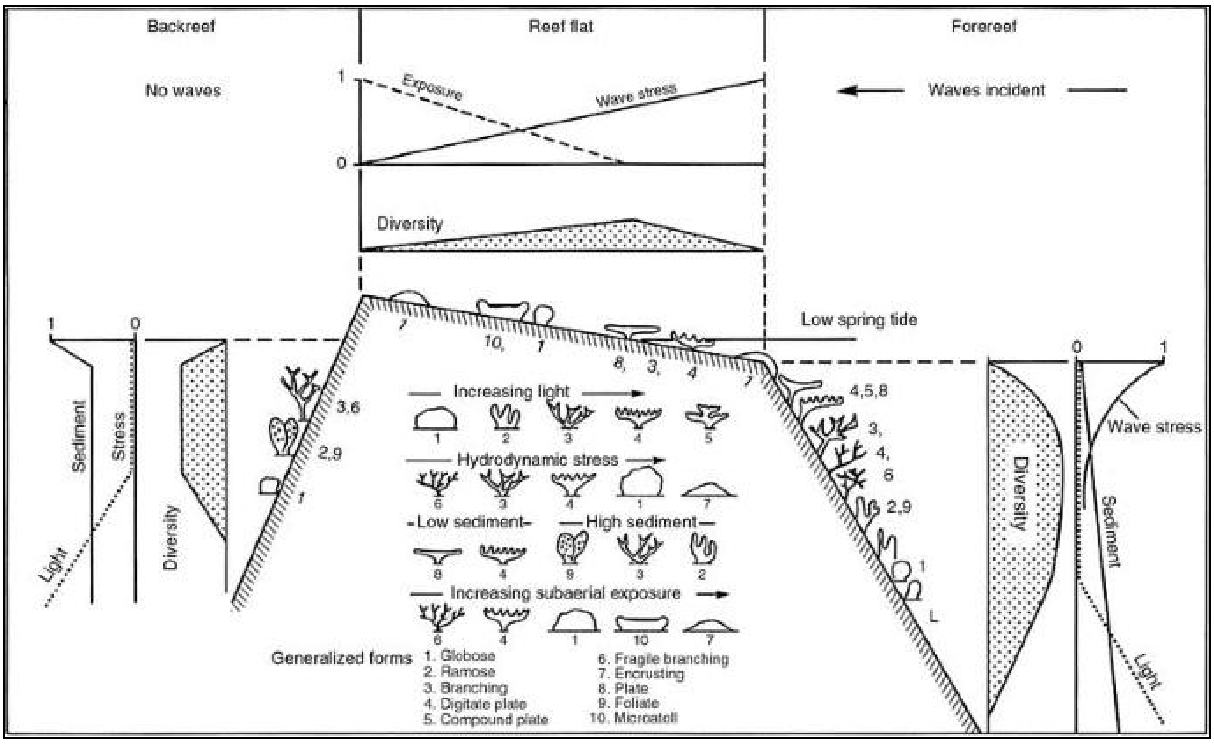

Figure 2 *Idealised variation of coral community forms and diversity from sums of stresses across a simple reef section and coral form responses to environmental stresses (Chappell 1980).*

The successional stage of coral communities is the third predictor of reef fragility. Significant changes in community composition occur along depth gradients of less than 30 m, primarily as a result of changes in wave energy and light irradiance (Done 1982), as well as the frequency and intensity of disturbances (Madin and Connolly 2006). Reefs that suffer more frequent or recent disturbances are likely to have early successional communities with relatively low coral cover, whereas, reefs undisturbed for a long period of time feature late successional communities consisting of fewer taxa, but with higher coral cover and larger mean colony size (Done et al. 2010). Research into coral species diversity along depth gradients has shown that species richness is highest in intermediate depths, 15–35 m (Huston 1985). Light-dependent corals are eventually limited by declining solar irradiance with increasing depth; however, coral assemblages in deeper waters (> 20 m) are also less exposed to disturbances such as severe storms and coral bleaching events and are therefore more ecologically stable than shallower reefs (Smith et al. 2014). The capability of corals to inhabit deeper water is considered to be a crucial factor mitigating extinction risk (Carpenter et al. 2008).

1.3 | Threats to Coral Reef Ecosystems in the Great Barrier Reef

Based on the world's most extensive time series data on reef condition, with 2,258 surveys undertaken on 214 reefs between 1985-2012 in the GBR, a major decline in coral cover was found from 28.0% to 13.8% (an average of 0.53% y^{-1}), a loss of 50.7% of initial coral cover (De'ath et al. 2012). In a more recent survey conducted between August 2022 and May 2023, the northern, central, and southern sectors of the GBR showed declines in hard coral cover of 0.8%, 1.8%, and 0.1%, respectively (*Figure 3*) (AIMS 2023). A majority of reefs underwent little change in 2023, however, coral cover losses from the 2022 mass coral bleaching event, TC Tiffany in January 2022, coral disease and crown-of-thorns starfish (COTS) on some reefs offset increases on other reefs less (or not) affected by such disturbances (AIMS 2023).

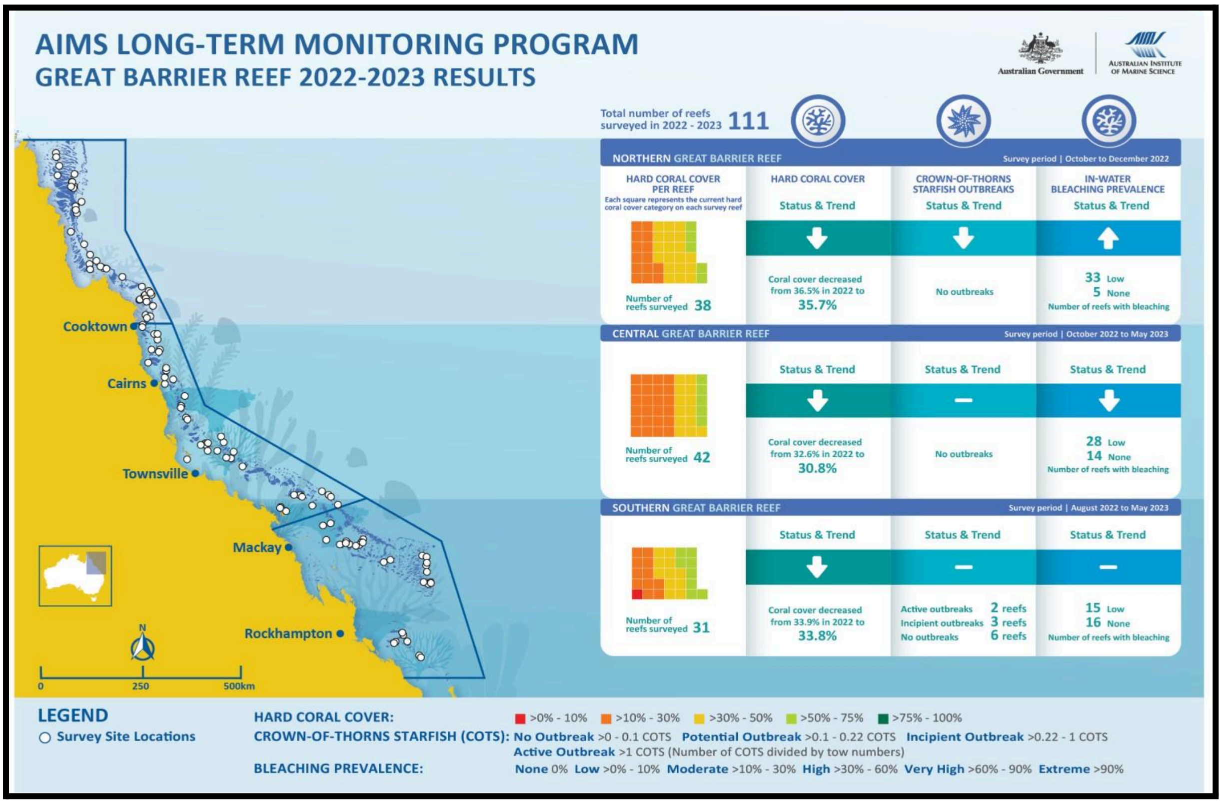

Figure 3 *Summary of the results from the AIMS GBR long-term monitoring program coral reef condition report for the 2022-2023 period demonstrating the hard coral cover, crowns-of-thorns starfish outbreaks and in-water bleaching prevalence status and trends for the northern, central and southern GBR (AIMS 2023).*

Although COTS outbreaks have persisted on some southern GBR reefs in 2022-23, the number of outbreaks on the surveyed reefs have largely decreased (AIMS 2023). However, reefs surveyed between August 2023 and June 2024 have shown an increase in the number of detected COTS in the northern (four reefs) and central (two reefs) GBR, with outbreaks continuing to persist on four southern GBR reefs (*Figure 3*) (AIMS 2024a).

The annual summary report on coral reef condition for the 2023-24 period shows an overall increase in hard coral cover across all three sectors of the GBR, with the southern GBR showing the highest increase of 5.1% (*Figure 4*) (AIMS 2024a). However, it is important to note that these recent increases in hard coral cover can be quickly reversed, as many coral reefs remain highly susceptible to elevated heat stress, wave damage, COTS predation, disease and other anthropogenic impacts (AIMS 2024a).

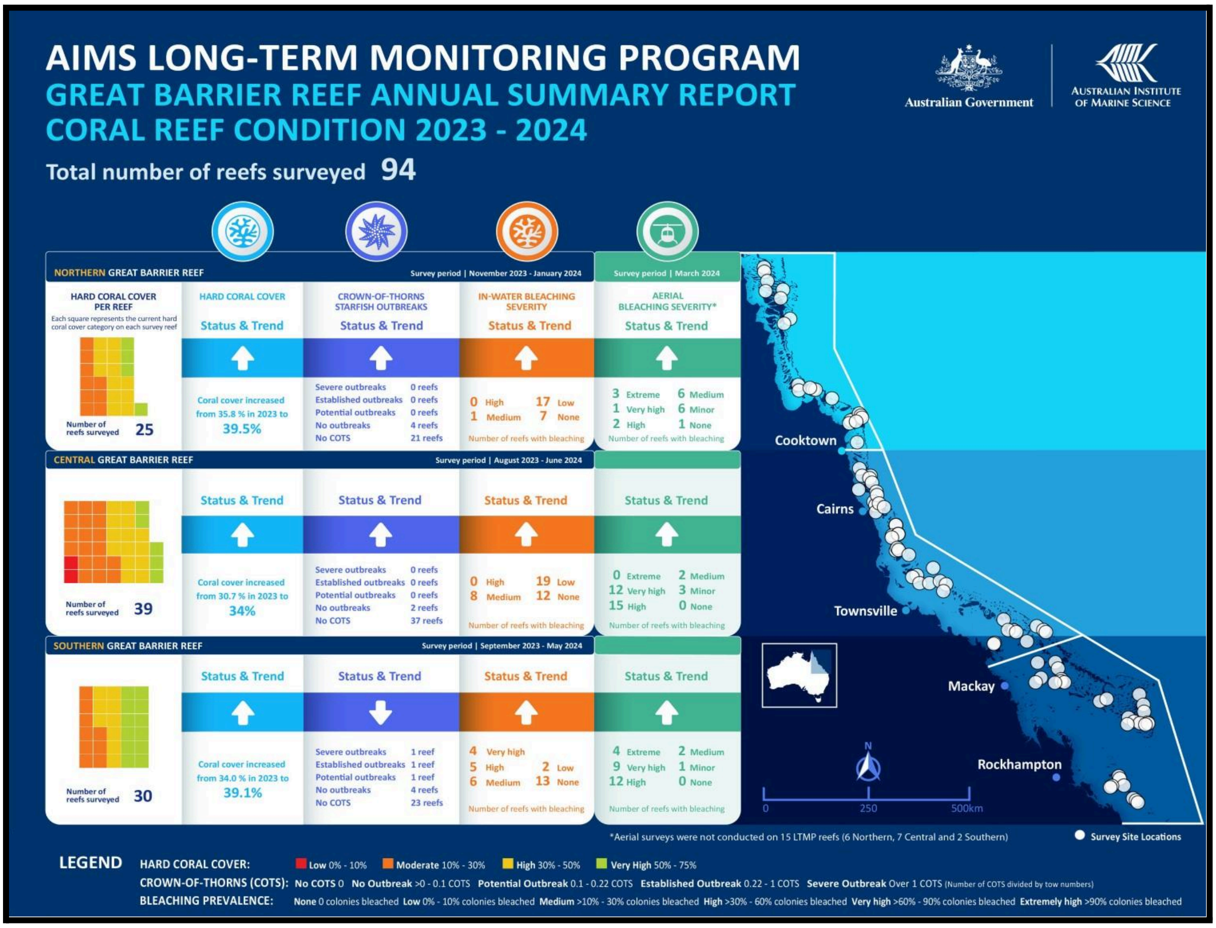

Figure 4 *Summary of the results from the AIMS GBR long-term monitoring program coral reef condition report for the 2023-2024 period demonstrating the hard coral cover, crowns-of-thorns starfish outbreaks, in-water bleaching prevalence and aerial bleaching severity status and trends for the northern, central and southern GBR (AIMS 2024a).*

Human-induced threats originating locally account for 60% of the global damage inflicted upon coral reefs, significantly influencing their recovery and resilience-building processes (Do, Saunders, and Kuleshov 2022). These threats include overfishing and destructive fishing practices, coastal development, and pollution from both watershed and marine sources, posing risks to 55%, 25%, 25%, and 10% of reefs, respectively (Do, Saunders, and Kuleshov 2022). The reefs of Australia are the least affected by local threats, with 15% affected by local stressors and only 1% at high or very high threat (Burke et al. 2011). Marine-based pollution and damage and watershed-based pollution have been identified as the major local threats to the GBR.

The threat of marine-based pollution and damage poses a moderate risk to 10% of the Great Barrier Reef (GBR), primarily influenced by the presence of busy shipping lanes traversing the GBR, with these shipping routes bringing vessels into relatively close proximity to coral reefs, especially in the northern region (GBRMPA 2009). In 2010, a 230 m long bulk coal carrier *Shen Neng 1* bound for China ran aground on Douglas Shoal (92 km northeast of Gladstone), with an initial assessment of 50% of the reef area within the track of the vessel revealing damage varying from severe to moderate across the area impacted, as well as contamination of the shoal and surrounding sediment with antifouling paint from the bottom of the ship (GBRMPA 2010). Despite this, between 1985 and 2008 only 54 major shipping incidents were recorded and the actual spatial impact of these incidents, including physical impacts and pollution, was quite small as a result of shipping being strictly managed (Burke et al. 2011).

Watershed-based pollution from agriculture and forest clearance has been widely recorded in the GBR, with 4% of the GBR threatened, including 2% at high threat (Bainbridge et al. 2009). Whilst only constituting a small percentage, this includes nearly all the nearshore reefs in the southern and central sectors of the GBR (Burke et al. 2011). These nearshore ecosystems not only host distinctive biodiversity but also hold significant importance for local communities (GBRMPA 2009). Overfishing and coastal development are individually assessed to pose a threat to only 1% of the GBR, mainly as a result of the considerable distances of most reefs from human habitation (Burke et al. 2011). Nonetheless, recorded impacts of fishing on remote reefs suggest that both recreational and commercial fishers likely travel greater distances than previously thought (Jackson et al. 2001).

COTS, scientifically identified as *Acanthaster* spp, are among the largest and most efficient coral predators in the Indo-Pacific region (Westcott et al. 2020). The starfish feed on corals, leading to the formation of plagues that beset reefs (Baird et al. 2013). In the GBR, the population dynamics of COTS exhibit cyclical booms, eventually spreading across a significant portion of the ecosystem (Pratchett 2005). Whilst COTS typically exist at low densities (often <1 starfish per ha^{1}) and exert minimal impact on reef coral abundance, their potential for devastation of coral communities becomes apparent during outbreaks when their numbers surge (Pratchett 2005). During the period between 1985–2012, average hard coral cover across the GBR halved, which was mainly attributed to recurrent population outbreaks of COTS (Westcott et al. 2020). A historical example occurred in 1962 at Green Island on the northern GBR, where an outbreak of *A. planci* killed 80% of scleractinian corals across the entire reef, spanning from the shallow reef crest (<2 m depth) to a depth of 40 m (Pratchett 2005). Throughout the evolutionary history of the GBR, elevated levels of COTS are believed to have occurred; however, the severity of COTS outbreaks is thought to be intensified by a combination of anthropogenic influences and climatic events (De'ath et al. 2012), although outbreaks are not necessarily more frequent (Fabricius, Okaji, and De'ath 2010).

Coral bleaching is a stress response in which the coral expels most or all of its endosymbiotic zooxanthellae (Brown 1997). In extreme cases, the bleaching response can be fatal to the coral host, leading to the potential devastation of entire reef ecosystems across expansive areas of ocean (Wooldridge 2009). There are a diverse range of stress factors that lead to coral bleaching, including low salinity, low temperature, high sedimentation, aerial exposure and cyanide exposure; however, the combination of high irradiance and abnormally warm sea surface temperatures (SSTs) is the primary triggering factor for modern large-scale mass bleaching events (Hoegh-Guldberg 1999). There are a wide range of biological and ecological effects of coral bleaching. The biological effects extend to reduced coral growth, reduced reproduction and increased mortality, whilst ecological implications include significant decreases in the cover of susceptible species, shifts in community composition, a drop in species diversity and associated declines in both reef growth and habitat diversity (Marshall and Baird 2000).

Mass coral bleaching events do not uniformly impact all reefs within a given reef province during an episode and rarely do bleached reefs experience equal severity of effects (Berkelmans et al. 2004). During the 1998 coral bleaching event, an aerial survey of the GBR revealed that up to 72% of the surveyed offshore reefs and 13% of inshore reefs remained unbleached (Berkelmans and Oliver 1999). Furthermore, the severity of bleaching varied, ranging from moderate (1–10% of cover) to extreme (>60% of cover), with all reefs falling into the extreme category located inshore, specifically on fringing and patch reefs, with none observed offshore (Berkelmans and Oliver 1999). In 2016, the GBR faced another significant bleaching event, comparable to the 1998 incident, where the region experienced its highest recorded temperatures to date (Stuart-Smith et al. 2018). An estimated 91.1% of reefs along the GBR experienced some bleaching (Hughes et al. 2017), resulting in an estimated loss of approximately 30% of live coral cover over the following six months (Hughes et al. 2018). The most recent mass coral bleaching episode occurred in 2024, where above-average water temperatures (sea-surface temperature anomalies of 1–2.5°C) occurred over the austral summer, peaking in March 2024 and resulting in the fifth mass coral bleaching event since 2016 (AIMS 2024a). This bleaching event resulted in a record-breaking spatial footprint of coral bleaching, with 49% of reefs having high levels (>30% of corals bleached) and 32% of reefs having very high to extreme levels (>60% of corals bleached) (AIMS 2024a).

Coral disease is challenging the resilience of coral reef communities and is of particular concern because it may interact with and increase the impacts of other threats to coral health (e.g. bleaching, overfishing, destructive fishing practices and coastal developments) (Willis, Page, and Dinsdale 2004). The incidence of coral disease outbreaks has experienced a significant surge in recent years, with a notable exponential increase in the number of documented diseases since an initial report in 1965 (Sutherland, Porter, and Torres 2004). This increase includes the appearance of new diseases, re-emergence of more harmful forms of known diseases, and an increase in the range of coral species affected (Roff et al. 2011). A number of novel diseases have emerged in the Indo-Pacific region including atramentous necrosis, white syndrome, skeletal eroding band, brown band disease, and *Porites* ulcerative white spot disease (Jones et al. 2004; Willis, Page, and Dinsdale 2004). These diseases are most common within the *Acroporidae* family, the coral family that is amongst the fastest growing and the most spatially dominant framework builder along the

GBR (Page and Willis 2008). Acroporidae are also the most susceptible to bleaching (Marshall and Baird 2000), which has been shown to increase susceptibility to disease (Maynard et al. 2011). Coral disease surveys conducted twice yearly between 2008 and 2011 at a turbid inshore reef in the central GBR spanned two disturbance events, a coral bleaching event in 2009 and a severe cyclone (cyclone 'Yasi') in 2011 (Haapkylä et al. 2013). The principal coral disease observed at the site was atramentous necrosis (AtN) which displayed a seasonal pattern of outbreaks during the wet season, and predominantly affected a crucial inshore reef-building coral *Montipora aequituberculata* from the Acroporidae family (Haapkylä et al. 2013). Mean prevalence of AtN on *Montipora spp* that reached 63.8 % (± 3.03) was three- to tenfold greater in the wet season of 2009, which coincided with the 2009 bleaching event, than in other years and the persistent wet season outbreaks of AtN combined with the impacts of bleaching and cyclone events resulted in a 50–80% proportional decline in total coral cover (Haapkylä et al. 2013).

TCs are a natural feature of the dynamics of many tropical ecosystems, including coral reefs (Busby, Motzkin, and Boose 2008). Cyclones produce exceptionally strong winds, alterations in sea level, and intense rainfall, all of which can impact coral reefs. With sufficient fetch, persistent high winds generate large waves that crash onto shallow reef areas, displacing sediments and causing physical damage to individual coral colonies and the reef structure itself (Puotinen 2004). Surveys conducted after Cyclone Ivor in 1990 revealed damage to the GBR, including the breakage and displacement of coral colonies, significant sediment and debris movement, and even the removal of entire sections of the reef framework (Van Woesik, Ayling, and Mapstone 1991; Done 1992). Between 1985 and 2015, 44 TCs generated gale force winds within the Great Barrier Reef Marine Park (GBRMP) (Beeden et al. 2015), with 34% of the coral mortality recorded between 1995 and 2009 being attributed to TCs (GBRMPA 2011). Cyclones have been predicted to increase in magnitude and possibly frequency under an enhanced greenhouse climate, consequently increasing their impact on coral reefs (Cheal et al. 2017).

Some coral taxa, such as acroporids, have somewhat evolved and adapted to cyclone disturbance during their long coexistence (Wolff et al. 2016). However, the combination of cyclone damage with additional stressors that may impede recovery rates can result in successive cyclones causing long-term changes in ecosystem conditions (Hughes and Connell 1999). There are significant spatial differences in coral reef damage following a TC; nonetheless, in rare instances where extreme TCs don't inflict extensive harm to coral reef ecosystems, they may weaken the substrate, rendering it susceptible to severe damage during subsequent, less intense storms (Lirman and Fong 1997). In cases of structural damage, recovery could span from decades to centuries, provided there is access to a sufficient larval pool (Hughes and Tanner 2000). If such damage recurs frequently, particularly when coupled with other disturbances and human-induced pressures, coral coverage may decline significantly, endangering the resilience of reefs to maintain themselves as coral-dominated ecosystems (Beeden et al. 2015).

1.4 | Wave Dynamics and Bed Shear Stress

The intense winds generated by the spatially compact and well-formed vortex structures of TCs generate large and potentially destructive ocean surface waves (Young 2017). For the GBR, the most severe wave conditions occur during TCs (Hardy, McConochie, and Mason 2003). Offshore from the GBR, under stronger non-cyclonic conditions characterised by southeasterly trade winds of ~15 m/s, maximum significant wave heights and peak periods are approximately 4 m and 10 seconds, respectively (Wolanski 1986). However, during TCs, significant wave heights in deep water beyond the GBR can frequently exceed 10 m and may reach heights as high as 20 m during exceptionally severe storms (Young and Burchell 1996). The distant passage of an intense category 3 TC generated highly energetic surface waves across a large region of the Australian North West Shelf (Drost et al. 2018). At two sites on the continental shelf, significant wave heights up to a maximum of 10 m were recorded, accompanied by near-bed wave orbital velocities, reaching up to 0.7 m s^{-1} at depths of 40 and 74 metres (Drost et al. 2018). Concurrent current profiles were measured between 0.5 and 8.5 m above the seabed at these sites, therefore allowing a detailed analysis of the wave-current interactions in the continental shelf bottom boundary layer (Drost et al. 2018). These observations unveiled substantial alterations in current profiles during the cyclone, including a significant increase in apparent bottom roughness (by up to two orders of magnitude) compared to the usual tide-dominated current conditions (Drost et al. 2018).

Wave breaking occurs at the seaward edges of reefs, then as the waves cross the reefs, bottom friction further reduces wave height (Young and Hardy 1993). As waves break and weaken, the mean water surface elevation increases, driving currents (Longuet-Higgins and Stewart 1962) and reef circulation (Angwenyi and Rydberg 2005). These currents have implications for the transport of sediments, pollutants, nutrients, plankton, and larvae (Lowe et al. 2005). The GBR is composed of a 'reef matrix', formed by thousands of individual reefs, with spaces between them that allow wave energy to pass through (Gallop et al. 2014). The proportion of these spaces relative to the total reef area is referred to as the "porosity" of the reef matrix and is represented by the 'porosity index' (Gallop et al. 2014). The porosity index was generated based on the volume of reef above the 40 m depth contour (*Figure 5*), between the forereef (100 m depth) and the lee of the reef (Gallop et al. 2014).

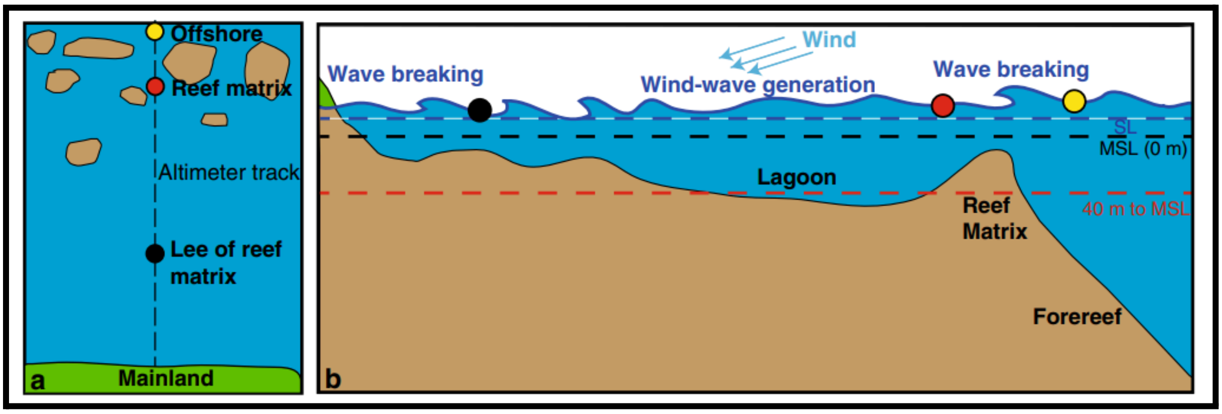

Figure 5 *Schematic of a typical cross section of the GBR matrix, (a) a plan view; and (b) the profile view (Gallop et al. 2014).*

A porosity index of 0 indicates that the entire volume above 40 m was reefs or seabed (i.e., 0% porous), while 1 specifies that there were no reefs or seabed above 40 m depth (i.e., 100% porous) (Gallop et al. 2014). There is a trend of increasing reef matrix porosity from north to south across the GBR (Gallop et al. 2014). In the north, porosity averages approximately 0.6 (i.e., 60% porous) where the shelf is narrower than 8 km (Gallop et al. 2014). From 15S as the shelf widens, porosity starts to increase, and the central GBR is mostly between 0.7 and 0.95 (Gallop et al. 2014). In the south, the shelf is up to 300 km wide, and there is an extensive lagoon that is more than 200 km wide in the far south, so this lagoon leads to high porosities of generally more than 0.8 (Gallop et al. 2014).

On the GBR, waves can travel through the reef matrix without entirely dissipating, resulting in the transmission of considerable wave energy (Thomas A. Hardy and Young 1996). This contrasts with mainland beaches and fringing reef-lagoon systems, where waves typically lose energy or transform into changes in water levels and currents (Lugo-Fernández, Roberts, and Suhayda 1998). The impact of reef matrix porosity on wave attenuation has been poorly understood in past research, with the frictional dissipation of waves being studied in much greater detail on the reef crest and reef flat compared to the high-energy environments of the forereef slope (Perris et al. 2024). Wave breaking on the forereef slope is the dominant form of wave energy dissipation in high-energy conditions (Osorio-Cano et al. 2018) with the high dissipation rates on the forereef being controlled by forereef morphology such as spurs and grooves (Monismith et al. 2013; Osorio-Cano et al. 2018). Spurs and grooves are shore-normal elongate ridges (spur) and troughs (groove) on the forereef slopes of many coral reefs (Duce et al. 2016). A recent study investigated the role of forereef spur and groove morphology in wave energy dissipation and transmission at the reef crest (Perris et al. 2024). Using XBeach on LiDAR-derived bathymetry from One Tree Island in the southern GBR, dissipation rates comparable to spur and groove field studies were reproduced (Perris et al. 2024). The study examined how wave energy dissipation differs between realistic bathymetry and bathymetry with spur and groove features removed, finding up to a 40% decrease in dissipation when spur and groove features were absent (Perris et al. 2024). This shows that spur and groove morphologies can increase wave dissipation by inducing breaking and increasing bed friction and should be considered in future research on wave dissipation (Perris et al. 2024).

There is a reasonable understanding of wave conditions offshore of the GBR, but data from within and in the lee of the reef matrix are limited (Hopley, Smithers, and Parnell 2007). A few studies have conducted in situ wave measurements within the GBR matrix, where in the lee of the reef, a bimodal sea state with low energy at 10 seconds and more energetic, shorter-period waves was observed (Murray and Ford 1983). Significant reductions in wave height and energy over John Brewer Reef in the central GBR and Yonge Reef in the northern GBR was also found, with wave periods longer than 8 seconds being completely attenuated (Young 1989; Hardy et al. 1991). It has also been suggested that wave height over reefs is primarily determined by the depth of reef submergence, indicating that waves are depth-limited; however, the data showed considerable variability, suggesting that other factors also play a pivotal role (Young 1989; Hardy et al. 1991). A combination of numerical models and measurements from four in situ instruments during a tropical cyclone were used and found that cyclone-generated waves seaward of the GBR matrix had significant wave heights of ~10 m, which were attenuated to 6 m in the lee of the matrix (Young and Hardy 1993). As well as this, the results also suggested that although not all wave energy was dissipated by wave breaking at the seaward edge of the reefs, most of the energy remaining was dissipated as a result of the bottom friction over reefs (Young and Hardy 1993).

Modelling coastal currents influenced by tides, waves, wind, and high roughness is complex, particularly when assessing bed shear stresses under wave-current interactions (Lan and Huang 2024). Few studies have explored this, especially in reef environments. The first direct assessment using a coupled wave-current model (Delft-3D) over an algal reef in the Taoyuan coastal area on the northwestern part of Taiwan main island, showed that the model generally replicates depth-averaged currents and bed shear stresses when all factors are considered (Lan and Huang 2024). Two models, with and without wind forcing, revealed that tides primarily drive currents, even in shallow waters within a depth of 3 m; however, wind speed and direction also significantly affect currents during high-wind events (Lan and Huang 2024). When wind and tidal current directions align, the current speed increases, highlighting the importance of wind stress on coastal currents (Lan and Huang 2024). Additionally, the study found that non-linear wave interactions significantly enhance bed shear stresses, reducing the model error and emphasising the importance of these complex interactions between waves and currents in predicting shear stresses during high-wave orbital motions (Lan and Huang 2024).

1.5 | Impacts of Climate Change and Sea Level Rise

The Intergovernmental Panel on Climate Change's (IPCC) Special Report on Global Warming of 1.5°C identifies tropical coral reefs as one of the most sensitive ecosystems, with mass coral bleaching and mortality projected to increase as a result of the combined effects of increasing ocean temperatures, ocean acidification, sea-level rise and the potential for an increase in the intensity and frequency of TCs (O. Hoegh-Guldberg et al. 2018). Sustained and ongoing increases in ocean temperatures and acidification are altering the structure and function of reefs globally (Hoey et al. 2016) making them more susceptible to impacts from additional stressors.

The Working Group 1 (WG1) contribution to the IPCC Sixth Assessment Report (AR6) presented findings on the physical science basis of climate change (Masson-Delmotte et al. 2021). The report released in 2021 shows improvements in observationally based estimates and information from paleoclimate archives since the release of the IPCC Fifth Assessment Report (AR5) in 2014 (Lee et al. 2021). The Shared Socio-economic Pathway (SSP) framework was developed and used in the Coupled Model Intercomparison Project Phase 6 (CMIP6) and focuses on five illustrative projections that cover a range of possible future developments of anthropogenic drivers of climate change: SSP1-1.9, SSP1-2.6, SSP2-4.5, SSP3-7.0 and SSP5-8.5 (Masson-Delmotte et al. 2021). In the SSP labels, the first number refers to the assumed pathway, and the second refers to the approximate global effective radiative forcing (ERF) in 2100 (Lee et al. 2021). As demonstrated in *Figure 6*, the SSPs start in 2015 and include scenarios with high and very high greenhouse gas (GHG) emissions (SSP3-7.0 and SSP5-8.5), where CO_2 emissions roughly double by 2100 and 2050, respectively (Masson-Delmotte et al. 2021). There are also scenarios with intermediate GHG emissions (SSP2-4.5), where CO_2 emissions stay around current levels until mid-century, and scenarios with low to very low GHG emissions, where CO_2 emissions decline to net zero around or after 2050, followed by varying degrees of net negative CO_2 emissions (SSP1-1.9 and SSP1-2.6) (Masson-Delmotte et al. 2021).

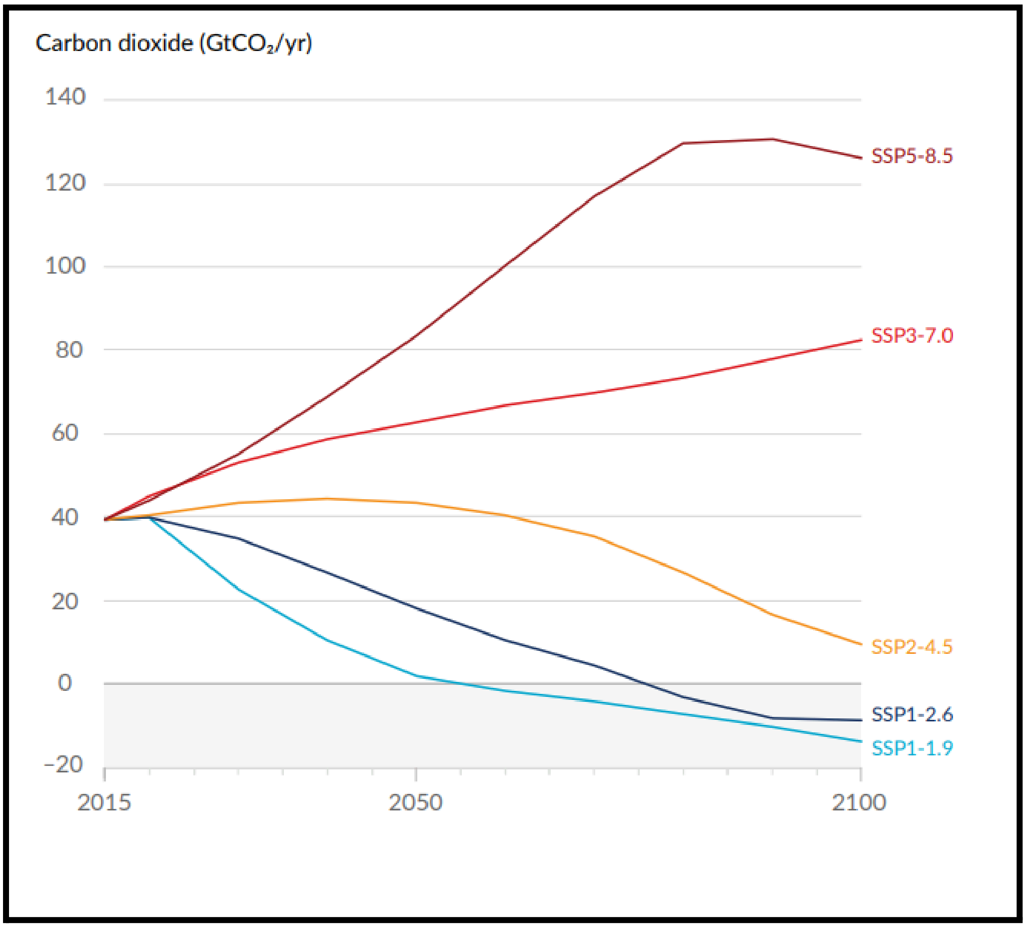

Figure 6 Annual anthropogenic emissions over the 2015–2100 period showing *the emissions trajectories for carbon dioxide from all sectors ($GtCO_2$/yr) (Masson-Delmotte et al. 2021).*

Global surface temperatures are projected to keep rising until at least the middle of this century across all considered emissions scenarios (Masson-Delmotte et al. 2021). Warming of 1.5°C and 2°C will be surpassed during the 21st century unless there are significant reductions in CO_2 and other greenhouse gas emissions in the coming decades (Masson-Delmotte et al. 2021). Compared to 1850–1900, global surface temperature averaged over 2081–2100 is very likely to be higher by 1.0°C to 1.8°C (*Table. 1*) under the very low GHG emissions scenario considered (SSP1-1.9), by 2.1°C to 3.5°C in the intermediate GHG emissions scenario (SSP2-4.5) and by 3.3°C to 5.7°C under the very high GHG emissions scenario (SSP5-8.5) (Masson-Delmotte et al. 2021).

Table 1 *Changes in global surface temperature, which are assessed based on multiple lines of evidence, for selected 20-year time periods and the five illustrative emissions scenarios considered. Temperature differences relative to the average global surface temperature of the period 1850–1900 are reported in °C. This includes the revised assessment of observed historical warming for the AR5 reference period 1986–2005, which in AR6 is higher by 0.08 [–0.01 to +0.12] °C than in AR5 (Masson-Delmotte et al. 2021).*

	Near term, 2021–2040		Mid-term, 2041–2060		Long term, 2081–2100	
Scenario	Best estimate (°C)	*Very likely* range (°C)	Best estimate (°C)	*Very likely* range (°C)	Best estimate (°C)	*Very likely* range (°C)
SSP1-1.9	1.5	1.2 to 1.7	1.6	1.2 to 2.0	1.4	1.0 to 1.8
SSP1-2.6	1.5	1.2 to 1.8	1.7	1.3 to 2.2	1.8	1.3 to 2.4
SSP2-4.5	1.5	1.2 to 1.8	2.0	1.6 to 2.5	2.7	2.1 to 3.5
SSP3-7.0	1.5	1.2 to 1.8	2.1	1.7 to 2.6	3.6	2.8 to 4.6
SSP5-8.5	1.6	1.3 to 1.9	2.4	1.9 to 3.0	4.4	3.3 to 5.7

Global mean sea level (GMSL) change is driven by warming or cooling of the ocean (and the associated expansion/contraction) and changes in the amount of ice and water stored on land (Arias et al. 2021). GMSL increased by 0.20m (0.15-0.25m) over the period 1901 to 2018, with a rate of rise that has accelerated since the 1960s to 3.7mm yr^{-1} (3.2-4.2mm yr^{-1}) for the period 2006-2018 (Arias et al. 2021). Sea level responds more gradually than global surface temperature in response to GHG emissions, resulting in a weaker scenario dependence over the 21st century (Arias et al. 2021). This delayed response causes long-term committed sea level rise (SLR) as a result of ongoing ocean heat absorption and slow ice sheet adjustment, continuing for centuries and millennia after emissions stop (Arias et al. 2021). By 2100, GMSL is projected to rise by 0.28–0.55 m under SSP1-1.9 and 0.63–1.01 m under SSP5-8.5, relative to the 1995–2014 average, with deep uncertainty regarding the higher CO_2 emissions scenarios for sea-level projections beyond 2100 as a result of unpredictable ice sheet responses (Arias et al. 2021). *Figure 7* shows the global projected sea-level change for the five SSP scenarios relative to a 1995-2014 baseline.

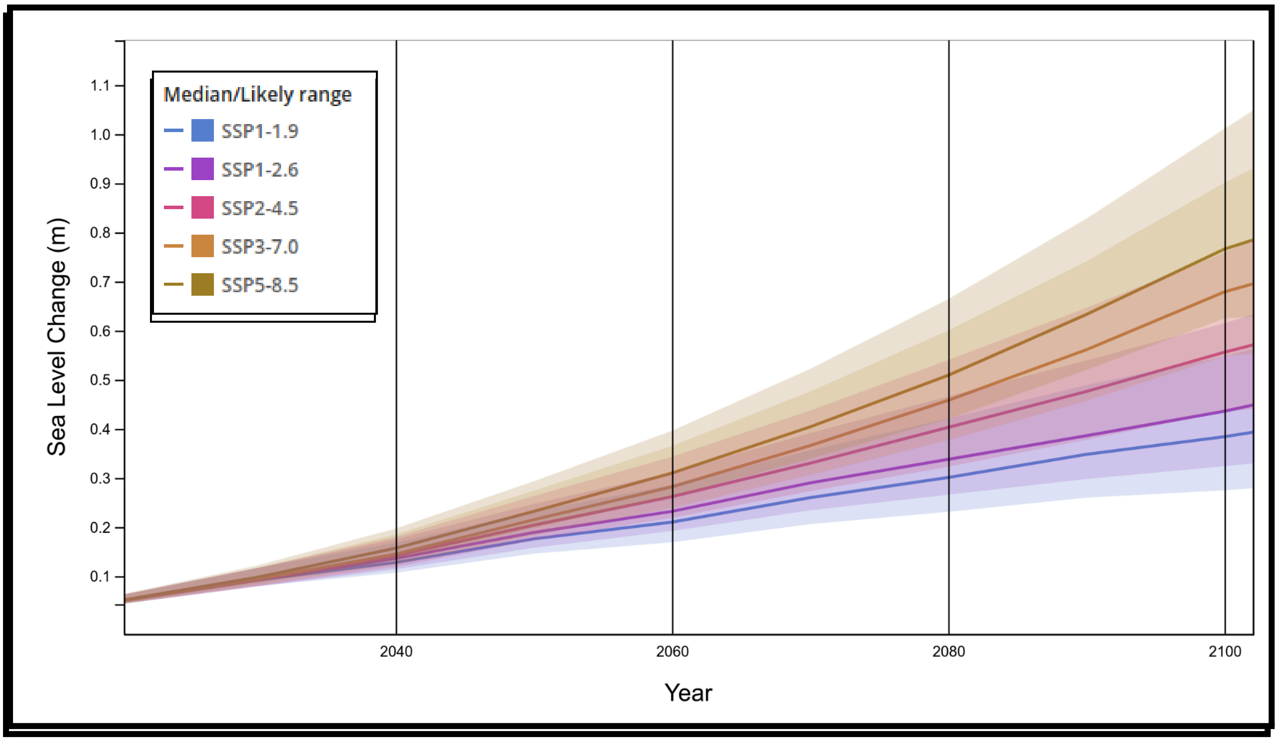

Figure 7 *Global projected sea level change for SSP scenarios resulting from processes in whose projection there is medium confidence. Shaded ranges show the 17th-83rd percentile ranges. Projections are relative to a 1995-2014 baseline (NASA 2024)*.

SLR is generally not considered a threat to coral reefs as long as coral growth remains robust enough to keep up with the rising water levels; however, other factors such as changes in sea temperature, increased sediment input, and acidity from future climate change are likely to reduce the growth of corals which suggests that some reef communities may struggle to maintain themselves under even the most minimum changes in sea level (Hoegh-Guldberg 2011). Coupled hydrodynamic and sediment-transport modelling suggests that a 0.5-1.0 m rise in sea level will likely increase coastal erosion, mixing and circulation, increase the amount of sediment resuspended and increase the duration of high turbidity on exposed reef flats (Storlazzi et al. 2011). This would result in decreased light availability for photosynthesis, increased sediment-induced stress on reef ecosystems and potentially affecting a number of other ecosystem processes (Storlazzi et al. 2011).

The impacts of future climate change on TC activity have been widely studied. Most global predictions of these impacts have focussed on frequency and intensity, with an increase in the relative frequency of the most intense TCs posing the greatest threat to coral reef communities (Cheal et al. 2017). Previous research generally shows an upward trend in TC intensity across various climate models (Emanuel, Sundararajan, and Williams 2008), with global average increases in intensity, as measured by maximum wind speeds, projected to range between 2% and 11% by 2100 (Knutson et al. 2010). These studies have also found that the proportion of TCs reaching category 4 and 5 intensity is projected to increase between 0-25% globally (Christensen et al. 2013), while the occurrence of lower-intensity storms is expected to decrease (Knutson et al. 2020). Under a medium emissions scenario (SSP2-4.5), the annual number of days with category four and five storms is projected to rise by 35% globally by 2100, and the total number of category four and five storms is expected to increase by 24%, indicating longer durations of intense storm conditions (Knutson et al. 2015). However, for the Southwest Pacific, most models contradict these projections and show a decrease in the frequency of category four and five TCs (Knutson et al. 2020), therefore there is a lot of uncertainty with predictions on TC intensity under a changing climate.

Despite the projected increase in TC intensity, a majority of climate model studies predict a decrease in the frequency of TC activity, or no change (Murakami et al. 2020), averaging at around -14% for +2 ℃ of warming (T. Knutson et al. 2020). Projections for the SW Pacific basin also align with these findings, showing a reduction in TC frequency (K. J. E. Walsh et al. 2016); however, the high natural variability in this region suggests that the projected reductions in at least some models are not statistically significant (K. Walsh 2015). Three separate reviews of climate projections found that the global frequency of TCs is most likely to remain stable or decrease by up to 40% by 2100 (Knutson et al. 2010; Christensen et al. 2013; Walsh et al. 2016); however, a separate study predicted substantial increases of 10-40% in the global mean frequency of TCs over the 21st century (Emanuel 2013). The varying projections across models regarding both the direction and magnitude of changes in global TC frequency under climate change have led to the suggestion that reaching a general consensus may be difficult for the foreseeable future (Emanuel 2013).

The potential impacts of climate change, including sea-level rise and the mortality of coral during warm conditions (Hoegh-Guldberg 2011) may reduce the effectiveness of fringing and barrier reefs as protection for islands, and directly change the hydrodynamics, nutrient supply and forces on reefs and corals (Perry et al. 2013; Storlazzi et al. 2011; Grady et al. 2013). Coupled hydrodynamic and sediment transport numerical modelling indicates that a 0.5–1.0 m increase in water depth on a 1–2 m deep exposed fringing reef flat would lead to higher significant wave heights and water setup, further raising water depths on the reef flat (Storlazzi et al. 2011). Larger waves would produce higher near-bed shear stresses, increasing the size and amount of sediment that can be resuspended from the seabed or eroded from nearby coastal deposits (Storlazzi et al. 2011). As water depth increases, stronger wave- and wind-driven currents would enhance the transport of water and sediment alongshore and offshore, moving them from the inner reef flat to the outer reef flat and fore reef, where coral growth is typically most abundant therefore could potentially affect coral reef growth (Storlazzi et al. 2011).

While wave heights increase under SLR, further research has found that changes in the wave-induced velocity are more complex, such that the changes vary reef by reef (Baldock et al. 2014). A one-dimensional wave model was used to investigate changes in reef top wave dynamics and wave forces under different SLR scenarios for a large sample of idealised reef profiles (Baldock et al. 2014). The model results predict that the impacts of SLR vary spatially and are strongly influenced by the bathymetry of the reef and coral type, showing that for many reef bathymetries, wave orbital velocities increase with SLR during average wave conditions and cyclonic wave forces are reduced for certain coral species (Baldock et al. 2014). Both of these changes suggest future SLR could be beneficial to coral health and colony resilience as a result of the potential for increased wave induced orbital motion under average wave conditions or less coral breakage under cyclonic conditions (Baldock et al. 2014). However, predicting the impact of SLR on individual reefs requires consideration of the reef bathymetry, the reef zone and the type of coral species (Baldock et al. 2014).

A study utilising a two-dimensional numerical model, SWAN, examined swell wave dynamics on idealised fringing reefs, exploring various bathymetries, climate conditions, and water depths (Baldock et al. 2020). The results highlight how reef geometry, bathymetry, coral species, and SLR influence hydrodynamic parameters and forces on corals, with one-dimensional models underestimating wave action on reef flats (Baldock et al. 2020). Wide short reefs and narrow, long reefs have similar wave heights at the centre, but as reef width increases, wave height decreases, peaks when width equals length, and then decreases again due to dissipation and refraction (Baldock et al. 2020). If reefs maintain their wave-breaking and refracting functions, SLR increases wave heights and orbital velocities on the reef flat. However, without coral growth, deeper reefs may lose these functions, reducing near-bed velocities (Baldock et al. 2020). SLR also affects hydrodynamic forces on corals differently by species, with intermediate corals behaving like branching corals in long-period swell and like massive corals in short-period swell, potentially altering reef complexity overtime based on regional wave climates (Baldock et al. 2020). Therefore, there is a delicate balance between how future climate change and SLR could impact coral reef growth, and how resultant changes in wave dynamics and bed shear stress may either support coral resilience or lead to further erosion and degradation of reef ecosystems.

1.6 | Modelling Tropical Cyclones on Coral Reefs

Significant advancements in the numerical modelling of TCs have greatly improved the accuracy and reliability of simulations; however, accurately estimating intensity and phase changes in high winds remains challenging as a result of the complexity of modelling the full range of physical processes involved (Yan and Zhang 2022).

One approach to analysing the observations near a TC is through the use of an analytical model of the sea level pressure and wind profiles (Holland 1980). Such a model enables interpolation between observational data points, allowing for objective estimation of critical parameters, including maximum wind speeds, the spatial extent of destructive winds, and other key characteristics of the cyclone (Holland 1980). One model extended (Schloemer 1954) negative exponential relation model to develop a universal and analytical model for the radial profiles of sea level pressure and winds in a TC (Holland 1980). This model was applied to three TCs in Australia and nine in Florida, and it successfully reproduced their profiles with two considerations: when applied to pressure observations, the model may underestimate maximum winds as a result of unresolved strong pressure gradients over short distances; however, this can be mitigated by applying the model to wind observations provided they are reliable (Holland 1980).

The cyclostrophic wind equation from (Holland 1980) wind field model was adapted to develop HURRECON, a simple meteorological model using information on the track, size and intensity of a TC, as well as the cover type (land or water), to estimate the surface wind speed and direction from a TC (Boose, Serrano, and Foster 2004). The model distinguishes between land and water sites as a result of the greater surface friction; however, the model does not take into account local topography which can modify wind speed and direction particularly in hilly terrain (Boose, Foster, and Fluet 1994). The model reconstructs large-scale surface wind conditions based on the assumption that the surface wind field in all TCs can be represented by simple equations, with parameters adjusted to each specific storm (Boose, Serrano, and Foster 2004). Consequently, the model's accuracy depends on the extent to which this is true and the significance of localised effects that the model cannot account for, such as intense convective cells (Boose, Foster, and Fluet 1994).

A further adaptation of Holland’s (1980) model is CycWind, a double vortex TC pressure and wind field model that incorporates a synoptic scale wind field capability (McConochie, Hardy, and Mason 2004). The pressure profile is based on (Cardone et al. 1994), which has a primary and secondary cyclone pressure profile specification used to determine gradient level wind speeds and directions (McConochie, Hardy, and Mason 2004). The synoptic scale wind field is merged into the cyclone wind field at gradient level and a boundary layer correction is applied to give wind speeds and directions at the surface (10m above sea level) (McConochie, Hardy, and Mason 2004). CycWind produced 64 cyclone wind fields over 33 years (1969-2002) of cyclone activity along Queensland's East Coast, suitable to be applied to wind, storm surge, and circulation modelling (McConochie, Hardy, and Mason 2004). Enhancements to the wind field model were highlighted, including adjustments to account for the effect of super-gradient winds (Kepert 2001; Mallett 2000) and for wind field asymmetries beyond those caused by the forward motion of the TC (McConochie, Hardy, and Mason 2004).

Analytical models, like those above, have been used widely for estimating the wind speed of a TC, where the storm-induced wind velocity is calculated as a function of the distance from the centre of the TC (Kalourazi et al. 2020). For these models, different parameters such as maximum wind speed, a radius of maximum wind, TC shape parameter, TC translation speed and the orientation of the trajectory affect the shape of a TC (Kalourazi et al. 2020). Analytical wind models are effective for simulating wind fields within a certain radius from the centre of a TC, but beyond that range, predictions become inaccurate as the TC may be influenced by other global weather systems (Kalourazi et al. 2020). Further advances in modelling TCs have led to the development of 2D and 3D numerical storm surge models which generally simulate the wind-driven and pressure-induced surge and tide caused by a TC (Sheng, Zhang, and Paramygin 2010). However, the wave-induced surge can be simulated by including the effects of waves on storm surge via a coupling between a storm surge model and a wave model (Sheng, Zhang, and Paramygin 2010) such as SWAN (Booij, Ris, and Holthuijsen 1999). Numerical storm surge models typically model the ocean assuming the relevant physics can be suitably approximated via discretisation of the shallow water equations (SWEs), and are coupled to meteorological models via terms for atmospheric pressure and surface stress as a result of wind (Warder, Horsburgh, and Piggott 2021). The SWEs govern a variety of coastal and environmental engineering problems, such as estuarine and coastal circulation, overland flow, surface irrigation, river or lake hydrodynamics, tidal wave runup, TC-induced storm surge, etc (Akbar and Aliabadi 2013). Typically, the SWEs are formulated in conservation form and solved using methods such as finite difference, finite volume, or discontinuous Galerkin finite element approaches (Akbar and Aliabadi 2013). These techniques generally provide accurate results when the water velocity and wave speed are of similar magnitudes; however, if the wave speed is significantly higher than the water velocity, the numerical scheme can become challenging (Akbar and Aliabadi 2013). In such cases, the governing equations are often written into non-conservation form, and two separate sets of equations are derived and solved individually (Akbar and Aliabadi 2013).

Various adaptations of the analytical wind field model have been used alongside numerical wave and storm-surge models to determine the impact of tropical cyclones on coral reef environments. A study used CycWind to evaluate the wind field during severe TC Lua (Puotinen et al. 2020), a category three TC that formed off the northwest Australian coast in March 2012 (BOM 2019). The modelled wind speeds and directions were used to force the Simulating WAves Nearshore

(SWAN) numerical wave model to evaluate the evolution of the surface wave fields across north-western Australia during Lua (Puotinen et al. 2020). The results of this model were used alongside benthic field surveys conducted before and after TC Lua tracked through Australia's northwest shelf region to determine the exposure of Australia's north-west shelf to damaging waves from TC Lua and the global implications for coral reefs (Puotinen et al. 2020).

A range of other numerical models have also been used to model TC-induced wave climates across coral reefs. The numerical model Delft3D-FLOW (Lesser et al. 2004) was used in combination with SWAN (Booij, Ris, and Holthuijsen 1999) to simulate the hydrodynamic conditions at Ningaloo Reef during TC Olwyn along Australia's Northwest Shelf in March 2015 (Cuttler et al. 2018). Delft3D-FLOW uses a structured grid to solve the unsteady shallow-water equations in two- or three-dimensions using a system of equations that consist of the horizontal momentum equations, the continuity equation, the transport equation, and a turbulence closure model (Lesser et al. 2004). The model has been used successfully in coral reef environments under both non-storm and storm conditions (Grady et al. 2013; Hoeke, McInnes, and O'Grady 2015; Cuttler et al. 2018). There are many other numerical models that have been used in studies modelling TCs and their impacts, including WAMGBR (Hardy, McConochie, and Mason 2003), Delft3D FM (Leijnse et al. 2022) and XBeach (Harter and Figlus 2017), all of which were considered prior to this research.

1.7 | Aims and Objectives

This project aims to numerically model multiple TCs over the GBR over a period of no more than 3 months. Bed shear stress data generated from the models will be used as a proxy for coral reef damage, with coral cover data before and after the TC impact used to determine the extent of coral reef damage. This project also aims to run multiple models with varied bathymetry based on the IPCC AR6 SSP projections for SLR to determine the possible impacts that SLR could have on bed shear stress in the future.

This research is important as understanding the physical impacts of TCs on coral reef systems is critical for predicting reef resilience under current and future climate conditions. This study addresses this need by numerically modelling multiple TCs over the GBR to estimate bed shear stress—a key driver of mechanical coral damage. By linking modelled stress with observed changes in coral cover, the research provides a method for assessing cyclone-induced reef degradation. Additionally, by incorporating projected SLR scenarios from the IPCC AR6 SSPs, the study explores how future changes in bathymetry could alter hydrodynamic forces on reef systems. These insights are essential for improving risk assessments and informing reef management under climate change, for both the GBR and other Pacific coral reef environments.

Chapter 2 | Numerically Modelling Tropical Cyclones

2.1 | Introduction

The increasing frequency and intensity of tropical cyclones (TCs) due to climate change pose significant challenges for forecasting and mitigating their impacts (Tissaoui 2024). The occurrence of a TC has frequently been reported to cause immediate mechanical destruction to reef habitats, because of extreme winds, waves and swells (Cheal et al. 2002). This study aims to numerically model TCs in the Great Barrier Reef (GBR) to investigate the effects of TCs on coral reef cover. Therefore, a numerical modelling method had to be chosen, along with several TCs spanning the entire GBR region over a maximum period of three months. There are many different numerical models that have been used in previous studies modelling tropical cyclones and their impacts, including Delft3D FM (Leijnse et al. 2022) and XBeach (Harter and Figlus 2017), both of which were considered for use in this study. The chosen modelling approach for this research needed to capture bed shear stress throughout the simulation, enabling the research to focus on how TCs influence bed shear stress compared to a tide-only environment and how this will impact coral reefs. The unstructured coastal-ocean model Thetis was selected for use in this study as it has been used successfully in previous studies to model tidal dynamics (Lee et al. 2022), storm surges (Warder, Horsburgh, and Piggott 2021) and the impacts of future sea level rise on tidal dynamics (Mawson, Lee, and Hill 2022).

In this chapter, I will detail the methods selected to simulate TCs over the GBR. This includes a description of the TCs chosen for the study, the configuration and validation of the numerical model Thetis, and an assessment of the model's suitability for this purpose.

2.2 | Methodology

2.2.1 | Site Description

The modelling domain covers the northern, central and southern sections of the GBR region along the Australian east coast. To evaluate model performance, eight tide gauge stations were used for validation in this chapter: Pelican Island, Cooktown, Cairns, Cardwell, Townsville, Cape Ferguson, Bowen and Breaksea Spit. These stations span a broad latitudinal range and represent a variety of coastal and shelf environments within the GBR. Their locations are shown in *Figure 8*, along with the model boundary and the regional bathymetry.

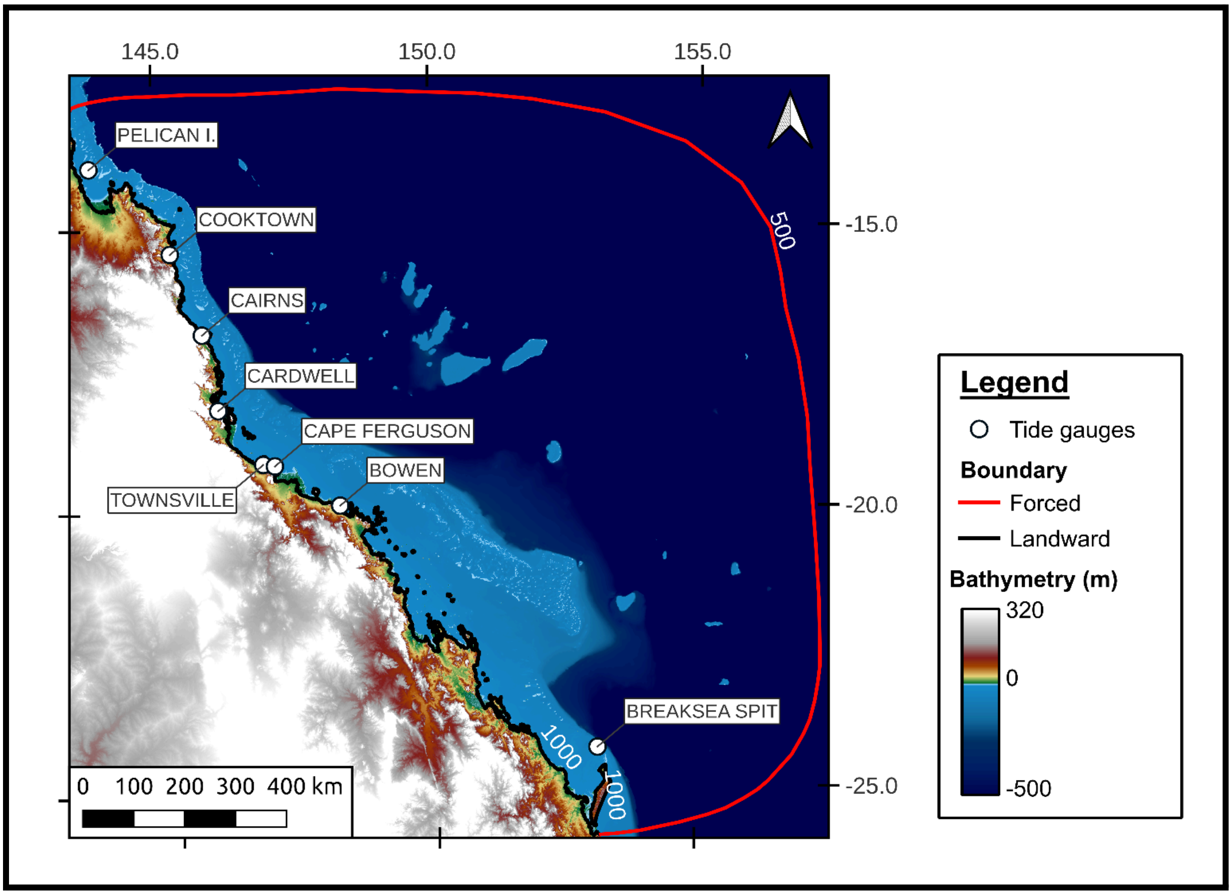

Figure 8 *Locations of the eight tide gauges depicted by the small white circles studied in this chapter for model validation. The model mesh domain is depicted by the black and red lines, with the black line representing the landward boundary and the red line indicating the forced boundary.*

2.2.2 | Tropical Cyclones

Four TCs were selected for this study using data sourced from the Australian Bureau of Meteorology (BOM 2024). The database contains historical tropical cyclone tracks spanning from 1907 to 2024. The chosen TCs, illustrated in *Figure 9*, were selected as a result of their diverse intensities ranging from category 1 to category 5 and different track locations across the GBR, covering a timeframe of no more than 3 months. *Table 2* provides an overview of the key information for each of these TCs.

In order to simulate TCs over the GBR, atmospheric data was required. Hourly data from the ERA5 reanalysis database was downloaded from the Copernicus website (Copernicus 2024). Three parameters were required for the storm model: the 10 m u-component of wind (m/s), the 10 m v-component of wind (m/s), and surface pressure (Pa). A NetCDF file containing data spanning the model domain was obtained from the website. The data within this file covers the period from 1st January 2014, to 30th April 2014. *Figures 10–13* present ERA5 reanalysis maps of the 10 m u-component of wind, 10 m v-component of wind, and surface pressure for each tropical cyclone studied in this research: Dylan, Edna, Hadi, and Ita.

Table 2 *The key information of each TC in this research, including the name, start and end dates, the maximum category (based on the Saffir-Simpson scale), the maximum wind speed and wind gust and the lowest central pressure (BOM 2024).*

Name	**Start Date**	**End Date**	**Maximum Category**	**Maximum Wind Speed (m/s)**	**Maximum Wind Gust (m/s)**	**Lowest Central Pressure (hPa)**
Dylan	24.01.2014	31.01.2014	2	30.9	43.7	974
Edna	31.01.2014	05.02.2014	2	25.7	36	985
Hadi	28.02.2014	17.03.2014	1	20.6	28.3	992
Ita	02.04.2014	15.04.2014	5	61.7	87.5	922

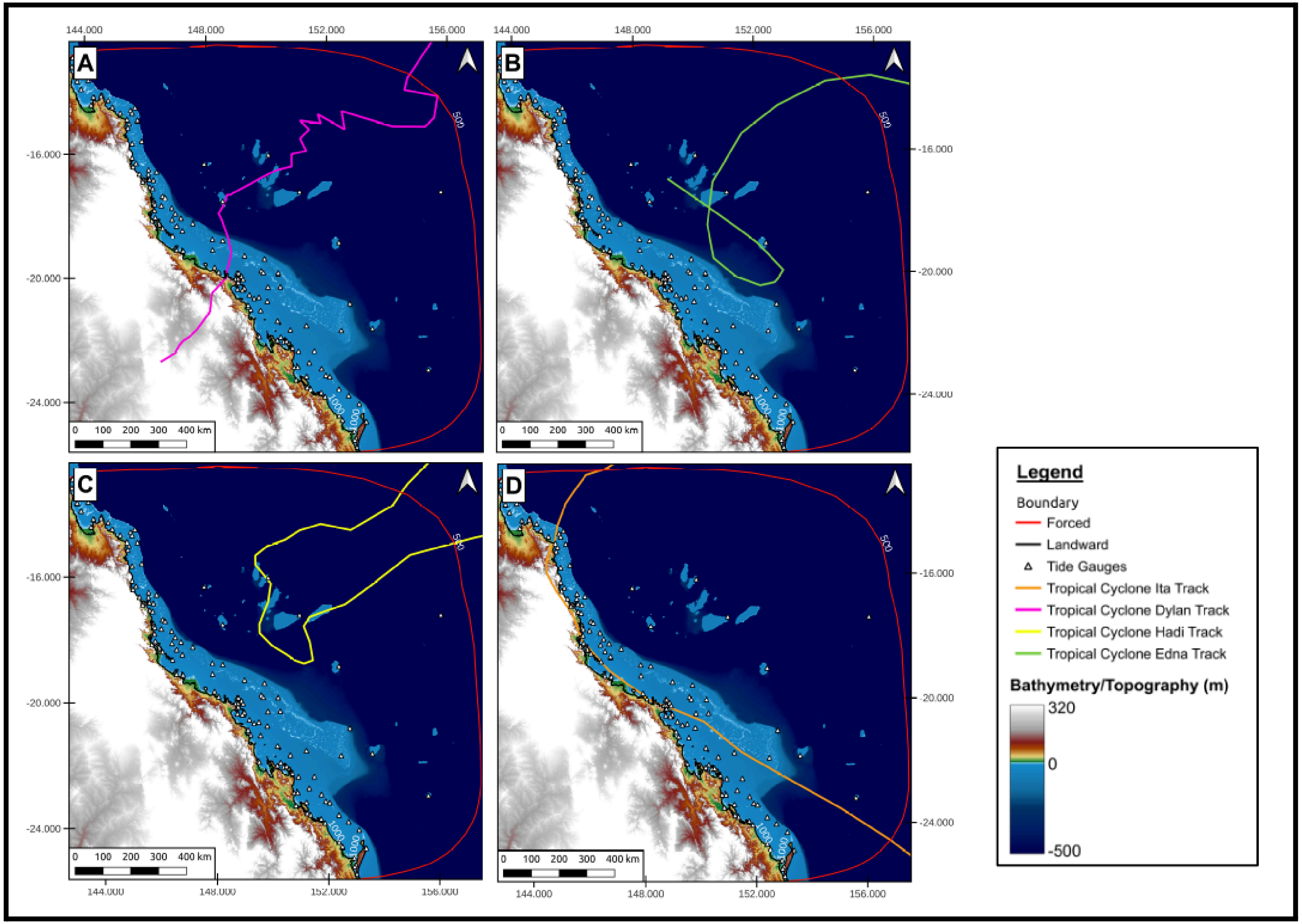

Figure 9 *Tracks of the four TCs studied in this project - **A**: TC Dylan, **B**: TC Edna, **C**: TC Hadi, and **D:** TC Ita - across the GBR. The model mesh domain is depicted by the black and red lines, with the black line representing the landward boundary and the red line indicating the forced boundary. Small white triangles denote tide gauge locations across the GBR.*

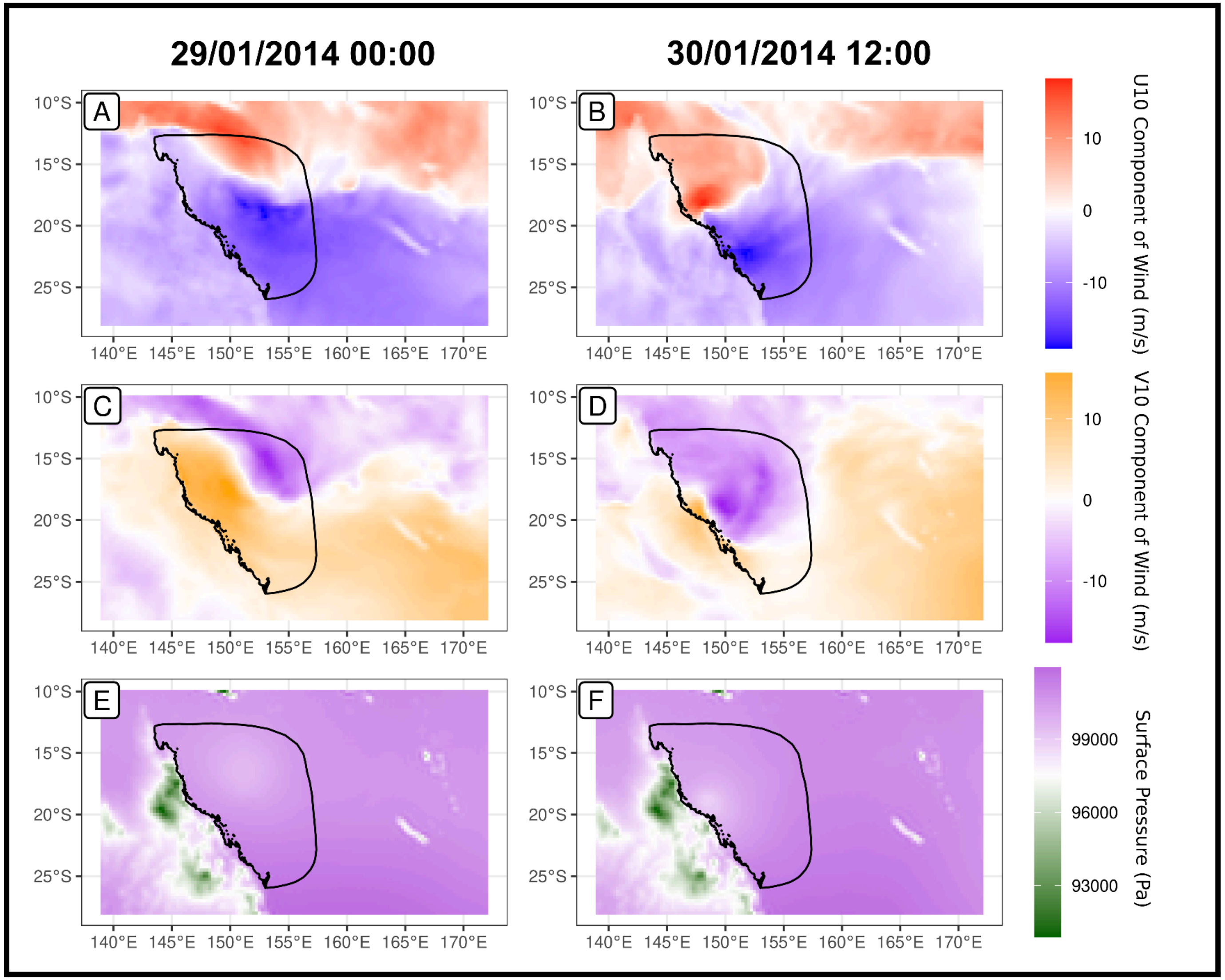

Figure 10 *Images of the ERA5 reanalysis data during TC Dylan on the 29/01/2014 at 00:00 (A, C and E) and the 30/01/2014 at 12:00 (B, D, F). A and B show the U10 Component of Wind (m/s), C and D show the V10 component of wind (m/s) and E and F show the Surface Pressure (Pa)*. *The model domain is outlined in black.*

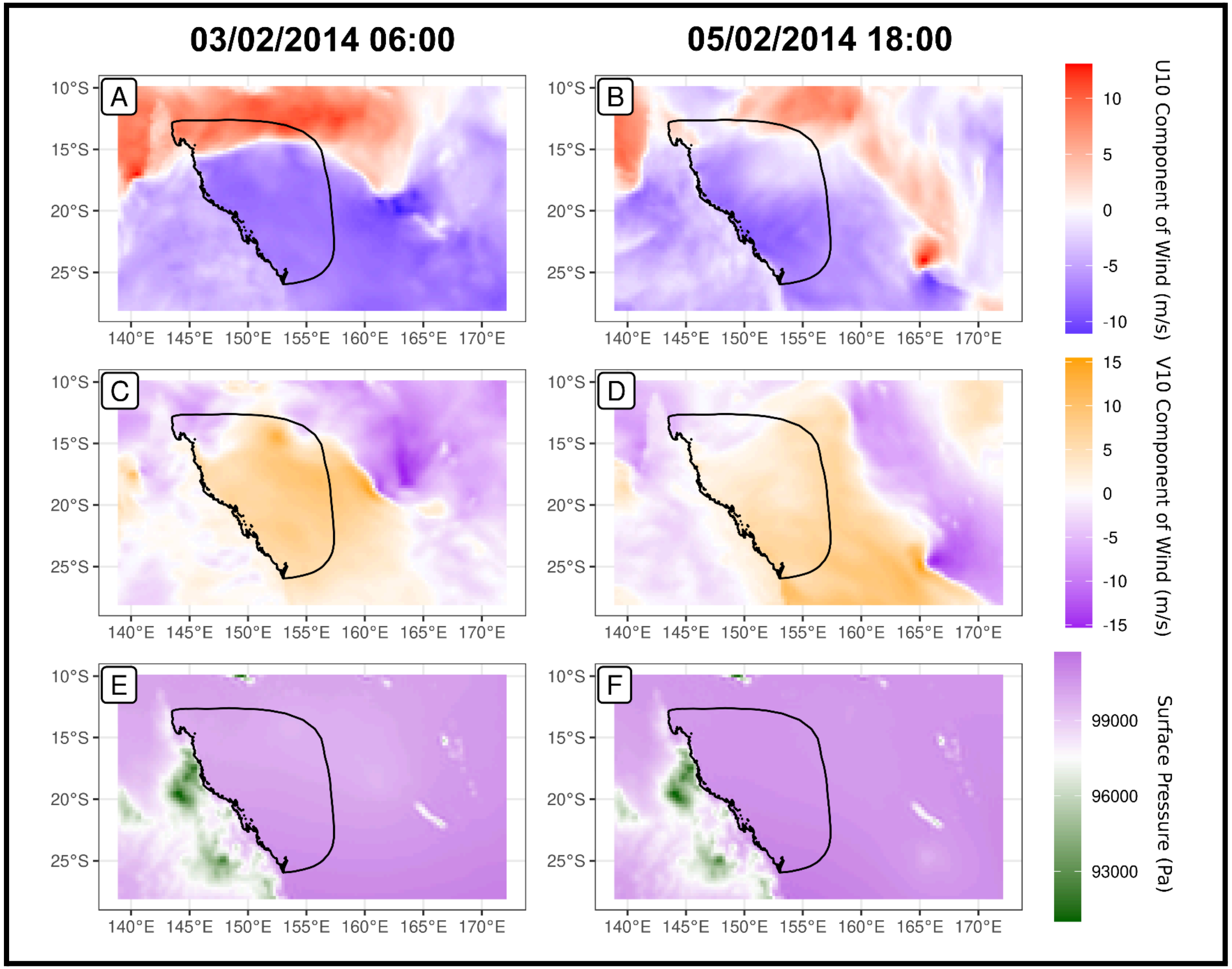

***Figure 11** Images of the ERA5 reanalysis data during TC Edna on the 03/02/2014 at 06:00 (A, C and E) and the 05/02/2014 at 18:00 (B, D, F). A and B show the U10 Component of Wind (m/s), C and D show the V10 component of wind (m/s) and E and F show the Surface Pressure (Pa). The model domain is outlined in black.*

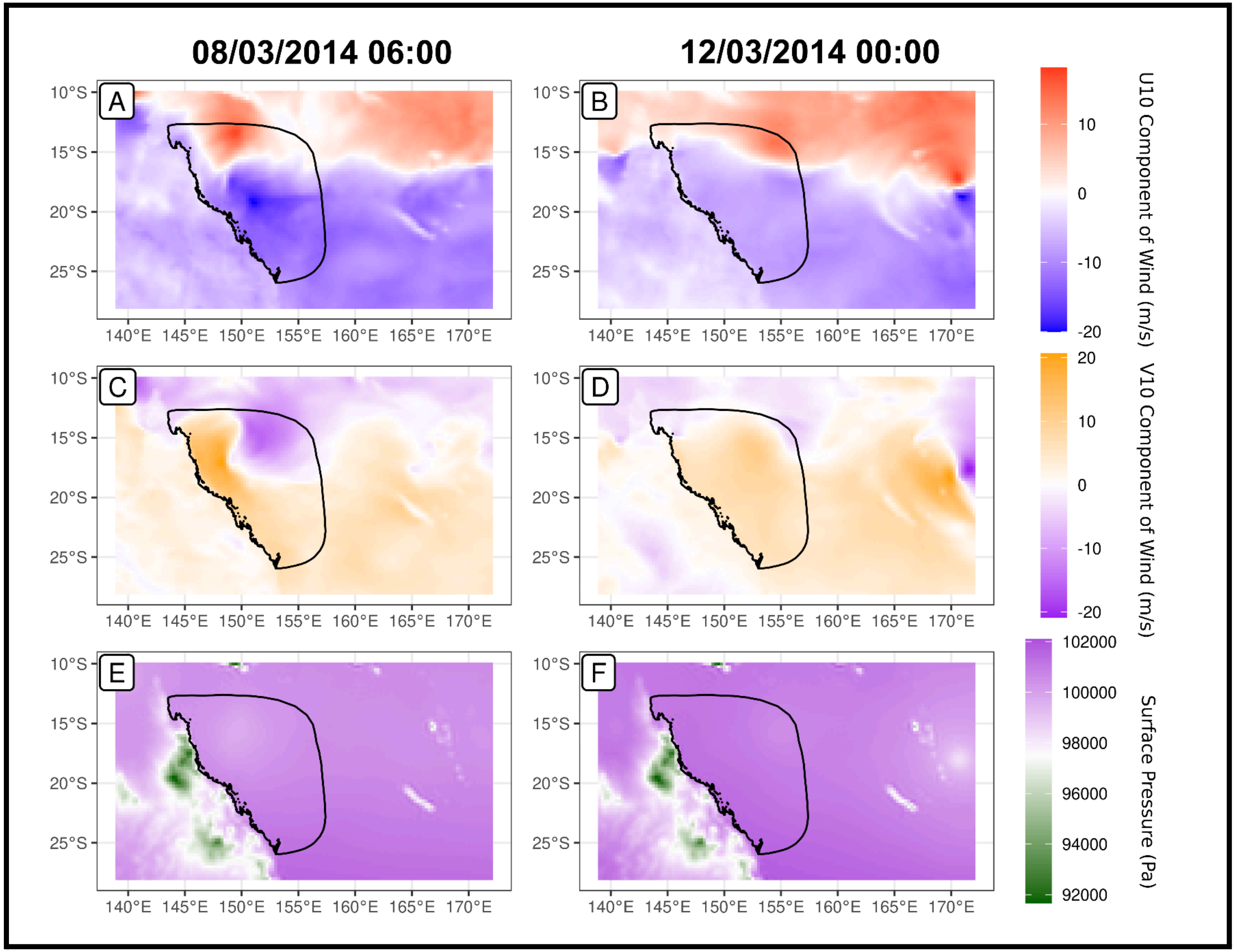

Figure 12 *Images of the ERA5 reanalysis data during TC Hadi on the 08/03/2014 at 06:00 (A, C and E) and the 12/03/2014 at 00:00 (B, D, F). A and B show the U10 Component of Wind (m/s), C and D show the V10 component of wind (m/s) and E and F show the Surface Pressure (Pa). The model domain is outlined in black.*

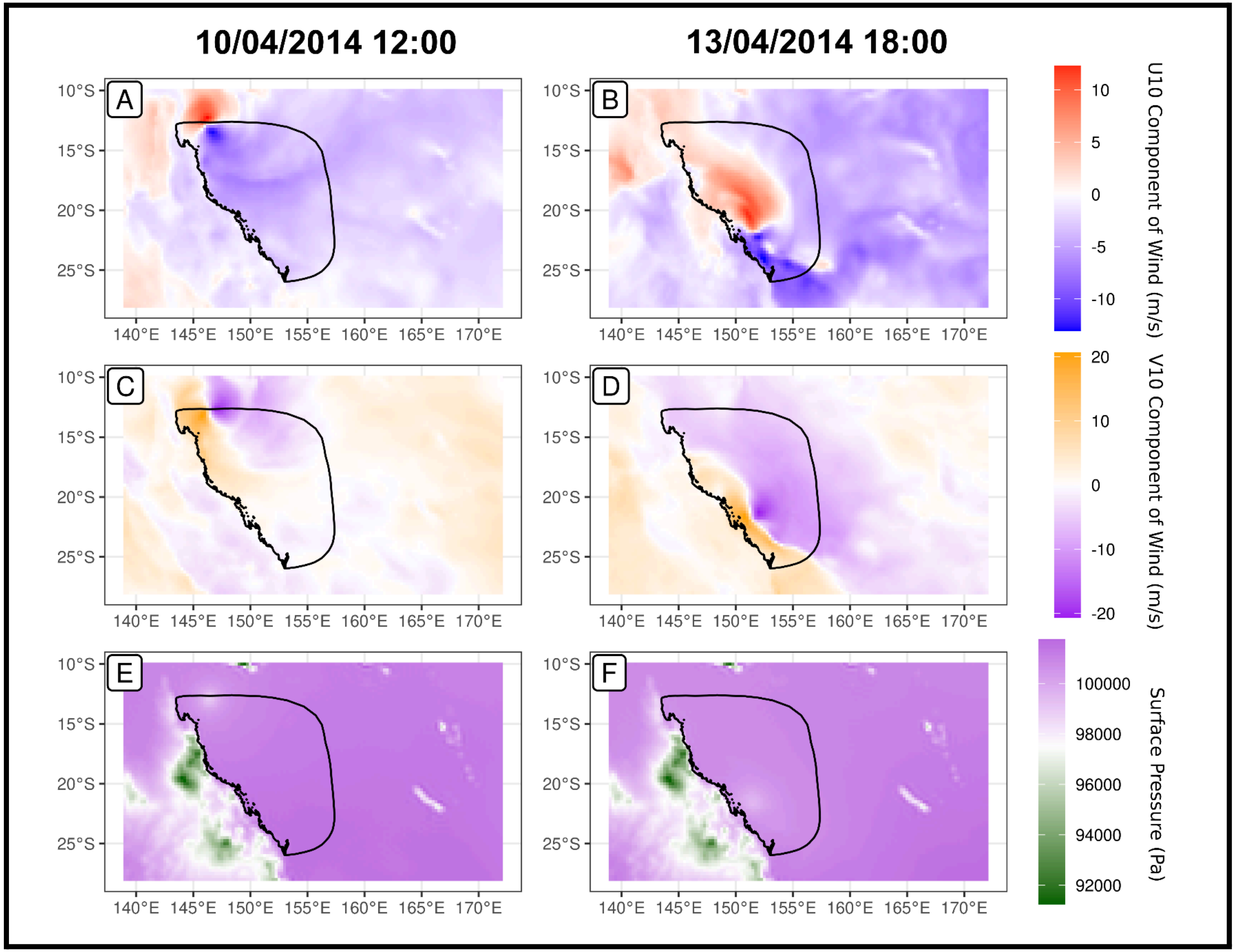

Figure 13 *Images of the ERA5 reanalysis data during TC Ita on the 10/04/2014 at 12:00 (A, C and E) and the 13/04/2014 at 18:00 (B, D, F). A and B show the U10 Component of Wind (m/s), C and D show the V10 component of wind (m/s) and E and F show the Surface Pressure (Pa). The model domain is outlined in black.*

2.2.3 | Model Framework and Set-up

Numerical models capable of simulating coastal ocean regions are instrumental in forecasting the changes in hydrodynamics as a result of tropical cyclones. Thetis (Kärnä et al. 2018), a flow solver proficient in both 2D and 3D simulations of coastal flows, was implemented within the Firedrake finite element partial differential equation solver framework (Ham et al. 2023) to simulate the effects of TCs on the GBR. This study implements Thetis to run tidal simulations with no atmospheric forcings and tidal simulations with added atmospheric parameters to simulate the TCs.

For the simulations incorporating atmospheric forcing, *Thetis* is applied in its 2D configuration (Warder et al. 2020), addressing nonlinear shallow water equations in their non-conservative form as described below:

$$\frac{\partial \eta}{\partial t} + \nabla \cdot (\tilde{H}\mathbf{u}) = 0, \tag{1}$$

$$\frac{\partial \mathbf{u}}{\partial t} + \mathbf{u} \cdot \nabla \mathbf{u} + F_c + g\nabla\eta + \nabla\frac{p_a}{\rho} = -\frac{\tau_s - \tau_b}{\rho\tilde{H}} + \nabla \cdot (\nu_h(\nabla\mathbf{u} + \nabla\mathbf{u}^T)), \tag{2}$$

where η is the free surface elevation, $H = \eta + h$ is the total water depth, h is the bathymetry (measured positive downwards), $\mathbf{u}$ is the two-dimensional depth-averaged velocity, F_C is the Coriolis force, g is the acceleration due to gravity, p_a is the atmospheric pressure at the surface, ρ is the water density, τ_s is the wind stress which acts on the free surface, τ_b is the bottom stress due to friction between the ocean and sea bed, and ν_h is the kinematic viscosity (S. Warder et al. 2020). The effects of bed shear stress (τ_b) are accounted for through the Manning's n formulation, expressed as:

$$\frac{\tau_b}{\rho} = gn^2\,\frac{|u|u}{H_d^{\frac{1}{3}}} \tag{3}$$

where n is the Manning coefficient (units s m $^{-1/3}$).

Surface stress induced by wind is characterised through the bulk formulae parameterisation (Large and Yeager 2009), where τ_s is estimated through a series of equations:

$$\tau_s = C_D\,\rho_{\mathrm{air}}|\mathbf{U_{10}}|\mathbf{U_{10}}, \tag{4}$$

$$\begin{aligned} C_D &= \frac{a_1}{\mathbf{U_N}} + a_2 + a_3\,\mathbf{U_N} + a_8\,\mathbf{U_N^6},\ \mathbf{U_N} < 33\ \mathrm{m/s} \\ &= 0.00234,\ \mathbf{U_N} \geq 33\ \mathrm{m/s} \end{aligned} \tag{5}$$

where a_1= 0.00270 m/s, a_2 = 0.000142 m/s, a_3= 0.0000764 m/s and a_8 = -3.14807x10^{-13} (m/s)$^{-6}$, $\mathbf{U_{10}}$ is the wind speed at 10 m height and $\mathbf{U_N}$ is the magnitude of $\mathbf{U_{10}}$ (Large and Yeager 2009).

2.2.4 | Generating a Mesh and Constructing the Model

In order to simulate the effects of TCs on the GBR using Thetis, a two-dimensional unstructured mesh was developed. The mesh was generated in a projection space of UTM 56S using contours extracted from digital elevation model (DEM) data to generate a coastal boundary and a forced boundary in the Pacific Ocean. The model encompasses a geographical range from 143.49 W to 157.37 E and -12.59 N to -25.96 S, with a resolution of between 1 km and 10 km.

The boundaries along the coast were delineated using contours derived from bathymetric and topographic data in QGIS (QGIS 2024). The mesh was created using *Qmesh* (Avdis et al. 2018) and *Gmsh* (Geuzaine and Remacle 2009). Two meshes were created, one had a coastal contour of 0 m, while the other incorporated a 10 m coastal contour. The coastal contour was utilised to define the inland boundary, with the 10 m contour facilitating wetting and drying processes, enabling the rise and fall of tides to inundate the land surface. 40-day simulations were conducted to determine which mesh is more accurate at simulating the GBR tides, each with an identical model configuration, with the exception of the mesh used. The results of both of these model simulations (*Figure 14*) show the 10 m coastal contour to be more accurate when simulating the tides of the GBR as the model output is closer to the expected value from tide gauge data. Therefore, a 10 m contour mesh was used for this project's simulations.

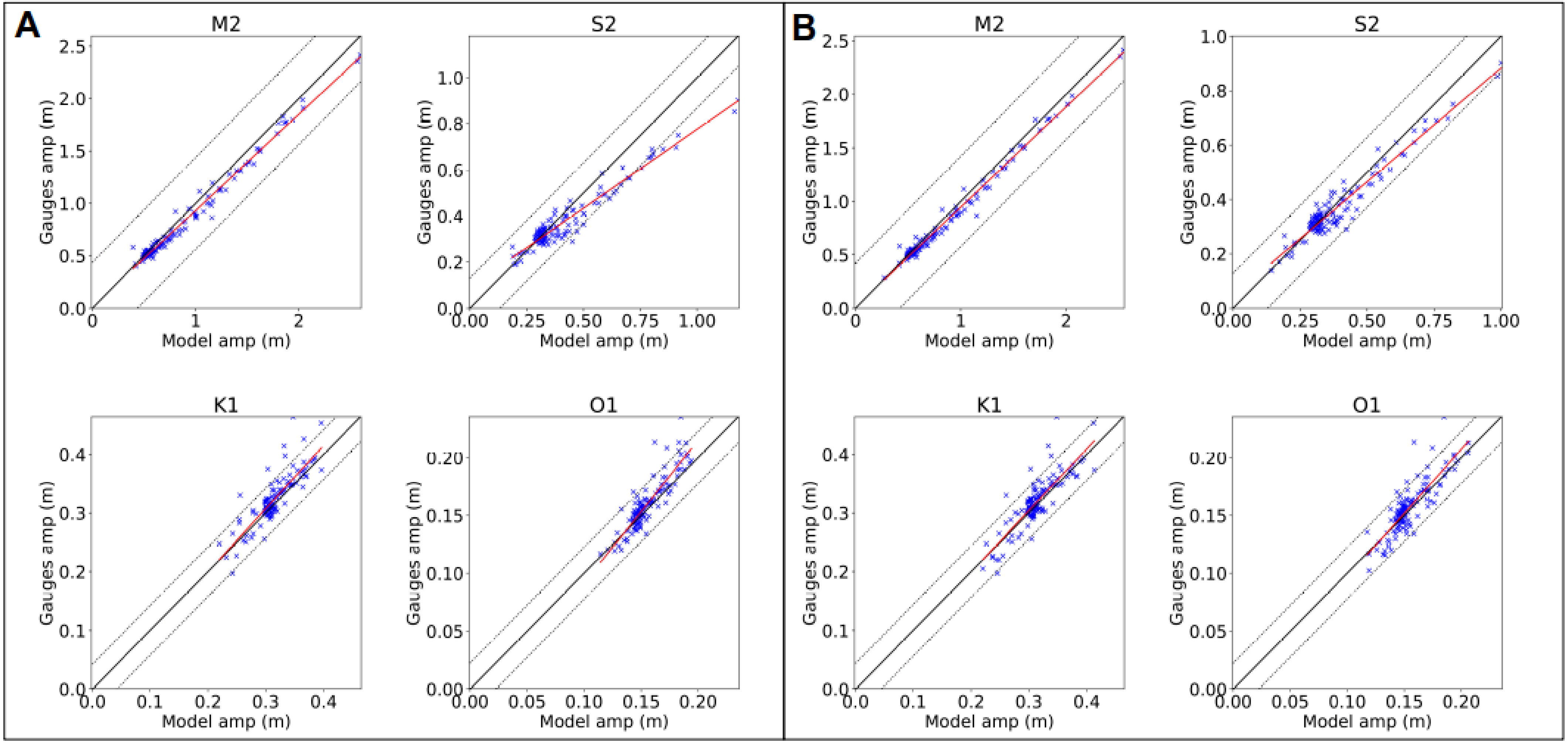

Figure 14 *Tidal model validation for 0 m coastal contour model (A) and 10 m coastal contour model (B) showing four tidal constituents (semi-diurnal M2 and S2 and diurnal K1 and O1) with the black line representing the expected tides and the blue points representing the model output values.*

The 10 m contour mesh (*Figure 15*) consisted of 190,924 nodes and 381,988 elements. This mesh was used for five tide-only simulations and four tide and wind simulations as described in Table 3. All model runs used a viscosity of 1.0 Ns/m^2 and a Manning's drag of 0.025. Element sizes varied from 1 km in the vicinity of islands and along the coastline to 10 km at the outermost boundary of the mesh.

The minimum resolution (1 km) is set on the coastline, which then increases away from the shoreline after a distance of 5 km to a resolution of 10 km after 20 km away from the boundary, this is the coastline metric, m_c. A depth-based metric, m_d, is also used, where a sigmoidal function is used to control the resolution using the following equation:

$$m_d = 10000 \frac{e^{((H-250)/115)}}{e^{((H-250)/115)}+1} \quad (6)$$

where H is the water depth. The final mesh metric is calculated using the minimum of both the coastline metric and the depth-based metric :

$$min\ (m_c, m_d) \quad (7)$$

Data for the models were provided from a range of sources. The bathymetry data consisted of a 400 m resolution DEM of the GBR region (Beaman 2010). The model incorporated the data utilising HRDS (Hill 2019), which employed bi-linear interpolation to integrate DEM data into the mesh. TPXO tidal levels (Egbert and Erofeeva 2002) were utilised to drive simulations at the open boundary. Nine tidal constituents (M_2, S_2, N_2, K_2, K_1, O_1, P_1, Q_1, M_4) were employed to drive the models, with no astronomical tidal forcing applied to the water surface. Although the models were driven by all nine constituents, approximately 182 days would be needed to separate all tidal constituents (according to the Rayleigh Criterion). Therefore, only four constituents were used during the tidal analysis (M_2, S_2, K_1, O_1) as only 14.77 days of simulation are required to separate the four constituents. Tidal forcing underwent updates at each timestep of the model (90 s).

Table 3 *The models used in this project, including the model ID, the configuration of the model (simulating tides only or tides and wind), the tropical cyclone they were simulating, total model runtime, the spin-up duration, and the start/end dates for each model.*

Model ID	Model Configuration	Tropical Cyclone	Model Run Length (days)	Spin-up (days)	Start Date	End Date
T_Val	Tides Only	*N/A*	40	5	01.01.2014	09.02.2014
T1_D	Tides Only	*Dylan*	11	2	22.01.2014	01.02.2014
T2_E	Tides Only	*Edna*	9	2	29.01.2014	06.02.2014
T3_H	Tides Only	*Hadi*	10	2	04.03.2014	13.03.2014
T4_I	Tides Only	*Ita*	7	2	08.04.2014	14.04.2014
W1_D	Tides + Wind	*Dylan*	11	2	22.01.2014	01.02.2014
W2_E	Tides + Wind	*Edna*	9	2	29.01.2014	06.02.2014
W3_H	Tides + Wind	*Hadi*	10	2	04.03.2014	13.03.2014
W4_I	Tides + Wind	*Ita*	7	2	08.04.2014	14.04.2014

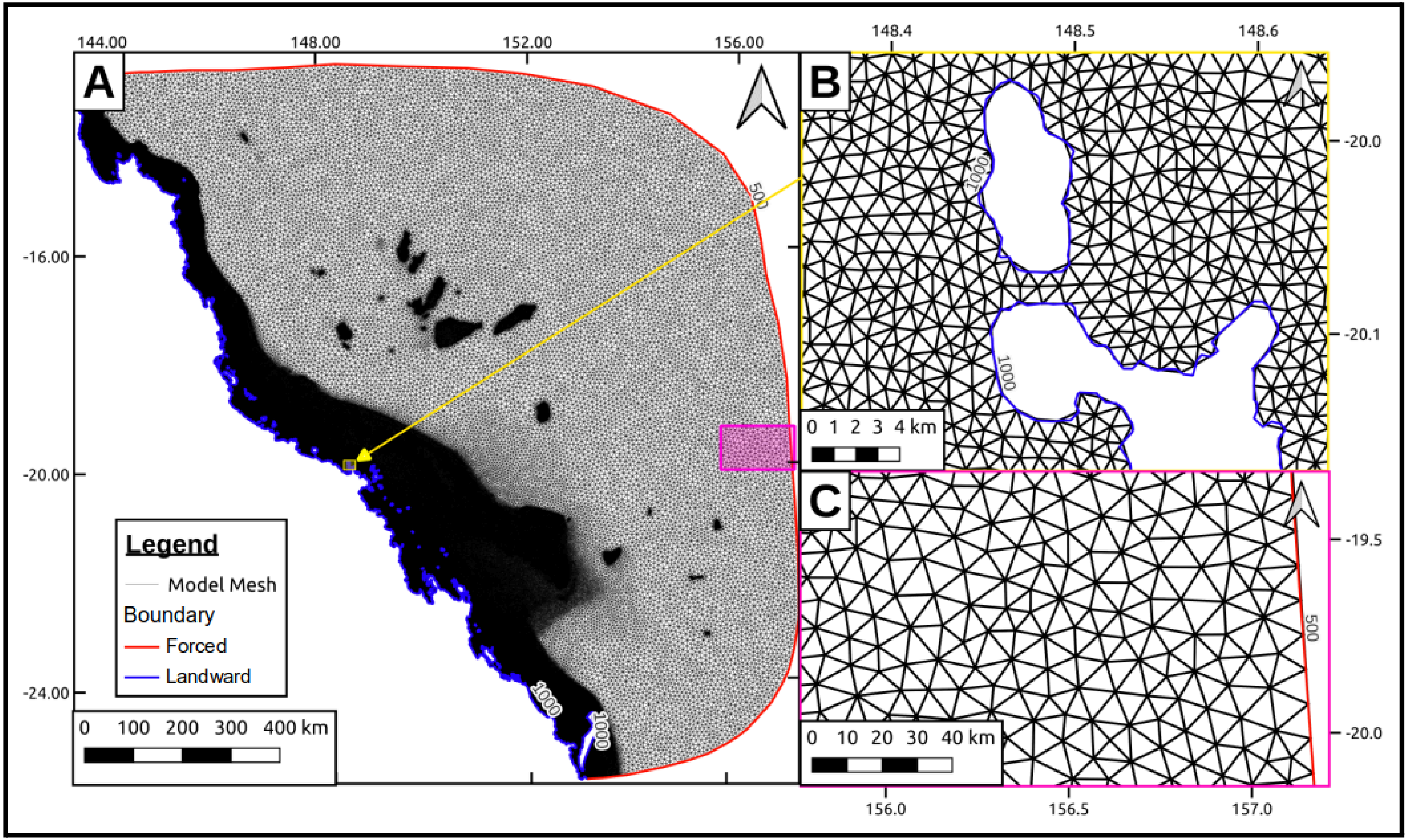

Figure 15 *The 10-m contour mesh with the contour depicted by the blue and red lines, with the blue line representing the landward contour and the red line indicating the forced boundary.* ***A****: the entire mesh domain;* ***B****: a section of the mesh showing the coastline;* ***C****: a section of the mesh showing the forced boundary within the Pacific Ocean.*

2.2.4 | Model Analysis

Following completion of the models, the difference between the modelled maximum water elevation and observed values from a BOM publication was computed using the expression in Eq.8. The results of this are shown in section 2.3.2.

$$Diff\ (\%)\ = \frac{|\,Observed - Modelled\,|}{Observed} \times\ 100 \qquad (8)$$

2.3 | Results

2.3.1 | Tide-Only Model Validation

The simulation *T_Val* was used to validate the tide-only models. In order to validate the Thetis simulation, a comparison with amplitude and phase data was carried out against data acquired from AusTides (Australian Hydrographic Office 2020). AusTides contains a list of the main 22 harmonic tidal constituents for over 80 primary and 600 secondary ports in Australia, Papua New Guinea, the Solomon Islands, Antarctica and Timor-Leste (Australian Hydrographic Office 2020). The model accuracy was calculated using 130 tidal gauges across the GBR, with four tidal constituents (M2, S2, K1 and O1) being compared to the AusTides tidal constituent data (*Table 4*).

Table 4 *Tidal constituent validation statistics for the T_Val Thetis simulation for four major tidal constituents (M2, S2, K1 and O1).*

Constituent	r-value	p-value	Standard Error (m)
M2	0.993	< *0.01*	0.009
S2	0.957	< *0.01*	0.019
K1	0.847	< *0.01*	0.067
O1	0.858	< *0.01*	0.067

The tidal constituents with the best fit predicted by Thetis were M2 and S2 (standard error of 0.9 cm and 1.9 cm, respectively). K1 and O1 were also acceptable with a standard error of 6.7 cm for both constituents. M2 and S2 are the most influential tidal constituents across the GBR, with K1 and O1 being less influential making their higher standard error values acceptable for this validation. All of the tidal constituent measurements were statistically significant with all p-values < 0.01.

A tidal gauge comparison of four selected tide gauges across the GBR are shown in *Figure 16.*

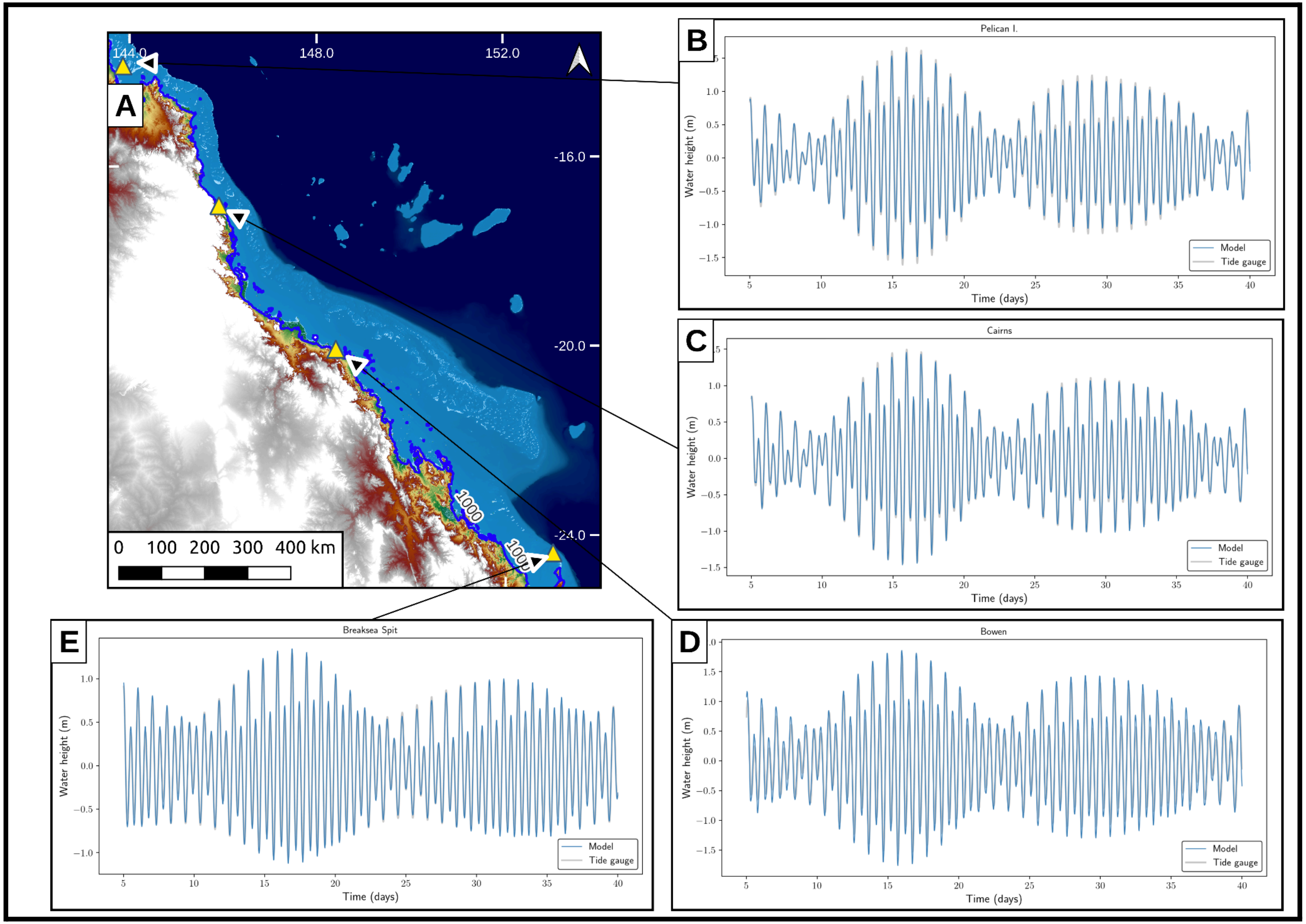

Figure 16 *T_Val model validation:* ***(A)*** *a map showing the location of four tidal gauges across different sections of the GBR coastline;* ***(B, C, D, E)*** *tidal gauge data comparison between AusTides data and modelled water elevation from Thetis at Pelican Island, Cairns, Bowen and Breaksea Split, respectively.*

2.3.2 | Tide and Wind Model Validation

The *W4_I* simulation was used to validate the tide and wind model. To validate the Thetis simulation, the modelled data was de-tided to isolate the surge component, which was then compared to data from a publication by the Australian Government's Bureau of Meteorology (Greenslade et al 2018). Observed de-tided station data during TC Ita was compared against the W4_I simulation de-tided data, with the observed tide gauge data reporting relative sea level at a set of point locations (Greenslade et al. 2018) (*Table 5*).

***Table 5** Comparison of the W4_I modelled maximum water elevation from the Thetis tide and wind model simulation and the observed maximum water elevation from the BOM publication (Greenslade et al. 2018) at six locations. The difference and percentage difference (Eq. 11) between the modelled and observed maximum water elevation has also been calculated.*

Tide Gauge Location	W4_I Modelled Maximum (m)	Observed Maximum (m)	Diff (m)	Diff (%)
Bowen	*0.18*	*0.56*	*-0.38*	*67.9*
Cairns	*0.51*	*0.57*	*-0.06*	*10.5*
Cape Ferguson	*0.31*	*0.62*	*-0.31*	*50.0*
Cardwell	*0.50*	*0.52*	*-0.02*	*3.8*
Cooktown	*0.52*	*1.09*	*-0.57*	*52.3*
Townsville	*0.35*	*0.51*	*-0.16*	*31.4*

The *W4_I* Thetis model underpredicted the surge maximum at all locations when compared to the observed data. The percentage error varied considerably across the six locations, with low percentage errors observed at Cardwell (3.8%) and Cairns (10.5%) and high percentage errors occurring at Bowen (67.9%), Cooktown (52.3%) and Cape Ferguson (50.0%).

Alongside a comparison with the observed tide gauge data, the *W4_I* simulation was also compared to surge-only data modelled using the Regional Ocean Modelling System (ROMS) (Greenslade et al. 2018) (*Table 6*). This model grids and uses parametric TC vortices derived from the BOM's official forecast track, which are used to force the hydrodynamic model ROMS (Greenslade et al. 2018). Wave set-up is derived from AUSWAVE-R and astronomical tides are linearly combined with the ROMS storm surge to provide forecasts of coastal sea level at a spatial resolution of approximately 2.5 km (Greenslade et al. 2018).

Table 6 *Comparison of the W4_I modelled maximum water elevation from the Thetis tide and wind model simulation and the ROMS modelled maximum water elevation from the BOM publication (Greenslade et al. 2018) at six locations. The difference and percentage difference (Eq. 11) between the modelled and observed maximum water elevation has also been calculated.*

Tide Gauge Location	W4_I Modelled Maximum (m)	ROMS Modelled Maximum (m)	Diff (m)	Diff (%)
Bowen	*0.18*	*0.34*	*-0.16*	*47.1*
Cairns	*0.51*	*0.50*	*0.01*	*2.0*
Cape Ferguson	*0.31*	*0.57*	*-0.26*	*45.6*
Cardwell	*0.50*	*0.61*	*-0.11*	*18.0*
Cooktown	*0.52*	*1.56*	*-1.04*	*66.7*
Townsville	*0.35*	*0.42*	*-0.07*	*16.7*

The *W4_I* Thetis model also underpredicted surge maximums at most locations when compared to the ROMS modelled data, with the exception of Cairns where Thetis predicted a 0.01 m higher maximum. Similarly to *Table 5,* the percentage error varied considerably across the six locations, with low percentage errors observed at Cairns (2.0%) and high percentage errors occurring at Cooktown (66.7%), Cairns (47.1%) and Cape Ferguson (45.6%).

The data in both *Table 5* and *Table 6* are illustrated in *Figure 17*.

As shown in *Figure 17*, a storm surge is evident at each location in the observed data, Thetis *W4_I* model data, and ROMS model data. However, each dataset displays differences in both the magnitude (*Table 5* and *Table 6*) and timing of the surge (*Table 7*).

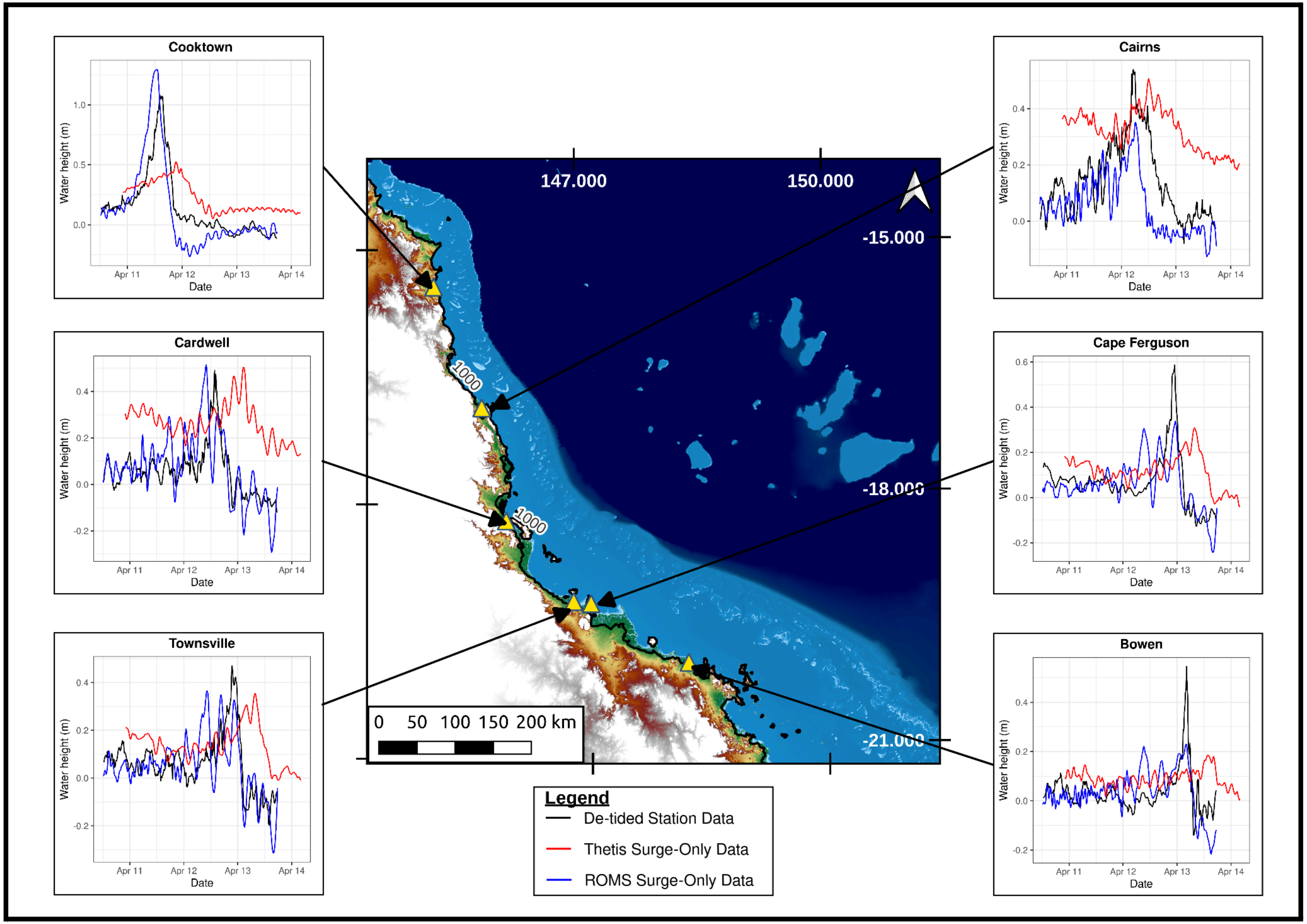

Figure 17 *A comparison of the water elevation modelled by Thetis for the W4_I simulation (red), the water elevation modelled by ROMS (blue) (Greenslade et al. 2018) and the observed de-tided tide gauge data (black) (Greenslade et al. 2018) between the 10th April 2014 and the 14th April 2014 at six locations across the GBR.*

Table 7 *Comparison of W4_I modelled peak water elevation times from the Thetis tide and wind model simulation, observed peak times, and ROMS modelled peak times (Greenslade et al. 2018) at six locations. Differences between Thetis modelled and observed peak times, Thetis modelled and ROMS modelled peak times and ROMS modelled and observed peak times, have also been calculated.*

Tide Gauge Location	W4_I Modelled Peak Time	Observed Peak Time	ROMS Modelled Peak Time	Thetis vs Obs Difference (mins)	Thetis vs ROMS Difference (mins)	ROMS vs Obs Difference (mins)
Bowen	*13 April 13:45*	*13 April 04:15*	*13 April 04:10*	*+ 570*	*+ 575*	*+ 5*
Cairns	*12 April 12:00*	*12 April 05:15*	*12 April 06:00*	*+ 405*	*+ 360*	*+ 45*
Cape Ferguson	*13 April 07:45*	*12 April 22:55*	*12 April 23:20*	*+ 530*	*+ 505*	*+ 25*
Cardwell	*13 April 02:30*	*12 April 14:05*	*12 April 09:50*	*+ 745*	*+ 990*	*- 255*
Cooktown	*11 April 21:15*	*11 April 15:25*	*12 April 13:00*	*+ 350*	*- 495*	*+ 1295*
Townsville	*13 April 07:45*	*12 April 21:25*	*12 April 22:20*	*+ 560*	*+ 505*	*+ 55*

The data indicates that Thetis consistently models peak times later than the observed values across all locations. Specifically, the differences range from +350 minutes at Cooktown to +990 minutes at Cardwell. Additionally, Thetis models peak times later than those predicted by the ROMS model for most locations, with the exception of Cooktown, where Thetis's predicted peak time is closer to the observed value. This demonstrates that while Thetis generally lags behind both the observed and ROMS values, Cooktown stands out as an anomaly where Thetis predictions align more closely with observations.

2.4 | Discussion

2.4.1 | Observed Tide Gauge Data

The observational data used to assess the Thetis modelled results has several limitations that could impact its accuracy. Tide gauges are placed at a limited number of locations, usually in sheltered harbours and structures such as jetties (Greenslade et al. 2018). Therefore, they are not ideally situated to capture the full range of storm surge events, as these events can be significantly influenced by wind, waves and coastal geography, which may not be fully represented at these sheltered sites (Greenslade et al. 2018). The measured sea level data also contains variability attributable to different phenomena across a broad range of temporal and spatial scales, including astronomical tides, storm surges, tsunamis, infra-gravity waves, seiching and seasonal variability which can have an effect on the measurements made (Greenslade et al. 2018). Despite this, although these locations are not ideal for sampling the extremes of storm surges, they currently provide the most fit-for-purpose objective data set available for this kind of study (Greenslade et al. 2018).

2.4.2 | Thetis vs ROMS

While comparing the modelled Thetis data to the modelled ROMS data can provide insights into the accuracy of the model used in this project, the differences in the model set-ups for both methods can also lead to variations in results and should be carefully considered (*Table 8*).

Table 8 *Comparison of the model set-ups for both Thetis and ROMS (Greenslade et al. 2018).*

Model Set-Up	Thetis	ROMS
Grid	*Unstructured*	*Structured*
Numerical method	*Finite Element Method*	*Finite Difference Method*
Drag parameterisation	*Spatially uniform Manning's Drag derived from the Quadratic Bottom Equation*	*Spatially uniform quadratic bottom drag*
Drag parameterisation	*Manning's drag of 2.5 x 10^{-2}*	*Drag coefficient of 1 x 10^{-3}*
Time Stepping	*90 seconds*	*6 seconds*
Wetting and Drying Settings	*On*	*On with critical depth of 0.1 m*
Domain boundary Conditions	*The external domain boundary conditions use symmetric velocity conditions*	*The normal component of the depth-average velocity is subject to the Flather boundary condition (Flather, 1976)*
Spatial Resolution	*1 km to 10 km Starting at 1 km near the coastline and increasing towards the outer boundary*	*1.9 km to 4 km with a mean resolution of 2.5 km*

There are some key differences between both Thetis and ROMS which may have an impact on the results produced from each model. Thetis uses an unstructured grid for the mesh generation, whereas ROMS uses a structured grid. The potential advantages of using an unstructured mesh are significant, for example, there are issues relating to boundary conditions when bathymetry and coastlines are represented by a 'staircase' regular structured mesh (Pain et al. 2005). The result of this can be an unintentional application of no-slip boundary conditions, and consequently problems with the transport of fluids along slopes (Pain et al. 2005). This process needs to be adjusted for staircase 'structured' grids, for example, by increasing diffusion in the cells near the ocean floor (Pain et al., 2005). Aligning the mesh with the bathymetry, such as for unstructured grids, helps avoid many of these issues (Adcroft and Marshall 1998) and enables fluid to move smoothly over the ocean floor (Pain et al. 2005).

The type of atmospheric forcing data used is also different for Thetis and ROMS. Thetis uses ERA5 data, a fifth generation ECMWF (European Centre for Medium-Range Weather Forecasts) reanalysis for the global climate and weather for the last eight decades (Copernicus 2024). ROMS focuses on storm surge hindcasts using ‘Best Track’ forcing (Greenslade et al. 2018). The ‘Best Track’ for any TC is a time series of TC parameters, produced by forecasters, or other analysts, after the end of the TC season, and taking into account all available observations (Greenslade et al. 2018). The wind stress and pressure forcing fields were generated from the ‘Best Track’ data using a series of equations, presented in its operational configuration as a 0.5^{o} resolution grid and interpolated into the hydrodynamic model grid using a cubic interpolation method (Greenslade et al. 2018). Variations in the atmospheric forcing data used may contribute to the differences in the modelled peak water elevation and modelled peak times for Thetis and ROMS described in *Section 2.3.2.*

2.4.3 | Thetis Tide and Wind Model Limitations

The results of the tide and wind Thetis model validation underpredicted the storm surge maximum height when compared to both the observed tide gauge data and the ROMS modelled data. Thetis also modelled the peak time later than both the observed and ROMS modelled data. Despite this, Thetis successfully modelled a storm surge; however, a few considerations are needed for future work using Thetis to model TCs.

Thetis successfully modelled the tides of the GBR region during the 40-day T_Val simulation with near-perfect tide gauges (*Figure 16*) and statistically significant and relatively low standard error measurements (*Table 4*). The tide and wind model set-up is identical to the tide-only model set-up, with the addition of an atmospheric forcing parameter and atmospheric forcing data (ERA5 reanalysis data).

ERA5 reanalysis data combines model data with observations from across the world into a globally complete and consistent dataset using the laws of physics (Copernicus 2024). This principle, called data assimilation, is based on the method used by numerical weather prediction centres, where every 12 hours (at ECMWF) a previous forecast is combined with newly available observations in an optimal way to produce a new best estimate of the state of the atmosphere (Copernicus 2024). Reanalysis works in the same way, but at reduced resolution to allow for the provision of a dataset spanning back several decades (Copernicus 2024). Despite the dataset being fairly robust, the results of the Thetis simulation when compared to the observed tide gauge data suggest that the ERA5 data did not represent the atmospheric conditions effectively for the simulations. A study by (Warder et al. 2020) successfully applied the Thetis tide and wind model to simulate a North Sea storm surge event that occurred between the 5th and 6th December 2013. The Thetis model set-up for the North Sea storm surge simulation was identical to the one used in this study, with a few key differences: (Warder et al. 2020) incorporated the Charnock parameterisation for surface wind stress and utilised Hindcast meteorological data provided by the National Oceanography Centre. The results of the Thetis North Sea model surge residuals were compared with those observed at tide gauges, as well as with equivalent model outputs from the CS3X hindcast (Warder et al. 2020) (*Figure 18*).

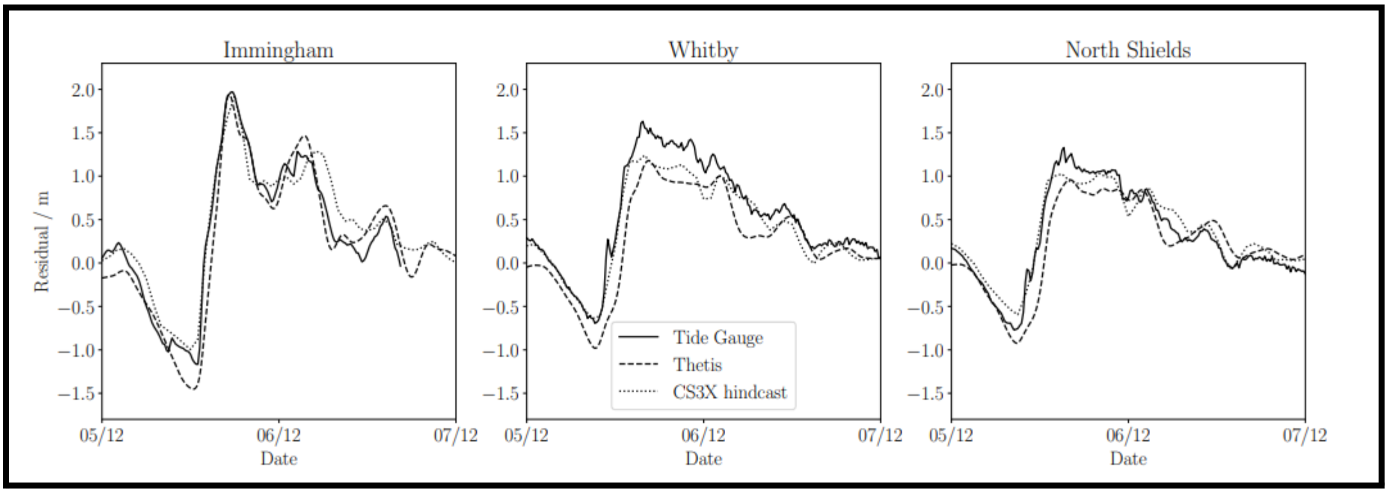

Figure 18 *Comparison of surge residual between Thetis model results, CS3X hindcast results, and British Oceanographic Data Centre tide gauges, for 5th-7th December 2013 (Warder et al. 2020).*

The Thetis surge residual results are comparable with those from CS3X and both capture the surge residual with reasonable accuracy for all three selected tide gauges (Warder et al. 2020). For all three gauges, the main features of the observed surge residual time series are captured well, although in most cases the models underestimate the peak surge residual as found in the *W4_I* simulation in this study (Warder et al. 2020). Therefore, it is reasonable to suggest that the ERA5 reanalysis data is not suitable for use in Thetis when modelling a TC storm surge and for future research it would be suggested to use other hindcast data similar to that used in (Warder et al. 2020) or follow methodologies using Best Track found in the (Greenslade et al. 2018) publication.

Additional variations of the *W4_I* model were tested, each with varying Manning's drag, viscosity and forcing (*Table 9*) (Hill 2024). *Figure 19* reveals minimal differences between the models, indicating that these parameters have little impact on model performance. This suggests that the current model configuration is optimised to a high standard, suggesting that these parameters are not likely responsible for the differences between Thetis and the observed tide gauge data. However, utilising the Charnock parameterisation for surface wind stress instead of the bulk formulae parameterisation may yield more accurate results in future studies (as demonstrated in (Warder et al. 2020)).

Table 9 *Values of the Manning's drag and viscosity used for the test simulations as well as the forcing used for each model (L&Y - Large and Yeager, 2009; Pond - Large and Pond, 1981; Smith - Smith and Banke, 1975). (Hill 2024)*

Model	Manning's Drag	Viscosity	Forcing
1	0.025	*1*	L&Y
2	0.03	*1*	L&Y
5	0.025	*1*	Pond
6	0.025	*1*	Smith
8	0.025	*0.1*	L&Y

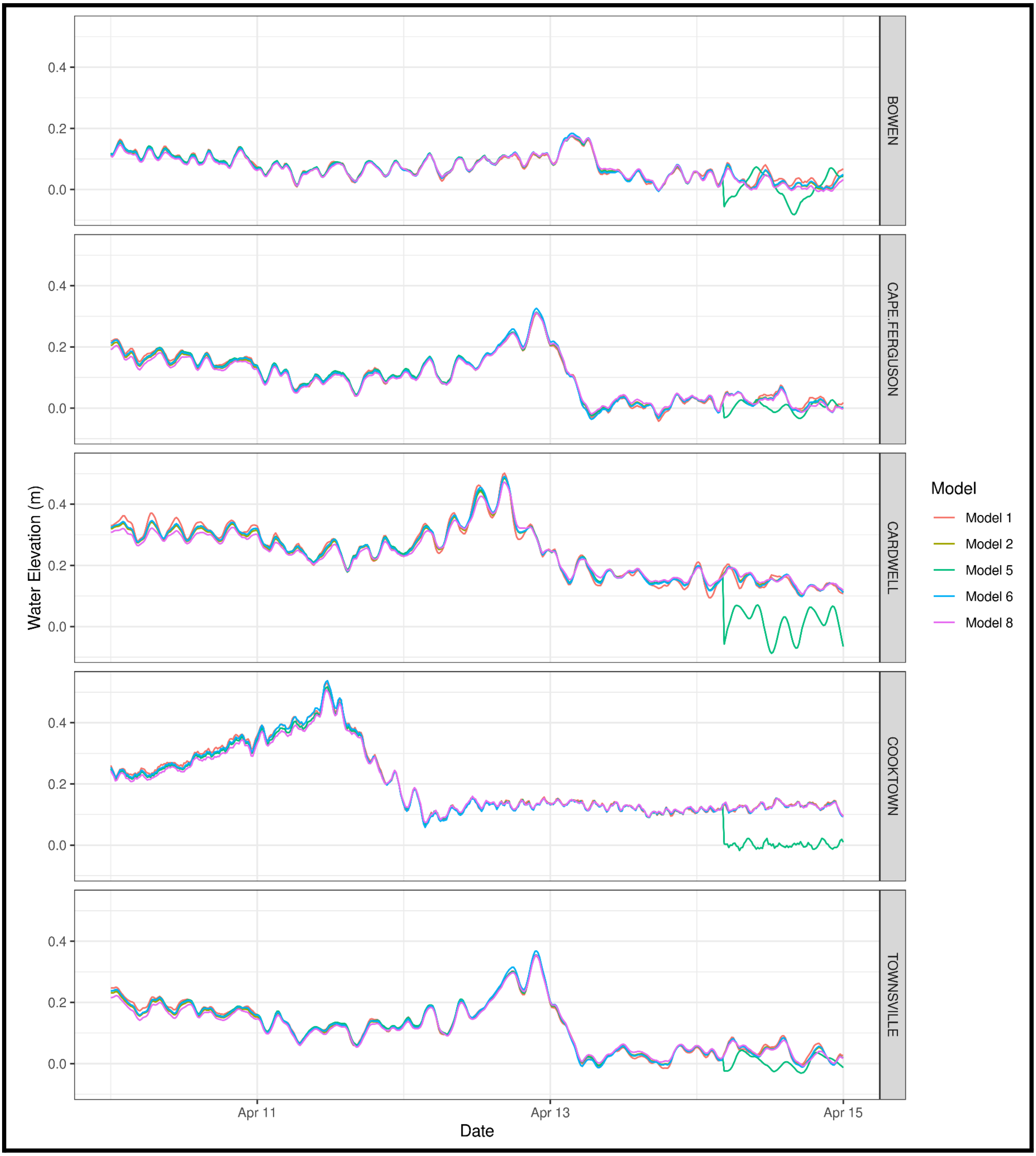

Figure 19 *Results of the test simulations described in Table 9. Note: Model 5 (green) storm surge model stopped after 14th April 2014 and only shows a tidal signal towards the end of the model. (Hill 2024).*

2.5 | Conclusions

In conclusion, this analysis highlights several critical considerations regarding the use of observational data and model configurations when modelling storm surge events. The comparative evaluation of the Thetis and ROMS models reveals significant differences in their configurations, including grid structures, atmospheric forcing data, and parameterizations. These discrepancies can lead to variations in model outputs and underscore the importance of carefully considering model design when interpreting results. Despite these challenges, Thetis demonstrated a strong capability for modelling tidal dynamics in the GBR region, achieving near-perfect agreement with tide gauge measurements during the *T_Val* simulation.

However, the validation results indicate that Thetis underpredicted storm surge maximum heights and peak times compared to both the observed data and ROMS model output. This suggests that future studies should explore alternative atmospheric forcing, such as the use of the Charnock parameterization for surface wind stress (Warder et al. 2020) and different hindcast meteorological data (Greenslade et al. 2018; Warder et al. 2020), to improve model accuracy further. The findings also indicate that variations in parameters like Manning's drag and viscosity had minimal impact on model performance, suggesting that the current configuration is optimised to a high standard.

Overall, while Thetis has demonstrated an adequate ability to model storm surge events, continued refinement of the model setup and selection of appropriate atmospheric data are crucial for enhancing its reliability in future simulations. However, the performance is sufficient to use in prediction of storm impacts with sea-level rise, but care must be taken in the interpretation of output.

Chapter 3 | Impacts of Tropical Cyclones on Coral Reefs

3.1 | Introduction

TCs are one of the major acute stressors on coral reefs and have structured coral reef assemblages over ecological to geological time frames (Castro-Sanguino et al. 2022). TCs are a significant contributor to coral decline on the GBR and coral recovery from these events is threatened by widespread coral loss as a result of consecutive mass bleaching events (Castro-Sanguino et al. 2022). The use of numerical models helps understand how TCs interact with and threaten coral reef environments and is therefore important for identifying priority areas for conservation and management efforts (M. Puotinen et al. 2020).

In this chapter, I will outline the methods used to assess the impact of TCs on a selected group of 15 coral reefs across the GBR. This includes a detailed description of the data utilised, the statistical tests applied, the resulting findings, the broader implications of these results and suggestions for future research.

3.2 | Methodology

3.2.1 | Coral Reef Data

This study uses all coral reefs within the model domain that have data available for before and after the TCs occur (Chapter 2). The data is from the Marine Monitoring Program (MMP) acquired from the Australian Institute of Marine Science (AIMS) website (AIMS 2024b). The objective of the MMP is to document the trends in the benthic reef communities on selected nearshore reefs (AIMS 2024b). These changes may be as a result of acute disturbances such as cyclonic winds, bleaching and crowns-of-thorns starfish, as well as those related to land runoff (e.g. floods), which disrupt processes of recovery such as recruitment and growth (AIMS 2024b). Coral community attributes are monitored at both 2 m and 5 m depths below the lowest astronomical tide at each of two sites on each reef (AIMS 2024b). Within site and depth combinations are five 20 m transects marked with steel pickets at the beginning and steel rod at the middle and each end (markers are maintained through time and compass directions are maintained for the entire site) (AIMS 2024b). Benthic cover is estimated from digital photos taken at 50 cm intervals along the upslope side of the marked transects (AIMS 2024b).

The MMP data was collected for 2013 and 2014 from the AIMS website. The dataset includes the reef name, the site number, latitude, longitude, reef depth, the sample date, the benthic group and the percentage of cover for each reef. The benthic groups are categorised as followed: Algae (combination of all algal forms including filamentous turf algae, fleshy macroalgae, and calcareous algae, Hard Coral (Order Scleractinia), Soft Coral (Order Alcyonacea and Helioporacea), Other - includes other benthic categories (e.g. sponge, tunicates, anthozoans, etc), and abiotics (e.g. rock, rubble, sand, silt, etc) (AIMS 2014). The absolute change (*Eq. 9*) and relative change (*Eq. 10*) were calculated for the change in coral cover between 2013 and 2014 for each benthic group. *Figure 20* shows the location of coral reefs used in this study within the extent of the model domain.

$$Absolute\ change\ = Cover\ in\ 2014\ -\ Cover\ in\ 2013 \tag{9}$$

$$Relative\ Change\ (\%)\ =\ \frac{Cover\ in\ 2014 - Cover\ in\ 2013}{Cover\ in\ 2013} \times\ 100 \tag{10}$$

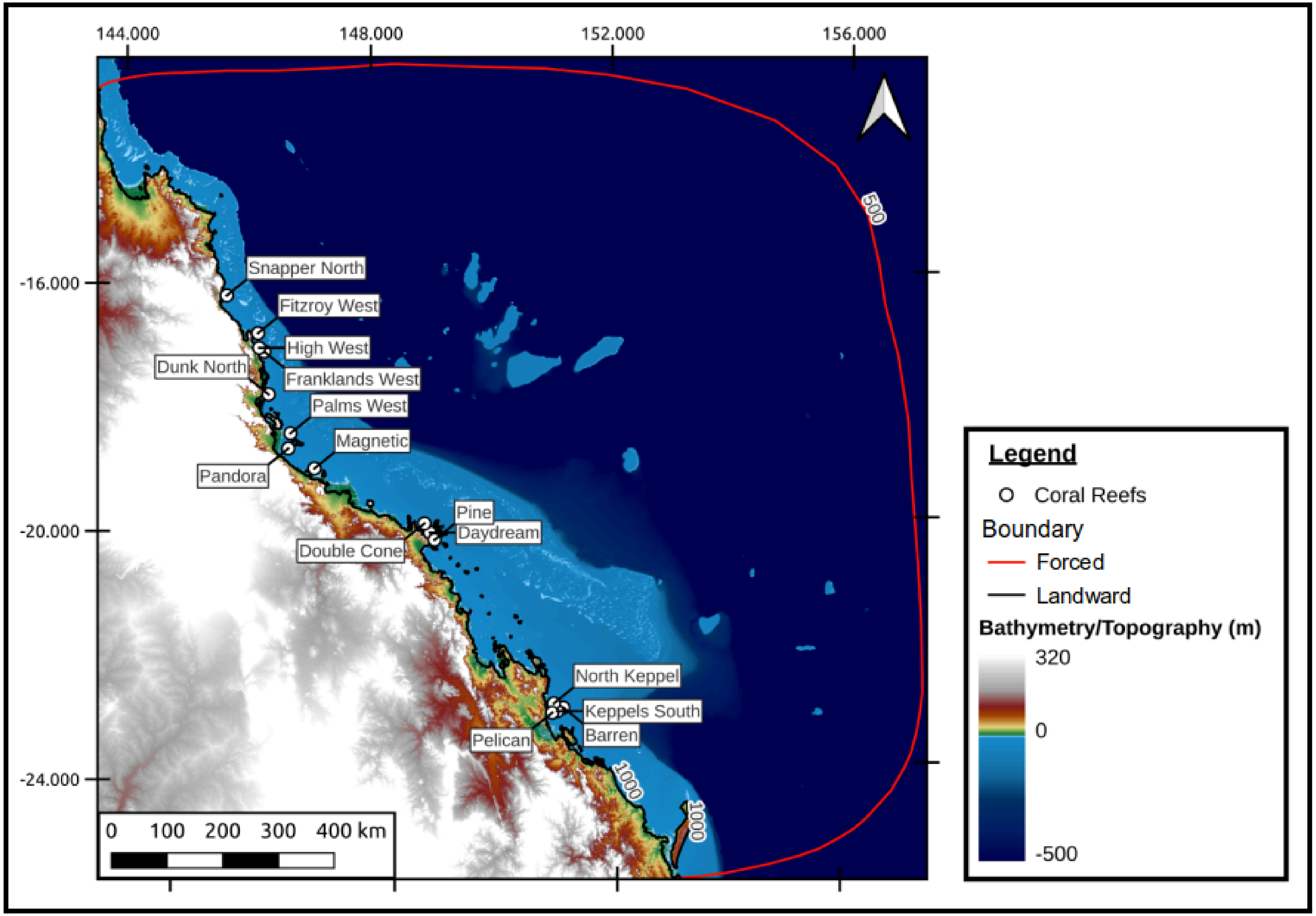

Figure 20 *The white points indicate the coral reefs within the model boundary that are used within this research. The model mesh domain is delineated by the black and red lines, signifying the landward boundary and forced boundary, respectively.*

3.2.2 | Numerical Model Data

The eight numerical models were post-processed to extract data on elevation, velocity, and bed shear stress. For each model, this data was extracted at each coral reef throughout the simulation period. Graphs were then created to display the water elevation, water velocity, and bed shear stress at each reef during each TC, comparing both tide-only models and combined tide and wind models.

From the tide and wind models (*W1_D, W2_E, W3_H, and W4_I*), the maximum bed shear stress and its occurrence time were also extracted. Using this occurrence time, bed shear stress was then extracted from the corresponding tide-only models (*T1_D, T2_E, T3_H, and T4_I*). The change in magnitude between the tide-only models and the combined tide-and-wind models was then calculated. Both the maximum bed shear stress and the change in bed shear stress magnitude were then used in the statistical analysis.

3.2.3 | Statistical Testing

A Shapiro-Wilk normality test was performed to assess whether the absolute change and relative change in total benthic cover for the four benthic categories of the MMP coral cover data followed a normal distribution. This test was necessary to determine the appropriate statistical methods for further analysis. Subsequently, Kendall's Tau test was conducted to determine the strength and direction of the association between the absolute and relative changes in coral cover for each benthic group and two variables: the maximum bed shear stress and the change in bed shear stress magnitude between the tide-only models and the tide-plus-wind models modelled at each reef during each simulation.

3.3 | Results

3.3.1 | Results of Simulations

Figures 22–25 present graphs illustrating the modelled bed shear stress, water elevation, and water velocity for both the tide-only and tide-plus-wind scenarios of the four tropical cyclones at a selected reef (*Figure 21*).

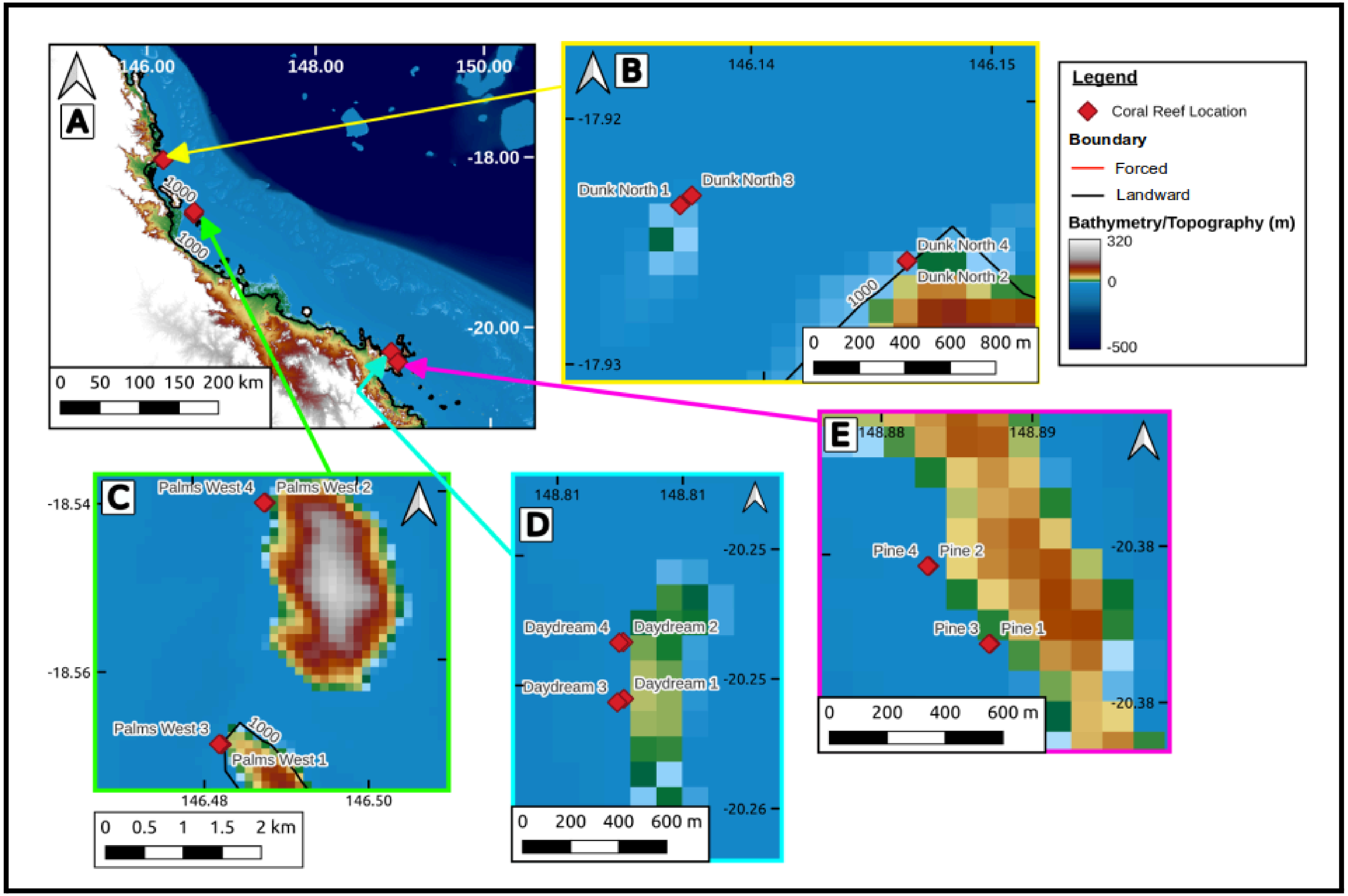

Figure 21 *Locations of the coral reefs Dunk North (B), Pine (E), Daydream (D) and Palms West (C) along the GBR for the graphs shown in Figures 16, 17, 18 and 19, respectively.*

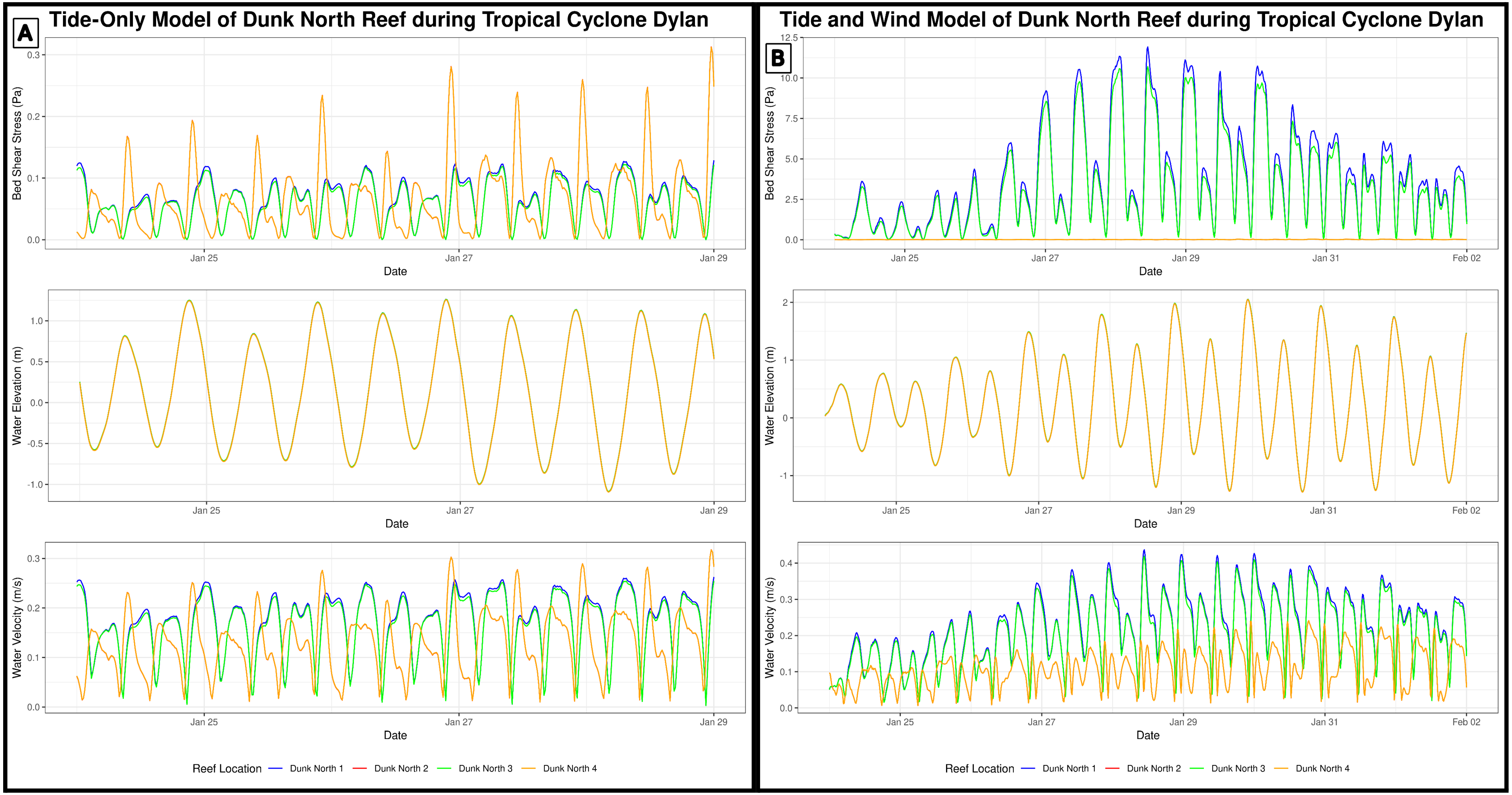

Figure 22 *Graphs showing the bed shear stress, water elevation and water velocity modelled for the T1_D simulation period (A), and the W1_D simulation period (B) for each location across Dunk North reef.*

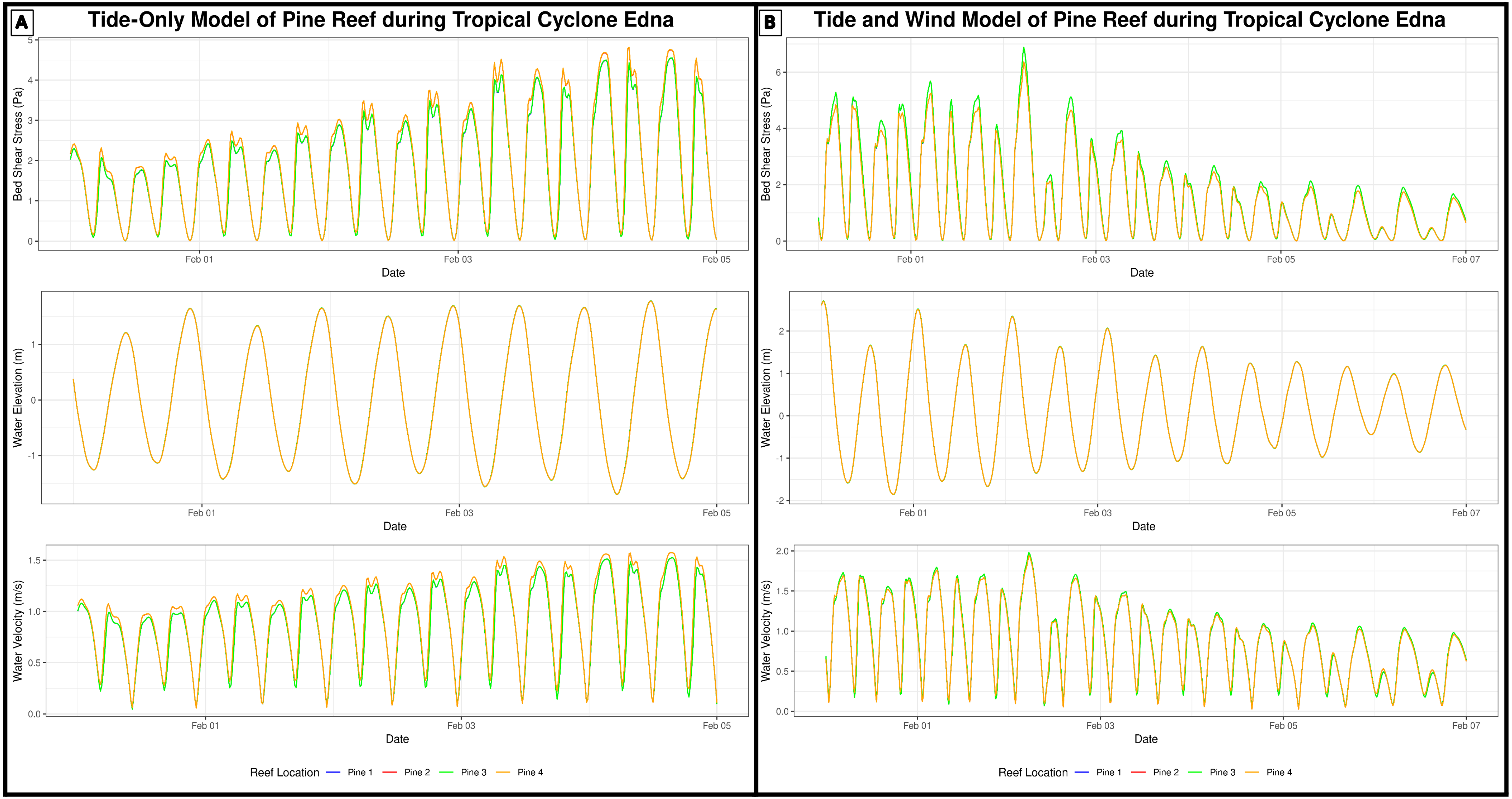

Figure 23 *Graphs showing the bed shear stress, water elevation and water velocity modelled for the T2_E simulation period (A), and the W2_E simulation period (B) for each location across Pine reef.*

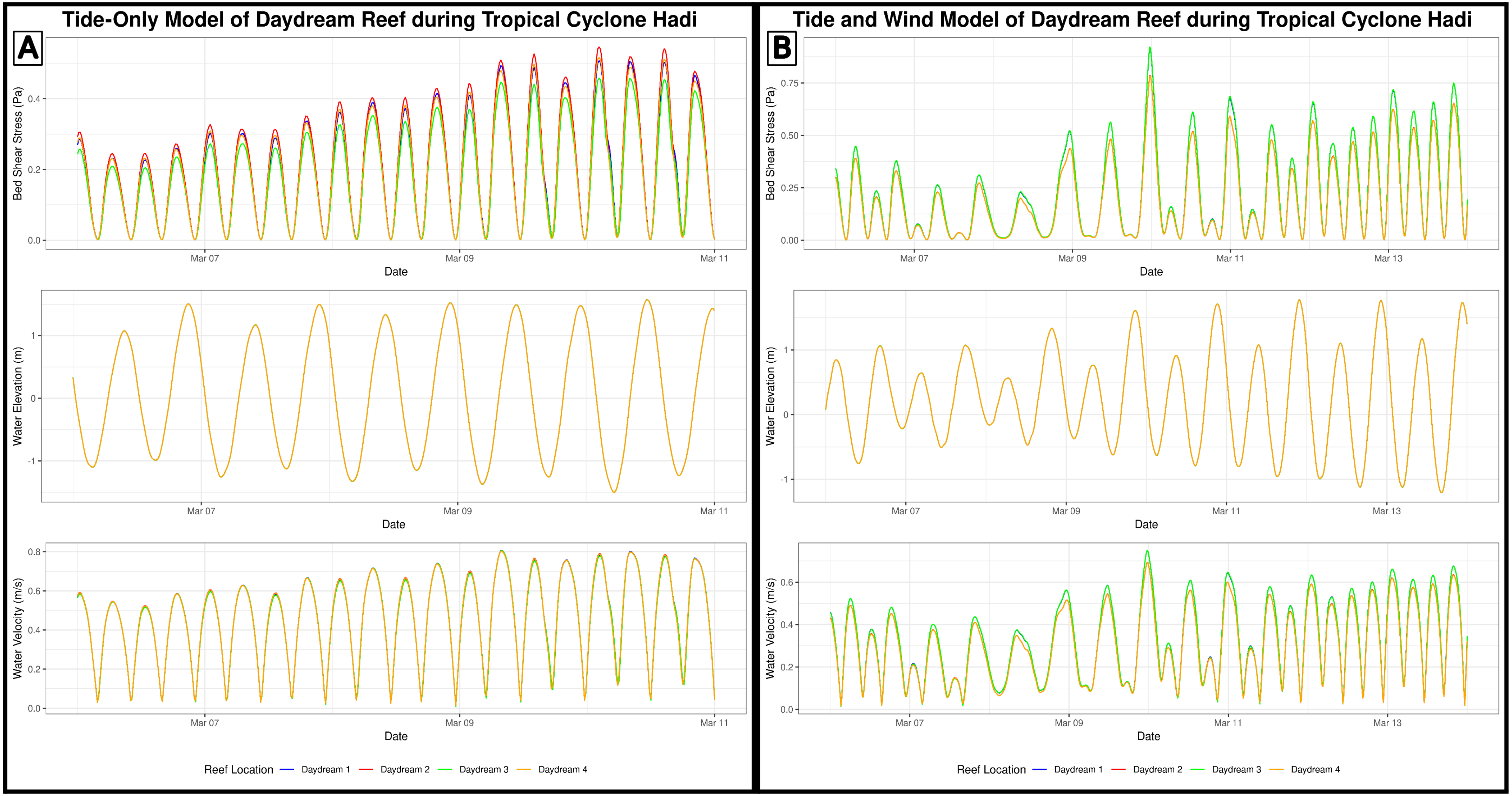

Figure 24 *Graphs showing the bed shear stress, water elevation and water velocity modelled for the T3_H simulation period (A), and the W3_H simulation period (B) for each location across Daydream reef.*

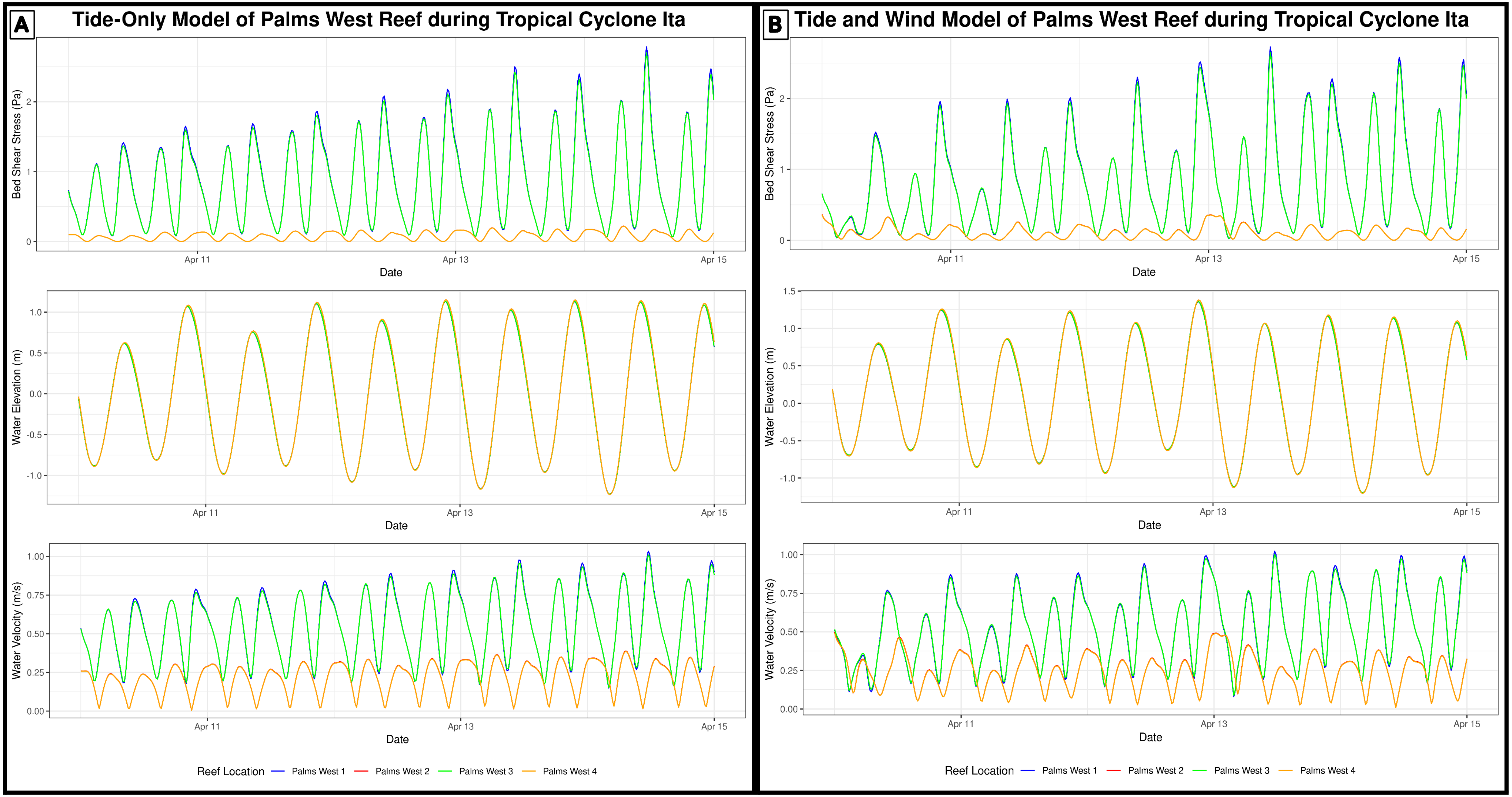

Figure 25 *Graphs showing the bed shear stress, water elevation and water velocity modelled for the T4_I simulation period (A), and the W4_I simulation period (B) for each location across Palms West reef.*

The graphs reveal a noticeable difference in magnitude between the tide-only and tide-plus-wind models for bed shear stress, water elevation, and water velocity. At Dunk North Reef (*Figure 22*), bed shear stress shows a significant increase, with a maximum of 0.18 Pa in the tide-only (*T1_D)* model compared to 11.9 Pa in the tide-plus-wind (*W1_D)* model. Water elevation and velocity also show notable increases at Dunk North Reef. The maximum water elevation rises from 1.68 m in the *T1_D* model to 2.05 m in the *W1_D* model, while the maximum velocity increases from 0.34 m/s to 0.44 m/s.

At Pine Reef *(Figure 23)*, the bed shear stress increases slightly between the tide-only (*T2_E*) and tide-plus-wind (*W2_E*) models, with maximum values of 5.88 Pa and 6.89 Pa, respectively. Similarly, the maximum water elevation increases from 2.5 m in the *T2_E* model to 2.72 m in the *W2_E* model, while the maximum velocity rises from 1.82 m/s to 1.98 m/s.

Daydream Reef (*Figure 24*) shows smaller changes between the tide-only (*T3_H*) and tide-plus-wind (*W3_H*) models. The maximum bed shear stress increases marginally from 0.83 Pa in the *T3_H* model to 0.92 Pa in the *W3_H* model. The maximum water elevation increases from 1.6 m to 1.78 m, while the maximum velocity rises slightly from 0.71 m/s to 0.75 m/s.

At Palms West Reef (*Figure 25*), the changes between the tide-only (*T4_I*) and tide-plus-wind (*W4_I*) models are minimal. The maximum bed shear stress is slightly lower in the *W4_I* model (2.73 Pa) compared to the *T4_I* model (2.79 Pa). However, the maximum water elevation increases from 1.15 m to 1.38 m, while the maximum velocity remains nearly unchanged, with values of 1.03 m/s in the *T4_I* model and 1.02 m/s in the *W4_I* model. These results demonstrate that the inclusion of wind in the models leads to varying degrees of impact across different reefs and TC scenarios.

3.3.2 | Shapiro-Wilk Normality Test

The results of the Shapiro-Wilk Normality test are summarised in *Table 10* with associated Q-Q plots presented in *Figure 26*. The results demonstrate that both absolute and relative changes in benthic cover, across all benthic categories, significantly deviate from normality (*$p < 0.001$*). This suggests that non-parametric statistical methods are more appropriate for further analysis of the data.

Table 10 *Results of the Shapiro-Wilk Normality test for absolute change and relative change in benthic cover for algae, hard coral, soft coral and other (NS – not significant ($p > 0.05$); * - significant to $p \leq 0.05$; ** - significant to $p \leq 0.01$; *** - significant to $p \leq 0.001$).*

Change in Cover	Algae	Hard Coral	Soft Coral	Other
Absolute	**0.93*****	**0.84*****	**0.72*****	**0.85*****
Relative	**0.94*****	**0.59*****	**0.42*****	**0.97*****

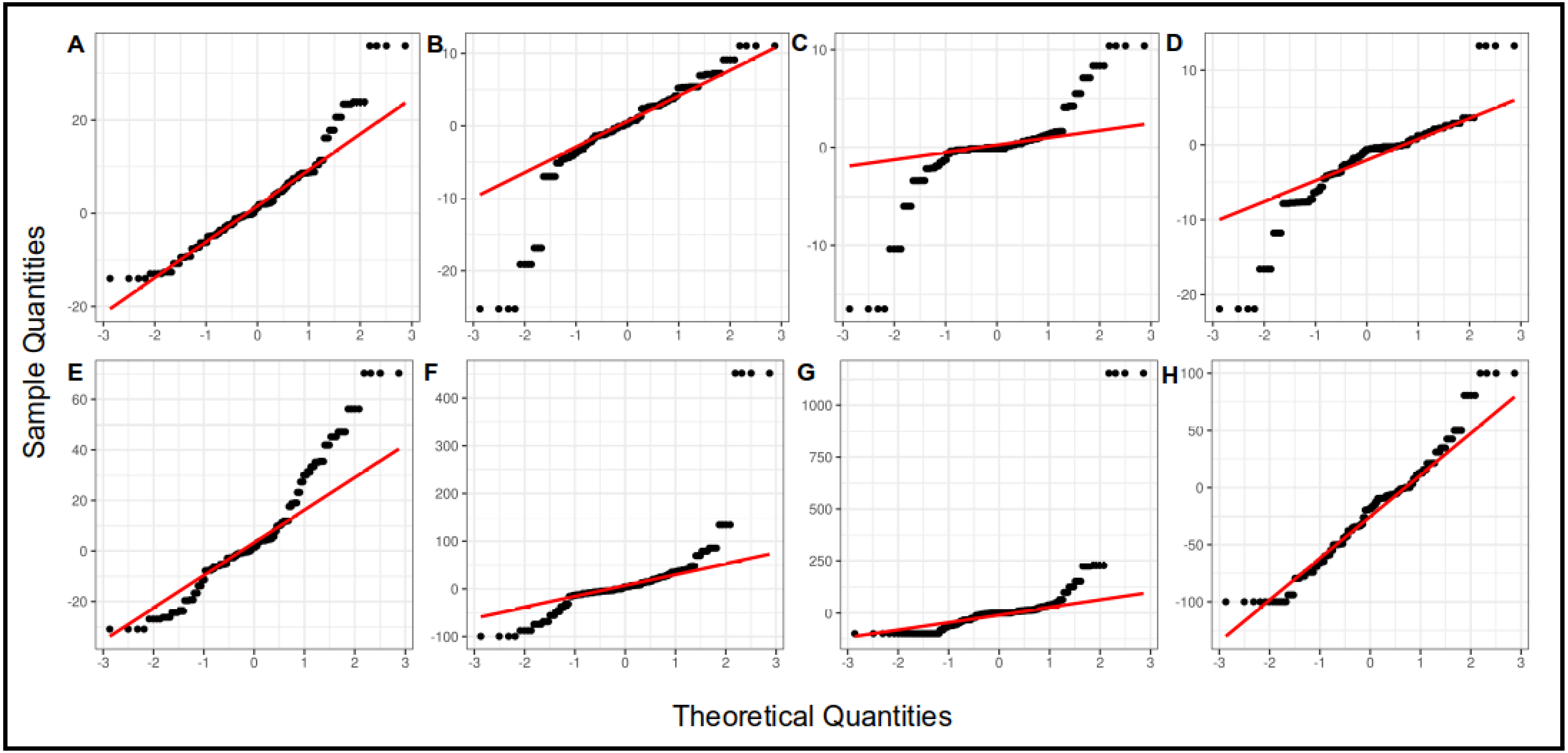

***Figure 26** Q-Q plots showing the results of the Shapiro-Wilk normality test for the four benthic categories for absolute and relative benthic change. Each plot represents the distribution of the variable comparing the observed (sample) data against a theoretical normal distribution. Deviations from the red line indicate variations from normality. Corresponding W-values and significance levels for the normality tests are presented in Table 10, respectively, with Algae - A and* E, Hard Coral - B and F, Soft Coral - C and G, Other - D and H and Absolute change in coral cover - A-D and Relative change in coral cover - E-H.

3.3.3 | Absolute Change in Benthic Cover

The results of the Kendall Tau's analysis examining the relationship between the absolute change in benthic cover (for algae, hard coral, soft coral and other) and both the maximum bed shear stress and change in bed shear stress magnitude modelled at each reef during each simulation is presented in *Table 11*, with corresponding graphs presented in *Figure 27*.

Table 11 *Results of the Kendall Tau's statistical analysis between the absolute change in benthic cover (for algae, hard coral, soft coral and other), and both the maximum bed shear stress modelled at each reef during each simulation (W1_D, W2_E, W3_H, W4_I) and the change in bed shear stress magnitude modelled at each reef during each simulation. (NS – not significant (p > 0.05); * - significant to p ≤ 0.05; ** - significant to p ≤ 0.01; *** - significant to p ≤ 0.001).*

Measurement of BSS	Algae	Hard Coral	Soft Coral	Other
Maximum	**0.19*****	-0.07^{NS}	0.01^{NS}	**-0.22*****
Change in Magnitude	**0.11****	-0.06^{NS}	0.04^{NS}	**-0.15*****

The results reveal a significant positive relationship between the absolute change in algae cover and both the maximum bed shear stress (τ = 0.19, p < 0.001) and the change in bed shear stress magnitude (τ = 0.11, p < 0.01). A significant negative relationship is also found between the absolute change in other benthic cover and both the maximum bed shear stress (τ = -0.22, p < 0.001) and the change in bed shear stress magnitude (τ = -0.15, p < 0.001). However, no significant relationships were found between the absolute change in hard coral or soft coral cover and both maximum bed shear stress (τ = -0.07, NS; τ = 0.01, NS, respectively) and the change in bed shear stress magnitude (τ = -0.06, NS; τ = 0.04, NS, respectively).

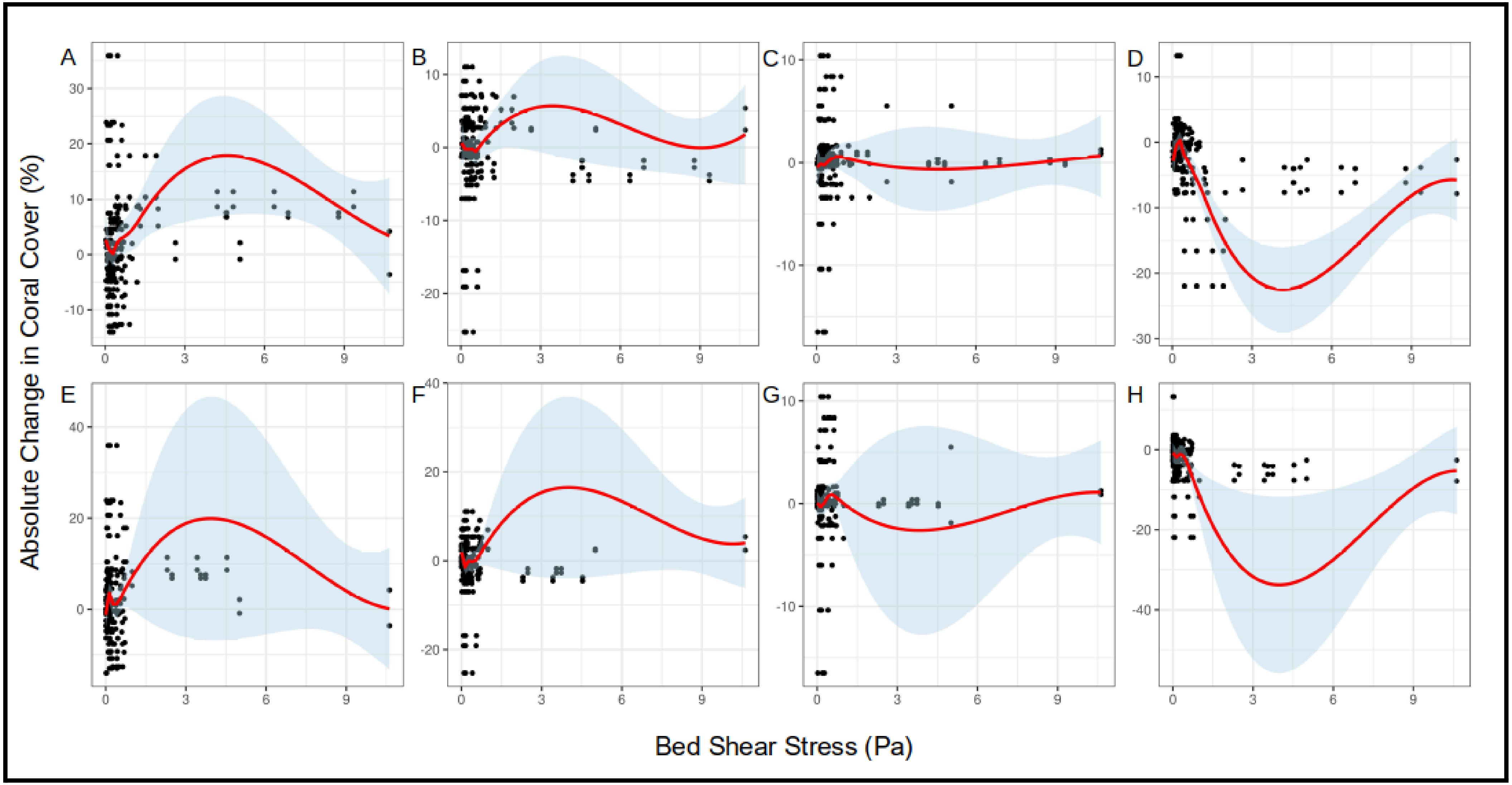

Figure 27 *Graphs showing the relationship between the absolute change in benthic cover (for algae, hard coral, soft coral and other benthic) and both the maximum bed shear stress and change in bed shear stress magnitude with Loess curves added to visualise trends in the data. Each plot corresponds to the statistical analysis results presented in Table 11, respectively, with Algae - A and E, Hard Coral - B and F, Soft Coral - C and G, Other - D and H, and Maximum Bed Shear Stress - A-D and Change in Bed Shear Stress Magnitude - E-H.*

3.3.4 | Relative Change in Coral Cover

The results of the Kendall Tau's analysis examining the relationship between the relative change in benthic cover (for algae, hard coral, soft coral and other) and both the maximum bed shear stress and change in bed shear stress magnitude modelled at each reef during each simulation is presented in *Table 12*, with corresponding graphs presented in *Figure 28*.

Table 12 *Results of the Kendall Tau's statistical analysis between the relative change in benthic cover (for algae, hard coral, soft coral and other), and both the maximum bed shear stress modelled at each reef during each simulation (W1_D, W2_E, W3_H, W4_I) and the change in bed shear stress magnitude modelled at each reef during each simulation. (NS – not significant ($p > 0.05$); * - significant to $p \leq 0.05$; ** - significant to $p \leq 0.01$; *** - significant to $p \leq 0.001$).*

Measurement of BSS	Algae	Hard Coral	Soft Coral	Other
Maximum	**0.19*****	-0.02NS	0.01NS	**-0.14****
Change in Magnitude	**0.11****	-0.07NS	0.03NS	**-0.18*****

The results reveal a significant positive relationship between the relative change in algae cover and both the maximum bed shear stress ($\tau = 0.19$, $p < 0.001$) and the change in bed shear stress magnitude ($\tau = 0.11$, $p < 0.01$). A significant negative relationship is also found between the absolute change in other benthic cover and both the maximum bed shear stress ($\tau = -0.14$, $p < 0.01$) and the change in bed shear stress magnitude ($\tau = -0.18$, $p < 0.001$). However, no significant relationships were found between the absolute change in hard coral or soft coral cover and both maximum bed shear stress ($\tau = -0.02$, NS; $\tau = 0.01$, NS, respectively) and the change in bed shear stress magnitude ($\tau = -0.07$, NS; $\tau = 0.03$, NS, respectively).

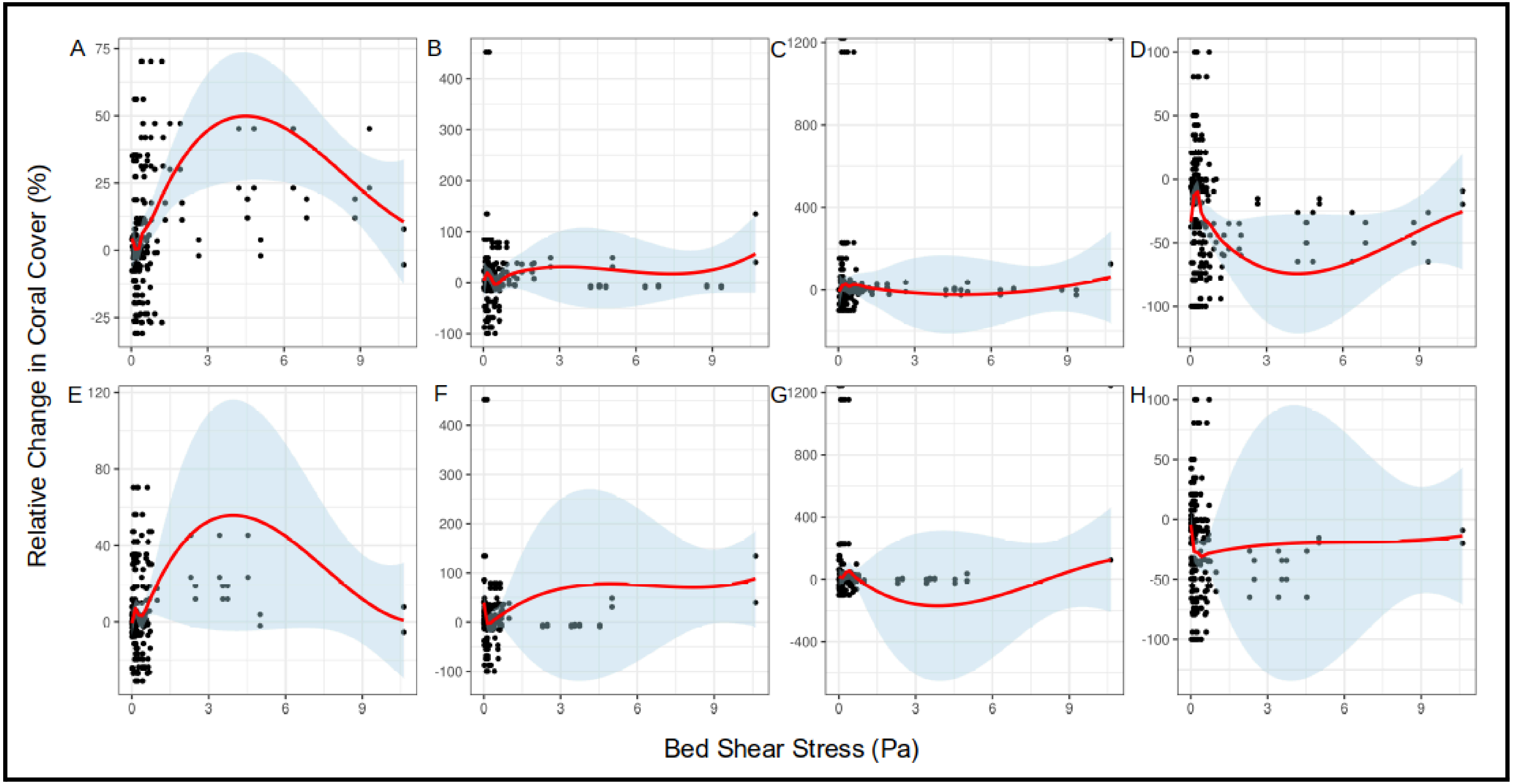

Figure 28 *Graphs showing the relationship between the relative change in benthic cover (for algae, hard coral, soft coral and other benthic) and both the maximum bed shear stress and change in bed shear stress magnitude with Loess curves added to visualise trends in the data. Each plot corresponds to the statistical analysis results presented in Table 12, respectively, with Algae - A and E, Hard Coral - B and F, Soft Coral - C and G, Other - D and H, and Maximum Bed Shear Stress - A-D and Change in Bed Shear Stress Magnitude - E-H.*

3.4 | Discussion

3.4.1 | Interpretation of Results

The analysis revealed significant trends in the response of algae and “other” to bed shear stress. Specifically, algae cover was found to significantly increase as bed shear stress intensified, while “other” (like sponges, tunicates and abiotics) showed a significant decrease in response to higher bed shear stress. These findings suggest a shift in reef composition, where the mechanical forces from TC-induced bed shear stress may reduce the abundance of sponges, sand, silt and rock, possibly as a result of dislodgement or physical damage and facilitate algal growth within the space created.

Despite limited research into the impacts of TCs on other benthic groups such as sponges and abiotics (e.g., sand, silt, rubble), some general insights can be drawn. Sponges, particularly erect and branching species, are highly vulnerable to TC-induced disturbances, experiencing damage that ranges from partial to complete mortality (Harmelin-Vivien 1994). This damage is often caused by abrasion, burial under sediment, or mechanical tearing of tissues and skeletons as a result of strong wave action and sediment movement (Harmelin-Vivien 1994). A decrease in sponge abundance and species richness was observed in Jamaica following Hurricane Allen, highlighting the potential for significant ecological impacts (Woodley 1980). However, research into these effects, especially across the GBR, remains minimal, highlighting a key knowledge gap.

In terms of abiotic impacts, higher bed shear stress during TCs has the ability to mobilise loose sediment such as sand, rock, and rubble within coral reef systems. This sediment is often transported and redeposited, depending on the cyclone's direction and intensity, with this redistribution of sediment possibly creating the space needed for the algal growth observed in this study.

Field surveys completed over a period of seven years recorded the development of a coral-macroalgal phase shift (> 7 years) observed on the GBR (Cheal et al. 2010). This shift followed extensive coral mortality at Havannah Island caused by coral bleaching in 1998 and subsequent cyclone damage (Cheal et al. 2010). Following the disturbances at Havannah Island, prolific macroalgae growth was consistently observed across the seven-year study period, where cover of brown macroalgae, (namely *Lobophora variegata* that contributed up to 73% of macroalgal cover), exceeded coral cover by 2001, reaching >40% by 2002 and remained high over the following five years (Cheal et al. 2010). Increases in algae cover were also found during impact assessment surveys following severe TC Yasi on the GBR in 2011, where extensive algal growth was observed on many of the damaged reefs, with green filamentous algae growing over remnant coral fragments and injured colonies, and blanketing large areas of damaged reef substrate (Beeden et al. 2015). These findings are consistent with the results of this study, highlighting a significant increase in algae cover on GBR coral reefs after disturbance events, particularly tropical cyclones. Algae seems to rapidly surge in areas cleared of coral and other benthic substrates, exploiting the available space and reduced competition (Beeden et al. 2015).

This study found no significant changes in hard or soft coral cover after the passage of the four TCs. However, numerous previous studies have reported significant changes in hard coral cover following the occurrence of a TC. TCs Hamish and Yasi drove 68% declines in the average cover of hard corals to ~9% cover between 2007 and 2011 over >1000 km of the outer central-southern GBR (Cheal et al. 2017). However, over the same 2007–2011 period, average coral cover remained stable in the unaffected northern region with no declines at individual survey reefs (Cheal et al. 2017). In the northern region between 2011 and 2015, TC Yasi and Ita were largely responsible for 13% declines in average hard coral cover on reefs spanning ~200 km, with the level of destruction being lower than that in the central-southern region and the remaining average coral cover was still almost three times higher (~26%) (Cheal et al. 2017). A different study researching the impacts of TC Yasi on the GBR found just over 15% of the total reef area was estimated to have sustained some level of coral damage, with ~4% sustaining a degree of structural damage (Beeden et al. 2015). Both studies identified significant impacts of TCs on coral cover; however, they used different methods to quantify the damage. The former study estimated the net effect of TCs on transect-scale hard coral cover in the impact region by developing a Bayesian hierarchical model that explicitly recognized the structure of the response (Cheal et al. 2017). The latter study used reef health and impact surveys to document the geographical extent, severity and patchiness of damage to reefs exposed to extreme winds (and consequently rough seas) during TC Yasi, followed by using a damage impact matrix to integrate the extent and severity scores for each survey into one of five levels of damage (Beeden et al. 2015). These differing approaches highlight how variations in methodology can influence the assessment of TC impacts on coral reefs. Unlike these studies, this research employed a different methodology and found no significant results, suggesting that the choice of approach may contribute to variations in findings.

Soft corals are not as extensively researched as hard corals; however, several studies have highlighted key findings regarding the impacts of TCs on soft corals. For example, a study reported a 29% decrease in soft coral cover at Low Isles along the GBR, following TC Rona in 1999 (Cheal et al. 2002). TC Rona's path exposed Low Isles, an inshore reef, to the full force of southeast winds, yet soft corals demonstrated greater survival rates compared to hard corals (A. Cheal et al. 2002). Similarly, soft corals were relatively unaffected by a previous cyclone at Low Isles in 1950 (Stephenson, Endean, and Bennett 1958), likely as a result of their elastic skeletons, which are more resilient to the destructive forces generated during TCs (Cheal et al. 2002). A different study found that at sites with severe coral damage following TC Yasi in 2011, the majority of large soft corals had either suffered substantial tissue loss or had been completely removed, as evident by layers of spicules formed where the coral had been attached to the substrate (GBRMPA 2011). These findings suggest that while soft corals may show greater resilience to some TC impacts, they are still vulnerable to significant damage, particularly in extreme TC occurrences. In contrast to these studies, this research found no significant changes in soft coral cover, indicating that different methodologies or environmental factors may also lead to varying outcomes in assessing TC impacts on soft corals.

3.4.2 | Methodological Insights

TC impacts are highly spatially variable as a result of complex hydrodynamic processes, and the coral-specific sensitivity to wind-induced impacts (Castro-Sanguino et al. 2022). This study used bed shear stress as a proxy for coral reef damage, an aspect that has not been extensively studied. While this research used a coastal flow model primarily driven by tidal dynamics, with the addition of an atmospheric forcing parameter to simulate TCs, most studies examining TC impacts on coral reefs across the GBR have used numerical wave models. For example, a recent study used the third-generation wave model SWAN to estimate the wave environment of surveyed reefs during TC Ita (Castro-Sanguino et al. 2022). A generalised additive model was then used to explore the influence of multiple predictors on observed changes in coral cover following the cyclone impact (Castro-Sanguino et al. 2022). The set of predictors used in the study were: cyclone-generated (Ita-U*b*) and non-cyclonic (nc-*Ub*) near-bed horizontal wave velocity amplitude, cyclone-generated cumulative wave energy flux (W_f), minimum distance to track and the time of the survey post-Ita (Castro-Sanguino et al. 2022). The response of coral assemblages to TC Ita were evaluated by the relative change in Acroporids cover ('total' and as per 'coral category') for four categories: *Acropora*, *Porites*, Other branching and MSE (Massive, submissive, encrusting) (Castro-Sanguino et al. 2022). Among the tested predictors, the relative abundance of Acroporids and Ita-U*b* were the most important predictors of the relative change of total coral cover, with losses in total coral cover strongly correlated with increasing Ita-U*b* levels (Castro-Sanguino et al. 2022). While bed shear stress and near-bed horizontal wave velocity are linked to fluid motion near the bed, they describe different aspects of that motion, therefore the use of a different proxy for damage will generate different results. This study found no significant relationship between either the maximum or the change in magnitude of bed shear stress and both the absolute and relative changes in hard coral cover, therefore alternative predictors of damage should be explored in future research.

At the coral colony scale, damage is always patchy because the size and spatial arrangement of colonies determine the extent to which physical damage from a potentially damaging wave actually occurs (Madin and Connolly 2006). As well as this, coral community composition (the abundance and traits of specific coral morphologies) is also an important predictor of reef damage (Castro-Sanguino et al. 2022). This research used broad categories for the coral reef data (Algae, Hard Coral, Soft Coral and Other), whereas many previous studies have looked at coral cover change post-TC at a species-level, rather than a broad benthic category to account for the differences in species resilience and susceptibility to cyclone impacts, providing a more detailed understanding of how specific coral taxa respond to extreme weather events. For example, research found that the composition of hard coral assemblages on the northeast flank of Low Isles in the GBR had changed by March 1999 following TC Rona in 1998 (Cheal et al. 2002). They found that the magnitude of decreases varied among life-forms: sub-massive (4.5±0.3 to 0.6±0.2% cover, mainly *Porites rus*, *P. annae*), branching (3.6±0.8 to 0.8±0.4% cover, *Porites cylindrica*), massive (3.8±1.5 to 1.8±0.9% cover, *Porites spp*.), and foleaceous (5.4±1.1 to 2.7±0.6% cover, *Echinopora spp*., *Pachyseris rugosa*, and *Pavona cactus*) (*Figure 29*) (A. Cheal et al. 2002).

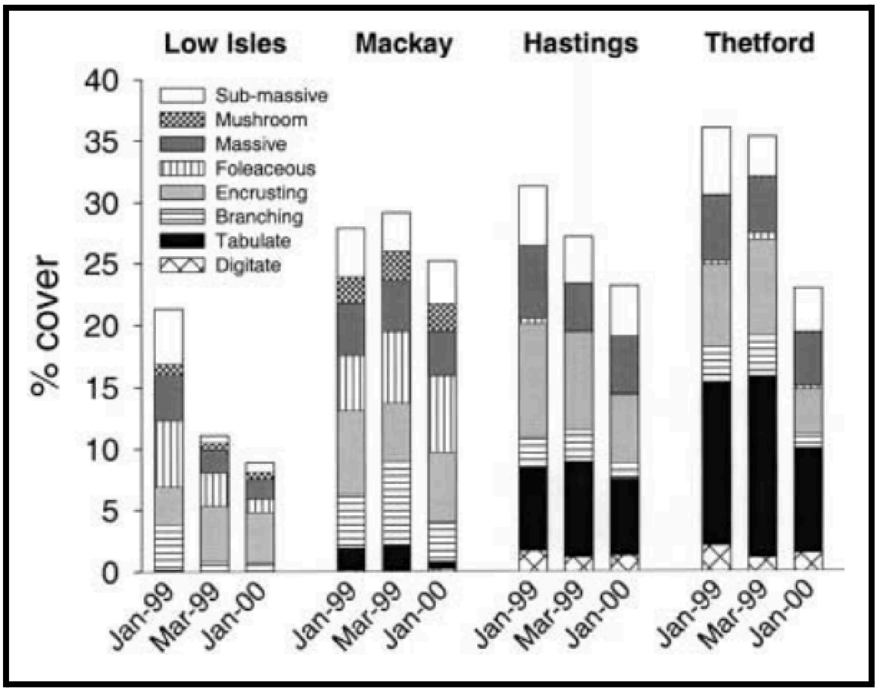

Figure 29 *Percentage cover of hard coral life-forms on four reefs from before TC Rona (Jan-99) to 1-2 months after the TC (Mar-99) to 11-12 months after Cyclone Rona (Jan-00) (Cheal et al. 2002).*

The results presented in *Figure 29* reveal differences not only between coral reefs but also among individual coral species, suggesting that the broad categories used in this study may oversimplify the complexity of coral ecosystem dynamics and species-specific responses to TC-induced impacts.

Therefore, a species-level breakdown of the MMP data used in this research was analyzed further to investigate whether examining the composition of each reef would yield different results. *Tables 13–15* summarise the results of Kendall Tau tests conducted for each benthic species observed across all reefs in this study, analyzing their relationships with both the maximum bed shear stress and the change in bed shear stress magnitude for all modelled TCs (only algae, hard coral and soft coral are presented as the data on the AIMS website did not include a breakdown of the category Other (AIMS 2024a)).

Table 13 *Results of the Kendall Tau's statistical analysis between the absolute change in benthic cover for all species of algae found across all reefs, and both the maximum bed shear stress modelled at each reef during each simulation (W1_D, W2_E, W3_H, W4_I) and the change in bed shear stress magnitude modelled at each reef during each simulation. (NS – not significant (p > 0.05); * - significant to p 0.05; ** - significant to p 0.01; *** - significant to p 0.001).*

Benthic Species	Maximum Bed Shear Stress	Change in Bed Shear Stress Magnitude
Brown Macroalgae	-0.019^{NS}	-0.003^{NS}
Coralline Algae	**0.228^{***}**	0.062^{NS}
Green Macroalgae	**0.15^{*}**	**0.121^{*}**
Other Macroalgae	**0.144^{*}**	-0.037^{NS}
Red Macroalgae	**0.248^{***}**	**0.186^{***}**
Turf Algae	**0.179^{***}**	**0.141^{**}**

Significant correlations were observed for specific algae types, such as red macroalgae (highly significant for both maximum bed shear stress and changes in bed shear stress magnitude) and turf algae. Brown macroalgae, coralline algae and other macroalgae showed no significant relationship with changes in bed shear stress magnitude, and brown macroalgae also showed no significant relationship with maximum bed shear stress. All results, except for three, indicate a positive relationship, reflecting an increase in algae cover. In contrast, brown macroalgae and other macroalgae (only for change in bed shear stress magnitude) show a negative relationship, suggesting a decline in cover for these species.

Table 14 *Results of the Kendall Tau's statistical analysis between the absolute change in benthic cover for all species of hard coral found across all reefs, and both the maximum bed shear stress modelled at each reef during each simulation (W1_D, W2_E, W3_H, W4_I) and the change in bed shear stress magnitude modelled at each reef during each simulation. (NS – not significant (p > 0.05); * - significant to p 0.05; ** - significant to p 0.01; *** - significant to p 0.001).*

Benthic Species	Maximum Bed Shear Stress	Change in Bed Shear Stress Magnitude
Acropora	-0.086^{NS}	**-0.158*****
Dendrophylliidae	**-0.162****	**-0.242*****
Euphylliidae	-0.1^{NS}	**-0.182*****
Fungiidae	**0.183*****	**0.153****
Goniopora Alveopora	**0.237*****	-0.011^{NS}
Isopora	0.002^{NS}	0.083^{NS}
Leptastrea	-0.002^{NS}	-0.083^{NS}
Lobophylliidae	**0.127***	-0.004^{NS}
Merulinidae	0.035^{NS}	0.055^{NS}
Montipora	0.047^{NS}	-0.061^{NS}
Other	-0.09^{NS}	**-0.18*****
Pachyseris	**-0.354*****	**-0.21*****
Pocilloporidae	0.001^{NS}	-0.099^{NS}
Porites	-0.039^{NS}	0.047^{NS}
Psammocora	**-0.139***	**-0.115***

Responses among hard corals varied widely. For example, *Pachyseris* and *Dendrophylliidae* exhibited strong negative correlations with maximum and change in bed shear stress, indicating vulnerability to hydrodynamic changes. In contrast, species such as *Fungiidae* and *Goniopora Alveopora* showed positive significant correlations, suggesting resilience or adaptive benefits under certain conditions. However, many hard corals, including *Montipora* and *Isopora*, showed no significant relationships, emphasizing species-specific responses.

Table 15 *Results of the Kendall Tau's statistical analysis between the absolute change in benthic cover for all species of soft coral found across all reefs, and both the maximum bed shear stress modelled at each reef during each simulation (W1_D, W2_E, W3_H, W4_I) and the change in bed shear stress magnitude modelled at each reef during each simulation. (NS – not significant (p > 0.05); * - significant to p 0.05; ** - significant to p 0.01; *** - significant to p 0.001).*

Benthic Species	Maximum Bed Shear Stress	Change in Bed Shear Stress Magnitude
Alcyoniidae	0.004^{NS}	**0.151****
Cladiellidae	-0.02^{NS}	-0.044^{NS}
Gorgonian-like	-0.003^{NS}	-0.021^{NS}
Heliopora	**0.119***	-0.049^{NS}
Lobophytum	**-0.189*****	**-0.119***
Other	-0.026^{NS}	**-0.122***
Other encrusting soft coral	0.041^{NS}	-0.005^{NS}
Sarcophyton	-0.074^{NS}	**0.171*****
Sclerophytum	0.092^{NS}	0.087^{NS}
Xeniidae	0.002^{NS}	0.083^{NS}

Soft coral responses were similarly diverse. *Lobophytum* exhibited strong negative correlations with both variables, indicating sensitivity to bed shear stress, whereas *Sarcophyton* and *Alcyoniidae* had positive correlations, suggesting potential resilience. Several species, such as *Cladiellidae* and Gorgonian-like corals, showed no significant relationships, reflecting varied tolerances for soft corals.

The observed variability in these results demonstrates that grouping benthic species into broad categories may obscure critical variations in species-specific responses to TC-induced bed shear stress. The vulnerability of coral reefs to TC damage is likely related to the robustness and fragility of reefs, which varies according to (1) location, (2) coral community type, and (3) successional stage of coral development (Fabricius et al. 2008). By analyzing individual reefs rather than multiple, more precise insights could be obtained regarding local resilience and vulnerability, ultimately informing tailored conservation and management strategies for specific reef systems. As well as this, TC features (e.g. wind speed, translation speed, size) will also impact how a coral reef is affected, with many studies agreeing that there is a significant level of variability in the type and intensity of TC impacts, and several studies have aimed at identifying the best predictors for storm damage (Done 1992; Gardner et al. 2005; Puotinen 2007; Fabricius et al. 2008). The ecological effects of TCs on coral reefs can have impacts accumulated over years to centuries (Connell 1997), so it is important to further improve our understanding of the factors that determine differences in TC effects between reef locations and among coral community types (Fabricius et al. 2008).

3.4.3 | Other Ecological Disturbances and Implications

As highlighted in *Chapter 1 (Section 1.3),* coral reefs in the GBR are affected by numerous ecological disturbances every year. The MMP data available on the AIMS Reef Reporting Dashboard (AIMS 2024a) identifies significant ecological disturbances that occur at each reef throughout the entire monitoring period. Using this dashboard, disturbances from 2011 to 2014 were identified, prior to the passage of the TCs modelled in this study. Among the 15 reefs analysed in this study, five experienced coral disease at least once, two were affected by Crowns-of-Thorns starfish (COTS) predation at least once, three were impacted by severe TC Yasi in 2011, one was impacted by TC Oswald in 2013 and one experienced the effects of flood waters (AIMS 2024a). All of these disturbances could have also influenced benthic cover across each reef, with each disturbance potentially leading to varying levels of impact and requiring different recovery times, depending on the severity of the event and the resilience of the reef's ecosystem.

Coral disease is a major threat to coral reefs and is one the most recent of threats that is challenging the resilience of reef communities (Willis, Page, and Dinsdale 2004). The first record of coral disease on the GBR was made in 1994 (Miller 1996), but it has become increasingly clear that coral diseases play an important role in the ecology of the GBR (Haapkylä et al. 2013). Coral disease surveys were carried out twice a year from 2008 to 2011 at Magnetic Island, a turbid inshore reef located in the central GBR, which is also included in the current study (Haapkylä et al. 2013). The dominant coral disease at the study site was atramentous necrosis (AtN), primarily affecting the reef-building coral *Montipora aequituberculata*, with other diseases including growth anomalies, white syndrome, and brown band syndrome, impacting eight coral genera in total (Haapkylä et al. 2013). AtN outbreaks occurred only during wet seasons, showing a clear seasonal pattern, with repeated wet season outbreaks, combined with bleaching and TC impacts, leading to a 50–80% decline in total coral cover (Haapkylä et al. 2013). These findings highlight the significant impact of coral diseases on the health and resilience of reef ecosystems, especially when combined with other stressors.

COTS predation is another major threat impacting the coral reefs across the GBR. The first COTS outbreak identified within the GBR was recorded on reefs offshore from Cairns in 1962 (Endean 1969). This was followed by three subsequent outbreaks over the following decades, each persisting for 10-15 years and resulting in significant coral losses across much of the GBR (Matthews et al. 2024). COTS outbreaks accounted for approximately 40% of the coral loss recorded on the GBR between 1985 and 2012, corresponding to a decline in coral cover of approximately -1.42% per year (Matthews et al. 2024; De'ath et al. 2012). The same analysis indicated that even in the presence of coral bleaching and TC damage, prevention of COTS predation would have yielded a net increase in GBR-wide coral cover over the same period (Matthews et al. 2024; De'ath et al. 2012). These findings highlight the critical need for effective management of COTS outbreaks, as mitigating this could substantially improve coral cover and enhance the overall resilience of the GBR, even in the presence of other stressors like bleaching and TCs.

Floodwaters caused by cyclonic rain events are a major factor shaping the nature, location and extent of inshore coral reefs along the GBR (Jones and Berkelmans 2014). In December 2010, the highest recorded Queensland rainfall associated with TC Tasha caused flooding of the Fitzroy River in Queensland, Australia (Jones and Berkelmans 2014). A large flood plume inundated coral reefs lying 12 km offshore of the Central Queensland coast near Yeppoon and caused 40–100% mortality to coral fringing many of the islands of Keppel Bay down to a depth of ~8 m (Jones and Berkelmans 2014). A significant part of the damage to inshore coral communities from TCs is caused by the inundation of reefs near major catchments by floodwaters (Bostock et al. 2006). This results in low salinity exposure, which is largely influenced by the movement of the flood plume, driven by wind-induced currents and tides (Bostock et al. 2006). This highlights the significant impact of TC-induced floodwaters on inshore coral reefs, emphasising the vulnerability of coral reef ecosystems to extreme weather events and the critical need for strategies to mitigate their impacts.

This study focused on coral reefs located between 16°S and 23°S latitude, encompassing a broad geographic range and a diverse array of reef and measurement sites. Disturbances such as coral disease and COTS predation tend to be relatively localised, as evidenced by their variable occurrence across different reefs. These spatial differences suggest that the observed patterns in this research are most likely as a result of TCs clearing unconsolidated sediments and creating space for algal colonisation rather than other stressors. To better understand the impacts of TCs on coral reefs, particularly in the context of interacting stressors, this study could be repeated across different years. Doing so would help determine whether similar patterns emerge during periods when other major stressors, such as coral bleaching or COTS outbreaks, are absent.

3.4.4 | Coral Reef Recovery Patterns and Future Management Implications

During the 20th century (1950–1999), the mean annual arrival rate of TCs across the GBR was 2.25 TCs per year, with rates varying from a low of 1.22 to a high of 3.75 TCs per year (Callaghan, Mumby, and Mason 2020). The impact of multiple TCs, alongside other disturbances, can affect the recovery of coral reefs across the GBR. Variation among coral reef communities in vulnerability to, and recovery from, disturbances has received increasing attention as a result of concerns that anthropogenic activities are altering disturbance regimes for coral reefs (Johns, Osborne, and Logan 2014). For example, human-induced climate change is predicted to increase both the frequency and severity of bleaching events, as well as the occurrence of high-intensity TCs (Hoegh-Guldberg et al. 2007). Consequently, coral reef communities will experience more frequent disturbances, and the intervals between disturbances will likely shorten, reducing recovery periods (Nyström, Folke, and Moberg 2000).

Changes in the relative abundances of coral species during recovery from disturbance may lead to shifts in essential ecological processes on coral reefs (Johns, Osborne, and Logan 2014). Coral cover can return to pre-disturbance levels without the assemblage returning to its previous composition; however, this process is not well understood as a result of the lack of long-term studies (Johns, Osborne, and Logan 2014). A study of six coral communities that suffered substantial coral loss and subsequently regained at least 50% of their pre-disturbance coral cover found recovery periods of 11 years or less, either because of recurring disturbances or the time frame of the study (Johns, Osborne, and Logan 2014). Four of the six communities reassembled to their pre-disturbance composition in 8–13 years, while the trajectories of two communities suggested that they were unlikely to reassemble, and the remaining community did not regain pre-disturbance coral cover (Johns, Osborne, and Logan 2014). The communities that regained coral cover and reassembled had a high relative abundance of tabulate *Acropora spp*., whereas communities that failed to regain coral cover or reassemble were located in near-shore areas and had a high relative abundance of *Porites spp.* and soft corals (Johns, Osborne, and Logan 2014). In conclusion, while coral reefs may show signs of recovery in terms of coral cover, the ability to reassemble into their original ecological composition is influenced by factors such as species abundance, reef location, and disturbance frequency, highlighting the complexity of coral reef recovery processes.

Ocean warming under climate change threatens coral reefs directly, through fatal heat stress to corals and indirectly, by increasing the energy of TCs (Cheal et al. 2017). Most global predictions of changes in TC activity under climate change have focussed on TC frequency and intensity; an increase in the relative frequency of the most intense TCs would pose the biggest threat to coral reef communities (Cheal et al. 2017); however, it is likely that the frequency of TCs will remain stable or decrease by up to 40% by 2100 under enhanced greenhouse conditions (Knutson et al. 2010; Christensen et al. 2013; Walsh et al. 2016). Despite TCs are one of the major causes of coral decline around the world (De'ath et al. 2012), only heat-induced mass coral bleaching and ocean acidification were specifically listed as key risks to coral reef biodiversity and fisheries abundance in the 2022 IPCC report (Boudreau, Robinson, and Farooqi 2022). While TCs were noted as one of the drivers of change on coral reefs under climate change, the consequences of altered TC activity are not yet adequately resolved to allow clear risk attribution (Cheal et al. 2017). This knowledge gap in understanding the impact of future climate change on TC frequency and intensity makes it difficult to plan and manage the GBR for future disturbances by TCs. However, understanding patterns in impact severity and recovery enables managers to target local-scale actions to support reef resilience and recovery and conserve the ecological, social, cultural and economic values provided by coral reefs (Beeden et al. 2015). Examples of such actions include: crown-of-thorns starfish eradication, active reef restoration and the establishment of special management areas or temporary fishing closures (Beeden et al. 2015).

3.5 | Conclusions

In conclusion, in order to completely understand the impacts of TCs on coral reefs, it is essential to consider all aspects of disturbance, as well as the unique characteristics of individual reefs and species, highlighting the need of a holistic approach. Studying individual reefs is crucial, as generalisations across all reefs may overlook important variations, and when combined with other stressors, such as disease outbreaks, COTS infestations, and the secondary effects of TCs (e.g. floodwaters), the impacts on coral reefs are further exacerbated. This highlights the urgent need for integrated conservation and management strategies that address these multiple, compounding threats to coral reef ecosystems (Uthicke et al. 2016). As well as this, anthropogenic-induced climate change is predicted to increase the frequency and severity of coral bleaching events, and the frequency of high-intensity TCs (Hoegh-Guldberg et al. 2007). Consequently, coral reef communities will suffer more frequent disturbances and the intervals for recovery will be reduced (Nyström, Folke, and Moberg 2000). Therefore, research into the potential future impacts of TCs on coral reefs across a range of predicted climate scenarios is essential to better understand the long-term consequences, and guide conservation efforts in the face of a changing climate.

Chapter 4 | Uncertainty for the Future: Sea Level Rise

4.1 | Introduction

The IPCC Special Report on Global Warming of 1.5°C highlights coral reefs as among the most sensitive ecosystems, with projections indicating increased mass coral bleaching and mortality as a result of the combined effects of rising ocean temperatures, ocean acidification, sea-level rise (SLR), and potentially more intense and frequent tropical cyclones (TCs) (Hoegh-Guldberg et al. 2018). Global mean sea level increased by 0.20 [0.15 to 0.25] m between 1901 and 2018 (IPCC 2023). The average rate of sea level rise was 1.3 [0.6 to 2.1] mm yr^{-1} between 1901 and 1971, increasing to 1.9 [0.8 to 2.9] mm yr^{-1} between 1971 and 2006, and further increasing to 3.7 [3.2 to 4.2] mm yr^{-1} between 2006 and 2018 (high confidence) (IPCC 2023).

The AR5 report concluded that while some coral reefs may be able to keep up with the maximum rate of projected SLR rate of 15.1 mm yr^{-1} by the end of the century (medium confidence), factors such as lower net accretion rates (compared to the Holocene) (Perry et al. 2013) and increased turbidity (Storlazzi et al. 2011) will weaken this capability (very high confidence) (Wong et al. 2014). So, while SLR alone is not typically seen as a threat to coral reefs, provided coral growth can keep pace with rising waters, other climate-related factors—such as warming sea temperatures, higher sediment input, and increased ocean acidity—are expected to inhibit coral growth (Hoegh-Guldberg 2011). These challenges suggest that some reef communities may struggle to sustain themselves even under minimal sea-level changes (Hoegh-Guldberg 2011).

In this chapter, I will explore the impacts of various SLR scenarios on the depth of coral reefs across the GBR and the impacts on TC-induced bed shear stress and how this could impact coral reefs in the future.

4.2 | Methodology

4.2.1 | Shared Socio-Economic Pathways

The integrated assessment community quantified anthropogenic emissions for the shared socioeconomic pathway (SSP) scenarios, each of which represents a different future socio-economic projection and political environment (Meinshausen et al. 2020). For this research, two SSP scenarios were chosen to determine the potential future impacts of rising sea level on bed shear stress on coral reefs. The two scenarios chosen were SSP1-1.9 and SSP2-4.5.

The SSP1-1.9 holds warming to approximately 1.5°C above 1850-1900 levels in 2100 after a slight overshoot (median) and implies net zero CO_2 emissions around the middle of the century (NASA 2024). The SSP2-4.5 scenario deviates mildly from a 'no-additional- climate-policy' reference scenario, resulting in a best-estimate warming around 2.7°C by the end of the 21st century relative to 1850-1900 levels (NASA 2024). For sea level projections, likely ranges are assessed based upon the combination of uncertainty in the temperature change associated with the SSP scenarios and uncertainty in the relationships between temperature and drivers of projected sea level change, such as thermal expansion, ocean dynamics, and glacier and ice sheet mass loss (NASA 2024). *Figure 30* shows the predicted sea level change between 2020 and 2100 for both SSP1-1.9 and SSP2-4.5 at Bowen on the east coast of Australia (NASA, 2024). By 2100, it is predicted that under an SSP1-1.9 scenario sea level will rise by 0.42 m, and for SSP2-4.5 it will rise by 0.59 m (NASA 2024).

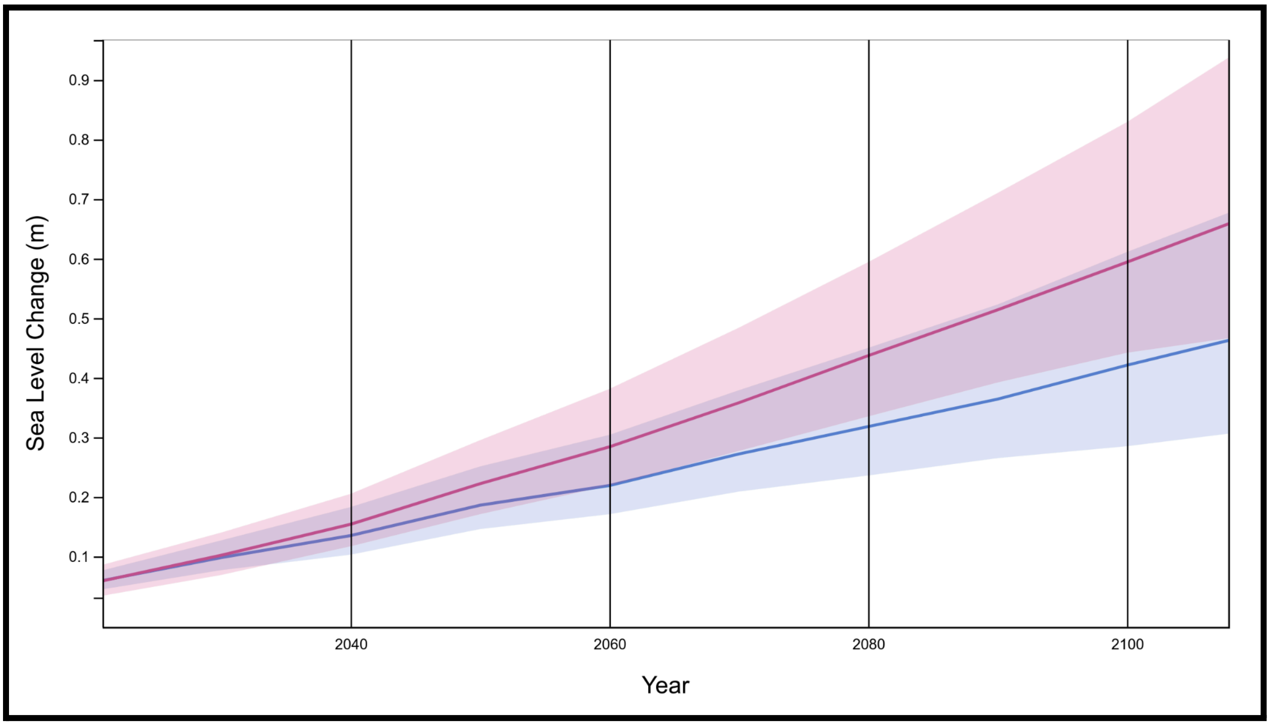

Figure 30 *Projected sea level change for Bowen for scenario SSP1-1.9 and SSP2-4.5 Shaded ranges show the 17th-83rd percentile ranges. Projections are relative to a 1995-2014 baseline (NASA 2024).*

4.2.2 | Bathymetry

IPCC AR6 sea-level change projection files (Fox-Kemper et al., n.d.; Kopp et al. 2023; Garner et al. 2021) were used to alter the current-day bathymetry data (described in *Chapter 2, Section 2.2.3*) for the two SSP scenarios. The files, in NetCDF format, provide time-series probability distributions for global sea level changes, including both levels and rates. An R script (*Appendix H*) was used to process the NetCDF file. The file was converted into a shapefile, allowing selection of the projection year (2100) and the quantiles of the sea-level change probability distribution (0.950). The shapefile was loaded into QGIS and converted into raster format using the Rasterize tool (*Figure 31*). The resulting raster was then clipped to match the extent of the current-day bathymetry data. Using the Raster Calculator, the sea level change raster was applied to modify the current-day bathymetry (*Eq. 15*), creating a new raster file representing the future sea level rise scenario. This was completed for both SSP1-1.9 and SSP2-4.5 projection files.

$$SSP\ scenario\ bathymetry\ =\ Current\ day\ bathymetry\ -\ Sea\ Level\ Change\ Raster \quad (15)$$

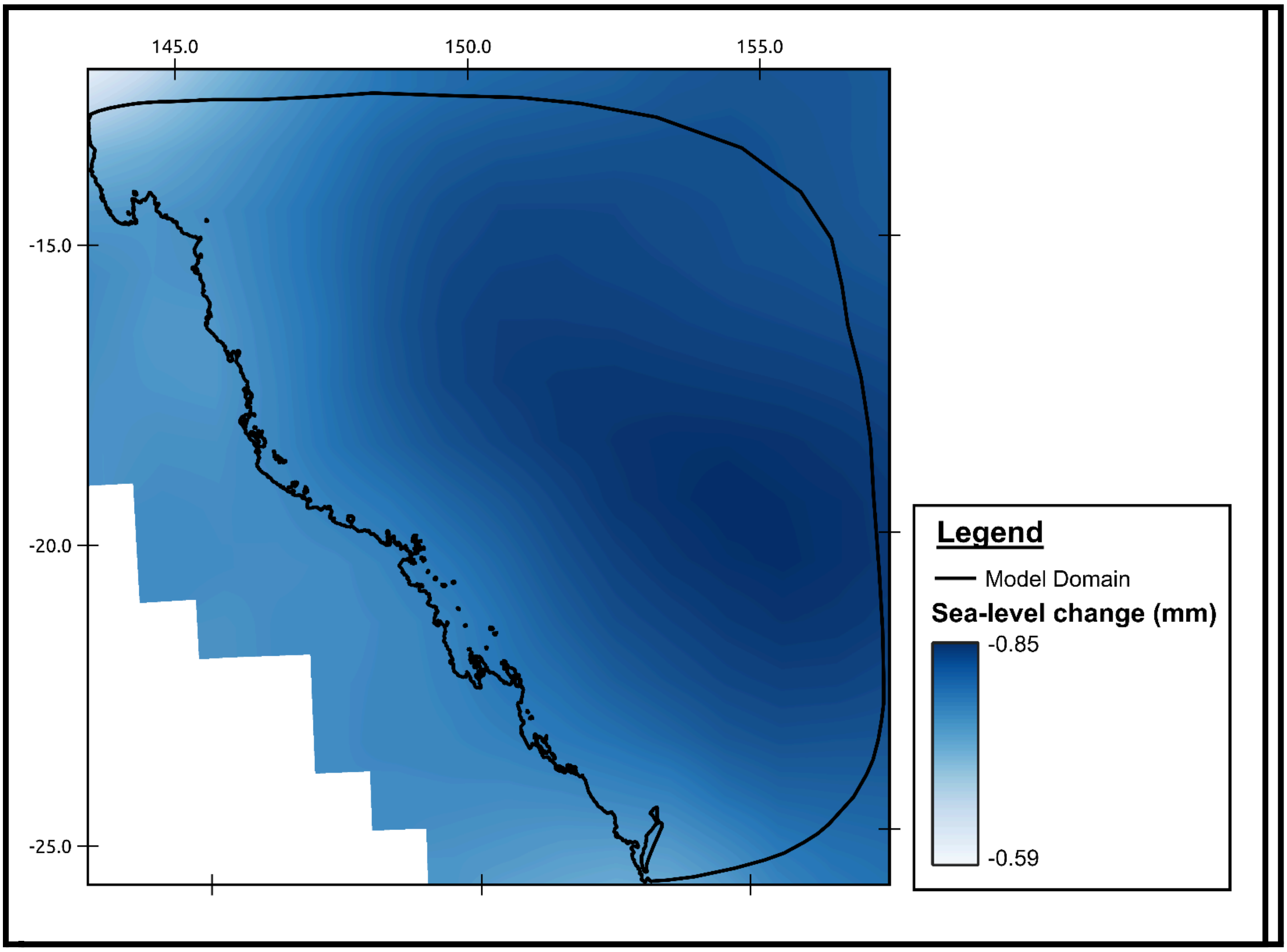

Figure 31 *Raster file from QGIS showing the variable level of sea-level change since the AR6 reference period for the SSP1-1.9 scenario.*

4.2.3 | Model Set-Up

Following the same model set-up as described in *Chapter 2 Section 2.2*, four models were run (*Table 16*), using the varied bathymetry for both SSP1-1.9 and SSP2-4.5.

Table 16 *The models used for the future sea level rise scenarios, including the model ID, the configuration of the model (simulating tides only or tides and wind), the tropical cyclone they were simulating, total model runtime, the spin-up duration, and the start/end dates for each model. For the model ID, 119 denotes the SSP1-1.9 scenario and 245 denotes the SSP2-4.5 scenario.*

Model ID	**Model Configuration**	**Tropical Cyclone**	**Model Run Length (days)**	**Spin-up (days)**	**Start Date**	**End Date**
W4_I	Tides and Wind	*Ita*	7	2	08.04.2014	14.04.2014
T4_I	Tides Only	*Ita*	7	2	08.04.2014	14.04.2014
W4I_119	Tides and Wind	*Ita*	7	2	08.04.2014	14.04.2014
T4I_119	Tides Only	*Ita*	7	2	08.04.2014	14.04.2014
W4I_245	Tides and Wind	*Ita*	7	2	08.04.2014	14.04.2014
T4I_245	Tides Only	*Ita*	7	2	08.04.2014	14.04.2014

4.2.4 | Numerical Model Data

The four numerical models were post-processed to extract data on elevation, velocity, and bed shear stress. For each model, this data was extracted at each coral reef throughout the simulation period. Graphics were then created to show the depth of each reef for models *W4_I, W4I_119* and *W4I_245*.

From the tide and wind models (*W4I_119 and W4I_245)*, the maximum bed shear stress and its occurrence time were also extracted. Using this occurrence time, bed shear stress was then extracted from the corresponding tide-only models (*T4I_119 and T4I_245*). The change in magnitude between the tide-only models and the combined tide-and-wind models was then calculated. Heatmaps of both the maximum bed shear stress and the change in bed shear stress magnitude were then created to compare the differences between *W4_I, W4I_119* and *W4I_245* models.

4.2.5 | Statistical Analysis

A Shapiro-Wilk normality test was performed to assess whether the maximum bed shear stress and change in bed shear stress magnitude data followed a normal distribution. Subsequently, a Kendall's Tau test was conducted to assess the strength and direction of the association between reef depth and the two measures of bed shear stress modelled for each of the three scenarios.

4.3 | Results

4.3.1 | Depth

Depths at a specific point on each reef were mapped in QGIS across all three scenarios (*W4_I, W4I_119,* and *W4I_245*) (*Figure 32*). Across all reefs, depth values become increasingly negative between *W4_I* and *W4I_119*, indicating a consistent increase in submersion under the projected scenario (SSP1-1.9) (*Table 17*). The magnitude of change varies among reefs, with Snapper North showing the smallest change in depth (-0.75 m) and Barren the largest (-0.78 m). Shallower reefs such as North Keppel (-0.78 m) and Pelican (-0.78 m) experience relatively larger depth increases compared to deeper reefs such as Franklands West (-0.76 m).

Table 17 *The depth of a point at each coral reef across 2 scenarios: current-day bathymetry (W4_I) and varied bathymetry using SSP1-1.9 sea level projections (W4I_119), with the change in depth calculated between each scenario.*

Reef	W4_I Depth (m)	W4I_119 Depth (m)	Change in Depth (m)
Magnetic	-9.2048	-9.97503	-0.77023
Palms West	-24.48586	-25.25337	-0.76751
Pandora	-18.27938	-19.04531	-0.76593
Barren	-14.60075	-15.38445	-0.7837
Keppels South	-9.86956	-10.65167	-0.78211
North Keppel	-2.65995	-3.44304	-0.78309
Pelican	-3.10255	-3.88363	-0.78108
Daydream	-24.05673	-24.83671	-0.77998
Double Cone	-18.63245	-19.41332	-0.78087
Pine	-17.36485	-18.14412	-0.77927
Snapper North	-7.73197	-8.48323	-0.75126
Fitzroy West	-15.67331	-16.43331	-0.75999
Franklands West	-21.82501	-22.58639	-0.76138
High West	-9.08523	-9.84524	-0.76001
Dunk North	-1.02922	-1.79197	-0.76275

Similar to SSP1-1.9, all reefs exhibit increased submersion under the SSP2-4.5 scenario, with depth values becoming increasingly negative between *W4_I* and *W4I_245 (Table 18)*. The magnitude of change varies among reefs, with Snapper North showing the smallest change in depth (-1.02 m) and Barren the largest (-1.04 m). This pattern is consistent with the findings for SSP1-1.9, indicating that the magnitude of depth changes are consistent across reefs for different future sea level scenarios. These results highlight spatial variations in reef submersion, driven by bathymetric changes associated with sea-level rise under SSP1-1.9 and SSP2-4.5 projections.

Table 18 *The depth of a point at each coral reef across 2 scenarios: current-day bathymetry (W4_I) and varied bathymetry using SSP2-4.5 sea level projections (W4I_245), with the change in depth calculated between each scenario.*

Reef	W4_I Depth (m)	W4I_245 Depth (m)	Change in Depth (m)
Magnetic	-9.2048	-10.23527	-1.03047
Palms West	-24.48586	-25.51237	-1.02651
Pandora	-18.27938	-19.30425	-1.02487
Barren	-14.60075	-15.64294	-1.04219
Keppels South	-9.86956	-10.90955	-1.03999
North Keppel	-2.65995	-3.70138	-1.04143
Pelican	-3.10255	-4.14111	-1.03856
Daydream	-24.05673	-25.09612	-1.03939
Double Cone	-18.63245	-19.67359	-1.04114
Pine	-17.36485	-18.40297	-1.03812
Snapper North	-7.73197	-8.74986	-1.01789
Fitzroy West	-15.67331	-16.69905	-1.02574
Franklands West	-21.82501	-22.85139	-1.02638
High West	-9.08523	-10.11028	-1.02505
Dunk North	-1.02922	-2.05403	-1.02481

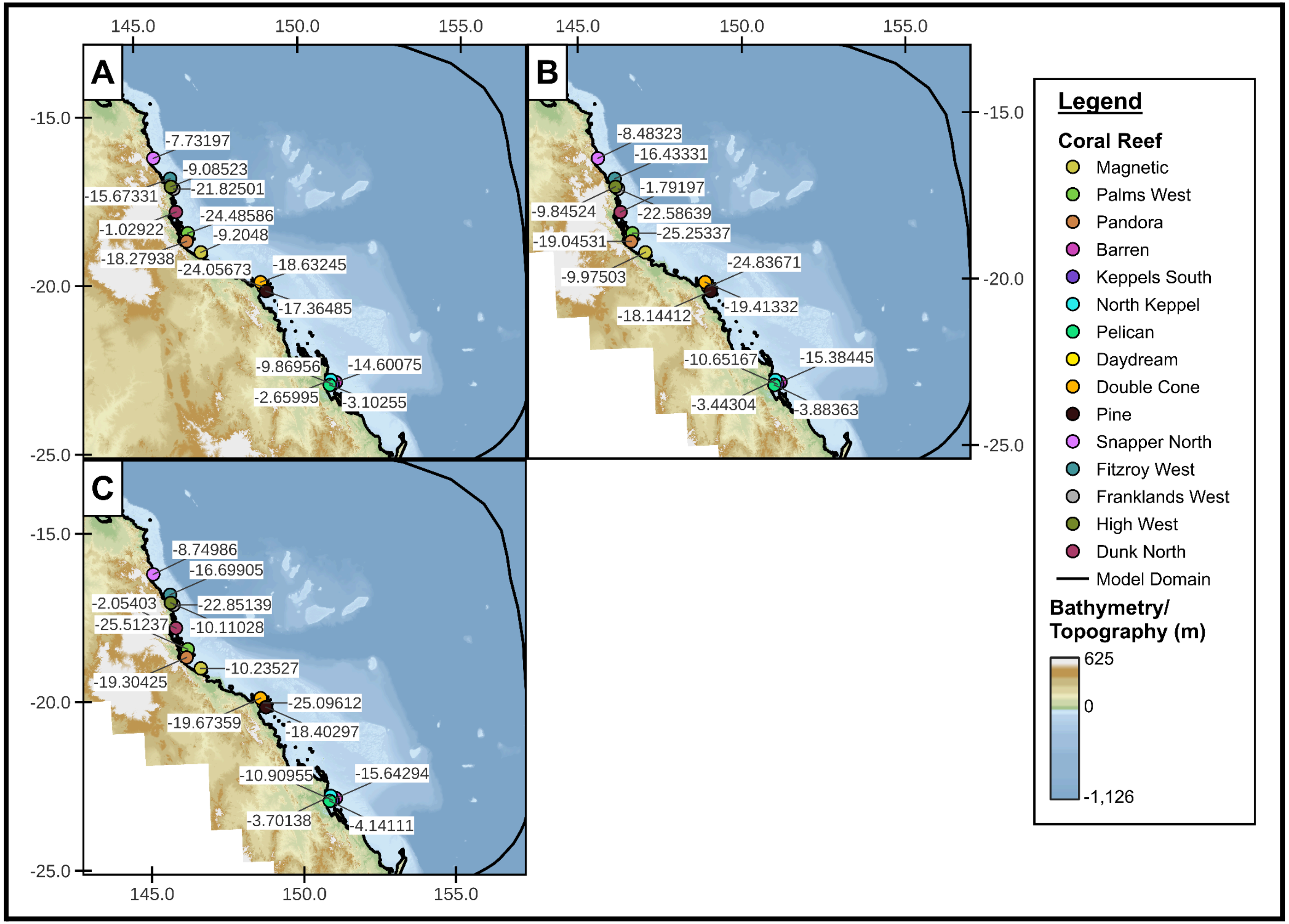

Figure 32 *Maps showing the depth measured at each coral reef used within this study under different bathymetric scenarios - (A) Current bathymetry; (B) varied bathymetry for SSP1-1.9 sea level projection; and (C) varied bathymetry for SSP2-4.5 sea level projection.*

4.3.2 | Maximum Bed Shear Stress

The average maximum bed shear stress for each scenario provides insight into the potential impact of SLR on bed shear stress across the GBR in the future. For the W4_I model, the average maximum bed shear stress across all reefs is 0.666 Pa. This increases to 0.976 Pa under the W4I_119 model (SSP1-1.9) and further to 0.985 Pa for the W4I_245 model (SSP2-4.5), indicating that rising sea levels are likely to result in higher maximum shear stress experienced at coral reefs.

For most reefs, the *W4I_119* (SSP1-1.9) scenario results in an increase in maximum bed shear stress from the current day scenario (*W4_I*) (*Figure 33*). For example, Magnetic Reef 1 sees an increase from 0.17 Pa (*W4_I*) to 1.7 Pa (*W4I_119*), while Palms West 1 increases from 2.7 Pa to 3.9 Pa. These increases suggest that under the modest sea-level rise of SSP1-1.9, reefs may experience heightened hydrodynamic stress due to altered flow dynamics caused by bathymetric changes. However, some reefs show minor changes in maximum bed shear stress. For example, Barren 1 only slightly increases from 0.61 Pa to 0.77 Pa, and North Keppel 1 rises from 0.44 Pa to 1.3 Pa. These results indicate that localized factors (e.g., reef-specific topography and hydrodynamic conditions) may influence the magnitude of change.

The differences between *W4_I* and *W4I_245* (SSP2-4.5) also show an increase in maximum bed shear stress for most reefs (*Figure 33*). For example, Magnetic Reef 1 increases from 0.17 Pa (*W4_I*) to 0.26 Pa (*W4I_245*), while Pine Reef 1 experiences a greater increase from 4.5 Pa to 5.8 Pa. Similarly, Palms West 1 increases from 2.7 Pa to 2.8 Pa, and Fitzroy West 1 increases from 0.17 Pa to 0.31 Pa. Despite the trend of increasing maximum bed shear stress, a few reefs show only modest changes. For example, Pelican 1 increases from 0.28 Pa to 0.3 Pa, while Barren 1 grows from 0.61 Pa to 0.78 Pa. These findings underscore the varying impacts of sea-level rise on different reefs, with some experiencing reduced bed shear stress while others may face heightened exposure to extreme hydrodynamic forces.

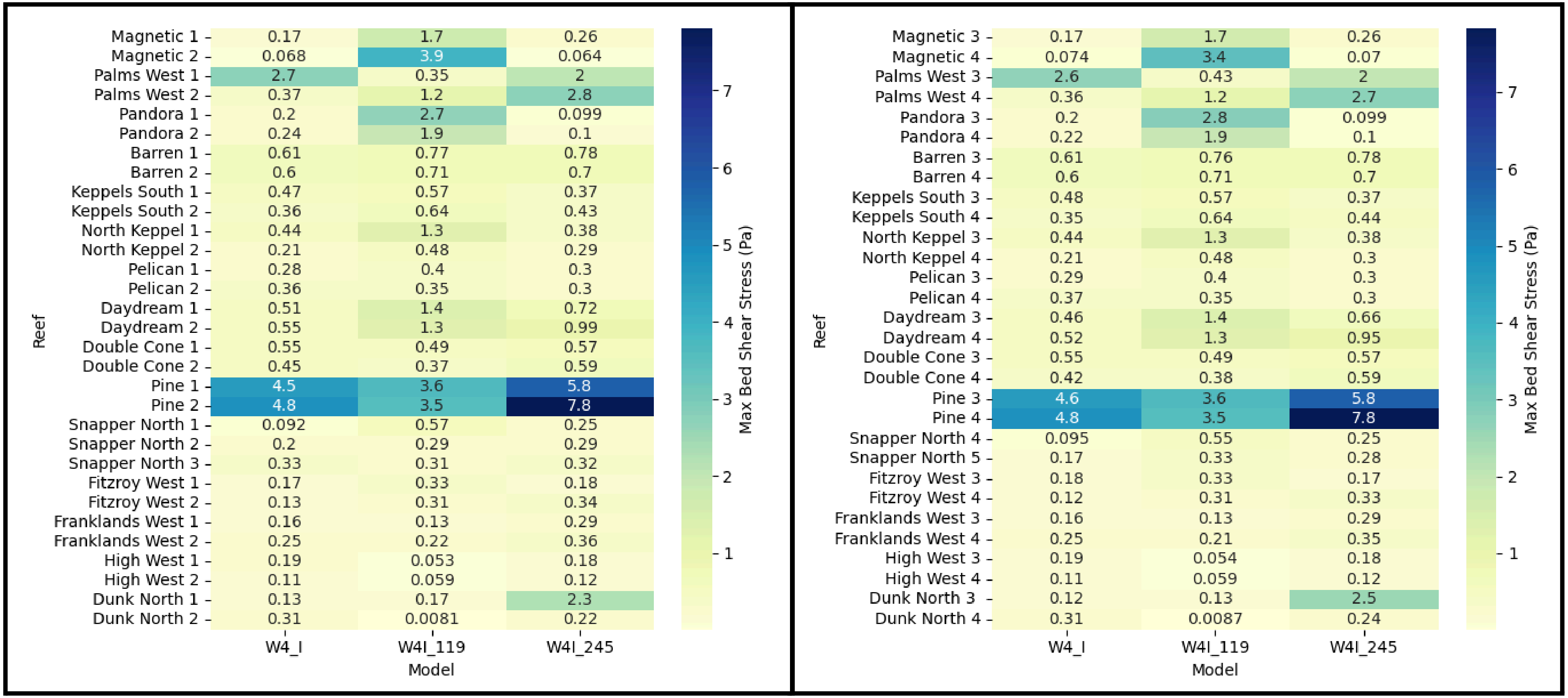

Figure 33 *Both the left and right figures are heatmaps showing the maximum bed shear stress (colour and value) extracted from each model (x axis) during the simulation period.*

4.3.3 | Tidal vs Cyclonic Bed Shear Stress Change in Magnitude

The average change in bed shear stress magnitude (from a tide-only environment to a tide and wind environment) for each scenario provides insight into the potential impact of SLR on bed shear stress across the GBR in the future (*Figure 34*). For the W4_I model, the average change in bed shear stress magnitude across all reefs is 0.173 Pa. This increases to 0.314 Pa under the W4I_119 scenario (SSP1-1.9); however, this decreases to 0.293 Pa for the W4I_245 scenario (SSP2-4.5). These results suggest that while sea level rise can increase changes in bed shear stress, the magnitude of this change may vary depending on the specific climate scenario.

For most reefs, the change in bed shear stress magnitude between the tide-only (T4_I and T4I_119) and the tide and wind (W4_I and *W4I_119)* models is highly varied for the W4I_119 model when compared to the W4_I model. For example, at Palms West 1, the change in bed shear stress magnitude is 0.062 Pa in *W4I_119*, compared to 0.53 Pa in *W4_I*, indicating a significant reduction in the change in magnitude between the tide-only and the tide and wind model under the SSP1–1.9 sea level rise scenario. Conversely, reefs such as North Keppel 1 show an increase in the change in bed shear stress magnitude, with 0.23 Pa in W4_I compared to 0.62 Pa in W4I_119, suggesting that bathymetric changes under SSP1-1.9 can alter the interaction of wind and tidal forces differently across reefs.

This is also found for most reefs when comparing the change in bed shear stress magnitude between the tide-only (T4_I and T4I_245) and the tide and wind (W4_I and *W4I_245)* models. For example, at Pine 3, the change in bed shear stress magnitude is 0.69 Pa in *W4I_245*, compared to 1.1 Pa in *W4_I*, indicating an increase in the change in magnitude between the tide-only and the tide and wind model under the SSP2–4.5 sea level rise scenario. However, reefs such as Keppels South 1 show a decrease in the change in bed shear stress magnitude, with 0.12 Pa in W4_I compared to 0.093 Pa in W4I_245. These results demonstrate that whilst some reefs experience reduced bed shear stress magnitude as a result of the altered bathymetry, others show an increase, highlighting the localized impacts of future bathymetric changes on bed shear stress dynamics during TC events

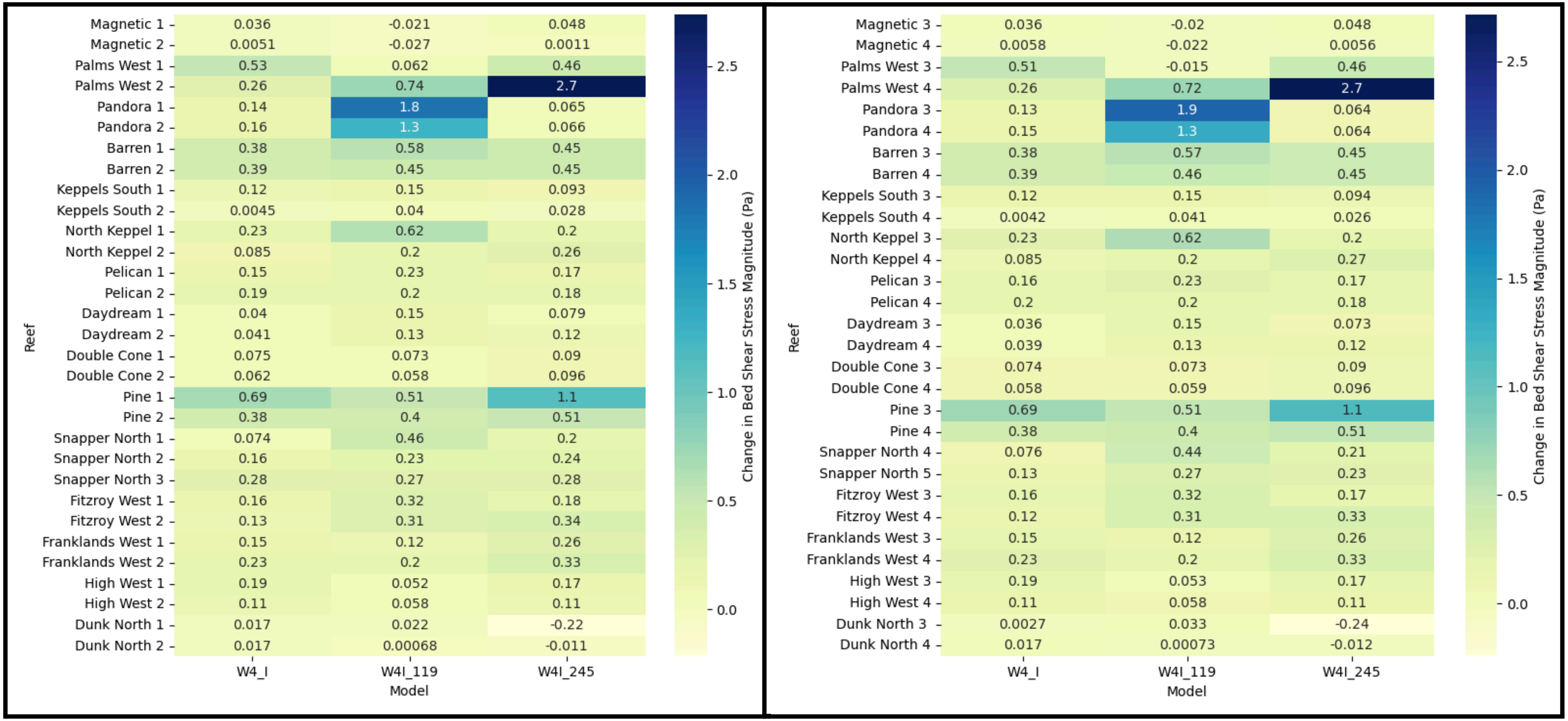

Figure 34 *Heatmap showing the change in bed shear stress magnitude calculated between the extracted maximum bed shear stress from the tide-only models (T4_I, T4I_119 and T4I_245) and the corresponding tide and wind models (W4_I, W4I_119 and W4I_245) for each scenario.*

4.3.4 | Relationship between depth and bed shear stress

The results of the Shapiro-Wilk Normality test are summarised in *Table 19*. The results demonstrate that both maximum bed shear stress and the change in bed shear stress magnitude significantly deviate from normality ($p < 0.001$). This suggests that non-parametric statistical methods are more appropriate for further analysis of the data.

Table 19 *Results of the Shapiro-Wilk Normality test for maximum bed shear stress and change in bed shear stress magnitude (NS – not significant ($p > 0.05$); * - significant to $p \leq 0.05$; ** - significant to $p \leq 0.01$; *** - significant to $p \leq 0.001$).*

Measurement of BSS	Shapiro-Wilk Result
Maximum	**0.59*****
Change in Magnitude	**0.60*****

The results of the Kendall Tau's analysis examining the relationship between the reef depth and the maximum bed shear stress and change in bed shear stress magnitude modelled at each reef during each scenario is presented in *Table 20*, with corresponding graphs presented in *Figure 35*.

Table 20 *Results of the Kendall Tau's statistical analysis between the reef depth and the modelled maximum bed shear stress and change in bed shear stress magnitude at each reef for each scenario (current-day bathymetry; varied bathymetry for SSP1-1.9 sea level projection; and varied bathymetry for SSP2-4.5 sea level projection) (NS – not significant ($p > 0.05$); * - significant to $p \leq 0.05$; ** - significant to $p \leq 0.01$; *** - significant to $p \leq 0.001$).*

Measurement of BSS	Kendall Tau Result
Maximum	-0.095^{NS}
Change in Magnitude	**-0.105^{*}**

The results reveal a weak insignificant negative relationship between the measured depth at each reef and the maximum bed shear stress modelled at each reef for each scenario of sea-level (τ = -0.095, $p > 0.05$). However, a significant negative relationship is found between the measured depth at each reef and the change in bed shear stress magnitude modelled at each reef for each scenario of sea-level (τ = -0.105, $p < 0.05$).

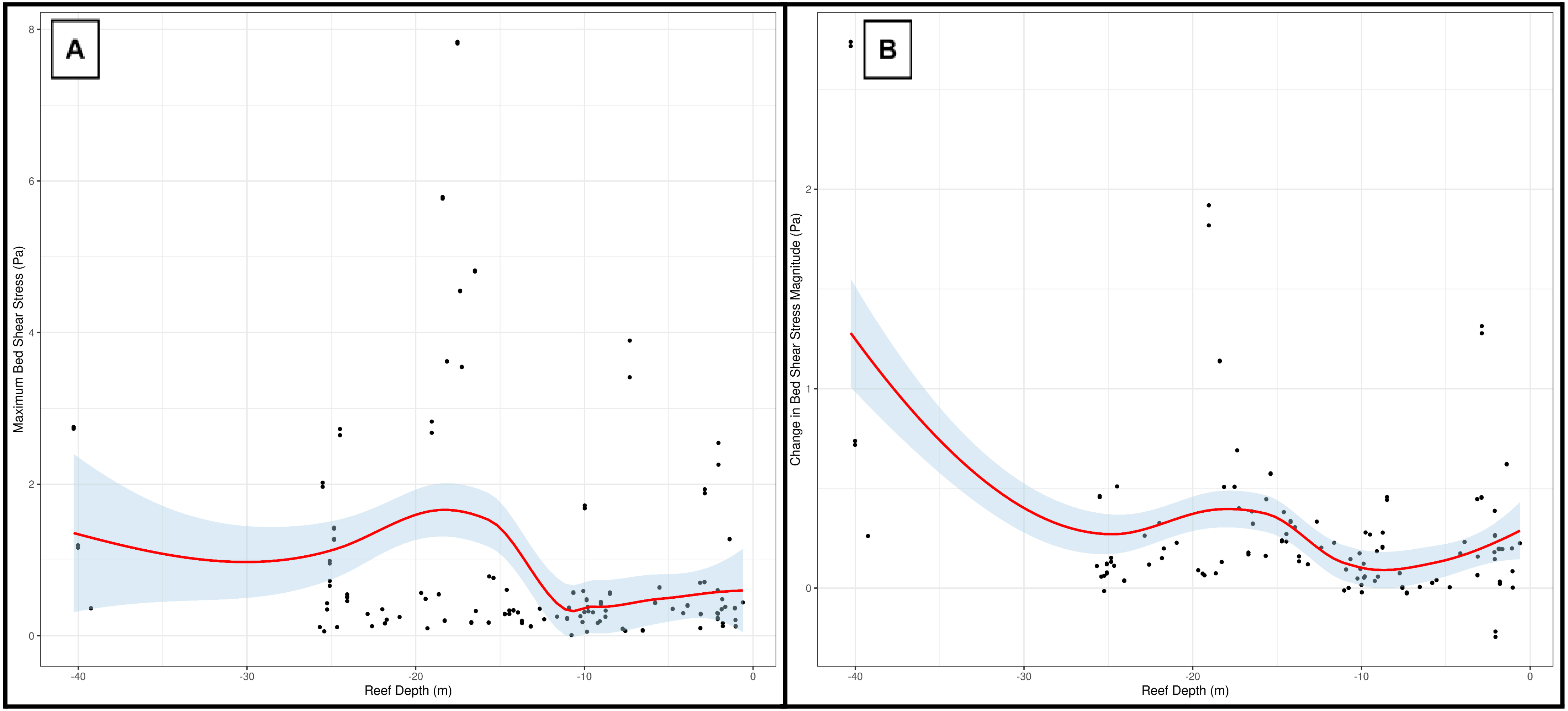

Figure 35 *Graphs showing the relationship between the reef depth and **(A)** the maximum bed shear stress and **(B)** the change in bed shear stress magnitude modelled at each reef during each scenario with Loess curves added to visualise trends in the data.*

4.4 | Discussion

4.4.1 | Implications of Sea-Level Rise on Coral Reefs

The model results show the change in depth, maximum bed shear stress and change in bed shear stress magnitude to vary at each reef for both scenarios. Some studies have explored the impacts of future sea-level rise on coral reefs; however, few have investigated the effects of tropical cyclones under future SLR scenarios.

A one-dimensional wave model was used to investigate the changes in reef top wave dynamics and wave forces for different scenarios of sea-level rise under non-cyclonic and cyclonic conditions (T. E. Baldock et al. 2014). The model results predicted that the impacts of SLR vary spatially and are strongly influenced by the bathymetry of the reef and coral type . The study found that while wave heights increased under SLR, changes in the wave-induced velocity were more complex as the changes varied reef by reef . For many reef bathymetries, wave orbital velocities increased with SLR during average wave conditions and cyclonic wave forces were reduced for certain coral species . Therefore, SLR was generally found to be beneficial as cyclonic wave forces decreased at all locations implying a reduced risk of cyclone damage in the future (T. E. Baldock et al. 2014). Across multiple reefs examined in this study, the cyclonic-induced maximum bed shear stress was increased for both SLR scenarios (W4I_119 and W4I_245 - 0.976 Pa and 0.985 Pa, respectively) when compared to the modern simulation suggesting that SLR may provide a form of natural protection to reef structures by mitigating cyclonic wave-induced stresses. However, predicting the impact of SLR on individual reefs requires consideration of the reef bathymetry, the reef zone and the type of coral species. I also neglect to account for coral growth during the time taken for sea-level rise. Although small, this could impact peak bed shear stress.

The analysis for this research revealed a significant negative relationship between the response of the change in bed shear stress magnitude from a tide-only to a tide and wind environment and the measured depth at each reef across each scenario of sea-level. This result indicates that as reef depth increases, the change in bed shear stress magnitude also increases. Consequently, this implies that deeper reefs are more affected by cyclonic forces as a result of their exposure to reduced tidal forces, which may put fragile, deeper corals at greater risk in the future. In contrast, for shallow reefs, the impact of cyclonic forces is comparable to that of tidal forces, as the changes in bed shear stress magnitude are smaller. This suggests that shallower reefs might be less affected by cyclonic forces in future sea-level rise scenarios.

4.5 | Conclusions

In conclusion, this study presents valuable insights into the impacts of SLR on reef depth and TC-induced bed shear stress with the results showing that the response of bed shear stress to SLR varies across different reefs. In future research, it is essential to consider reef bathymetry and coral species when assessing the impacts of SLR and TCs on coral reef ecosystems. Reef bathymetry is important for how wave energy and bed shear stress affect the seabed, with deeper reefs experiencing stronger cyclonic bed shear stress than shallower ones. The type of coral species is also important, as different species respond differently to hydrodynamic forces and TCs. Some coral species are more resilient to stress, while others may increase or decrease the impact of bed shear stress on the reef. It is important to note that generalising results across all reefs is difficult because each reef has different bathymetry, coral species, and environmental conditions, meaning the effects of SLR and TCs will vary from reef to reef and therefore studying individual reefs will provide a more accurate understanding of how they will respond to future SLR.

Chapter 5 | Conclusions

This project successfully modelled multiple TCs over the GBR, with Thetis demonstrating an adequate ability to model storm surge events. Bed shear stress data was generated successfully from the models and was used as a proxy for coral reef damage, alongside coral cover data before and after the TC impact to determine the extent of coral reef damage. The statistical analysis revealed significant trends in the response of algae and “other” to bed shear stress. Particularly, algae cover was found to significantly increase as bed shear stress intensified ($\tau = 0.19$, $p < 0.001$), while “other” showed a significant decrease in response to higher bed shear stress ($\tau = -0.22$, $p < 0.001$). These findings suggest a shift in reef composition, where the mechanical forces from TC-induced bed shear stress may reduce the abundance of sponges, sand, silt and rock, possibly as a result of dislodgement or physical damage and facilitate algal growth within the space created. This study found no significant changes in hard or soft coral cover after the passage of the four TCs; however, previous studies have reported significant changes in hard coral cover following the occurrence of a TC suggesting that variations in methodology can influence the assessment of TC impacts on coral reefs.

This project also successfully simulated TCs over the GBR using varied bathymetry based on the IPCC AR6 SSP projections for SLR (SSP1-1.9 and SSP2-4.5) to determine the possible impacts that SLR could have on bed shear stress in the future. The analysis for this research revealed a significant negative relationship between the response of the change in bed shear stress magnitude from a tide-only to a tide and wind environment and the measured depth at each reef across each scenario of sea-level. The results indicate that as reef depth increases, the change in bed shear stress magnitude also increases. This implies that deeper reefs are more affected by cyclonic forces as a result of their exposure to reduced tidal forces, which may put fragile, deeper corals at greater risk in the future. However, for shallow reefs, the impact of cyclonic forces is comparable to that of tidal forces, as the changes in bed shear stress magnitude were smaller. This suggests that shallower reefs might be less affected by cyclonic forces in future sea-level rise scenarios.

In conclusion, understanding the impacts of TCs on coral reefs requires considering all aspects of disturbance, along with the unique characteristics of individual reefs and coral species, emphasizing the importance of a holistic approach. Coral reefs across the GBR are affected by numerous ecological disturbances every year, including TCs, COTS infestations, coral disease, coral bleaching and anthropogenic-induced disturbances. Different disturbances do not impact all reefs, and during a disturbance event each reef rarely experiences equal severity of effects (Berkelmans et al. 2004). Studying reefs individually is vital for future research, as broad generalisations can overlook critical variations. When combined with other stressors the threats to coral reefs are further amplified therefore this underscores the urgent need for integrated conservation and management strategies to address these multiple, compounding threats to coral reef ecosystems (Uthicke et al., 2016). Additionally, climate change driven by anthropogenic activities is expected to increase the frequency and severity of coral bleaching events, as well as the occurrence of high-intensity TCs (Hoegh-Guldberg et al., 2007). As a result, coral reef communities will face more frequent disturbances with shorter recovery intervals (Nyström et al., 2000). This highlights the critical importance of researching the potential future impacts of TCs on coral reefs under various predicted climate scenarios to better understand the long-term consequences and inform conservation strategies in a changing climate.

Bibliography

Adcroft, Alistair, and David Marshall. 1998. “How Slippery Are Piecewise-Constant Coastlines in Numerical Ocean Models?” *Tellus A Dynamic Meteorology and Oceanography* 50 (1): 95.

AIMS. 2024a. “*Long-Term Monitoring Program Annual Summary Report of Coral Reef Condition 2023/24*.” AIMS. 2024a. https://www.aims.gov.au/monitoring-great-barrier-reef/gbr-condition-summary-2023-24.

———. 2014. “Great Barrier Reef Marine Monitoring Program - Coral (MMP).” https://doi.org/10.25845/5cc64f29b35a1.

———. 2021. “AIMS Long-Term Monitoring Program: Crown-of-Thorns Starfish and Benthos Manta Tow Data (Great Barrier Reef).” AIMS. 2021. https://apps.aims.gov.au/metadata/view/5bb9a340-4ade-11dc-8f56-00008a07204e.

———. 2023. “*Long-Term Monitoring Program Annual Summary Report of Coral Reef Condition 2022/23*.” AIMS. 2023. https://www.aims.gov.au/monitoring-great-barrier-reef/gbr-condition-summary-2022-23.

———. 2024a. “AIMS Reef Reporting Dashboard.” AIMS. 2024. https://apps.aims.gov.au/reef-monitoring/.

———. 2024b. “Great Barrier Reef Marine Monitoring Program - Coral (MMP).” AIMS. 2024. https://apps.aims.gov.au/metadata/view/c30cfb2d-46be-4837-9733-9bb60489b65b.

Akbar, Muhammad, and Shahrouz Aliabadi. 2013. “Hybrid Numerical Methods to Solve Shallow Water Equations for Hurricane Induced Storm Surge Modeling.” *Environmental Modelling & Software: With Environment Data News* 46 (August):118–28.

Angwenyi, Clive Migosi, and Lars Rydberg. 2005. “Wave-Driven Circulation across the Coral Reef at Bamburi Lagoon, Kenya.” *Estuarine, Coastal and Shelf Science* 63 (3): 447–54.

Arias, Paola & Bellouin, Nicolas & Coppola, Erika & Jones, Christopher & Krinner, Gerhard & Marotzke, Jochem & Naik, Vaishali & Plattner, Gian-Kasper & Rojas, Maisa & Sillmann, Jana & Storelvmo, Trude & Thorne, Peter & Trewin, Blair & Achutarao, Krishna & Adhikary, Bhupesh & Armour, Kyle & Govindasamy, Balasubramanian & Barimalala, Rondrotiana & Berger, Sophie & Zickfeld, Kirsten. 2021. “Climate Change 2021: Physical Science Basis. Contribution Working Group I Sixth Assessment Report Intergovernmental Panel Climate Change.” In .

Australian Hydrographic Office. 2020. “AusTides (AHP114).” Australian Hydrographic Office. 2020. https://www.hydro.gov.au/prodserv/publications/ausTides/tides.htm.

Avdis, Alexandros, Adam S. Candy, Jon Hill, Stephan C. Kramer, and Matthew D. Piggott. 2018. “Efficient Unstructured Mesh Generation for Marine Renewable Energy Applications.” *Renewable Energy* 116 (February):842–56.

Bainbridge, Zoe T., Jon E. Brodie, John W. Faithful, Damon A. Sydes, and Stephen E. Lewis. 2009. “Identifying the Land-Based Sources of Suspended Sediments, Nutrients and Pesticides Discharged to the Great Barrier Reef from the Tully–Murray Basin, Queensland, Australia.” *Marine and Freshwater Research* 60 (11): 1081–90.

Baird, A. H., M. S. Pratchett, A. S. Hoey, Y. Herdiana, and S. J. Campbell. 2013. “Acanthaster Planci Is a Major Cause of Coral Mortality in Indonesia.” *Coral Reefs* 32 (3): 803–12.

Baldock, T. E., A. Golshani, D. P. Callaghan, M. I. Saunders, and P. J. Mumby. 2014. “Impact of Sea-Level Rise and Coral Mortality on the Wave Dynamics and Wave Forces on Barrier Reefs.” *Marine Pollution Bulletin* 83 (1): 155–64.

Baldock, Tom E., Behnam Shabani, David P. Callaghan, Zhifang Hu, and Peter J. Mumby. 2020. “Two-Dimensional Modelling of Wave Dynamics and Wave Forces on Fringing Coral Reefs.” *Coastal Engineering* 155 (January):103594.

Beaman, R. J. 2010. *3DGBR: High-Resolution Depth Model Great Barrier Reef Coral Sea. Marine Tropical Sciences Facility (MTSRF) Project, 2, 13*.

Beeden, Roger, Jeffrey Maynard, Marjetta Puotinen, Paul Marshall, Jen Dryden, Jeremy Goldberg, and Gareth Williams. 2015. “Impacts and Recovery from Severe Tropical Cyclone Yasi on the Great Barrier Reef.” *PloS One* 10 (4): e0121272.

Bellwood, D. R., and T. P. Hughes. 2001. “Regional-Scale Assembly Rules and Biodiversity of Coral Reefs.” *Science* 292 (5521): 1532–35.

Berkelmans, Ray, Glenn De’ath, Stuart Kininmonth, and William J. Skirving. 2004. “A Comparison of the 1998 and 2002 Coral Bleaching Events on the Great Barrier Reef: Spatial Correlation, Patterns, and Predictions.” *Coral Reefs* 23 (1): 74–83.

Berkelmans, R., and J. K. Oliver. 1999. “Large-Scale Bleaching of Corals on the Great Barrier Reef.” *Coral Reefs* 18 (1): 55–60.

BOM. 2019. “*Severe Tropical Cyclone Lua 10-18 March 2012*.” BOM. 2019. http://www.bom.gov.au/cyclone/history/pdf/Lua_report.pdf.

———. 2024. “*Tropical Cyclone Databases*.” BOM. 2024. http://www.bom.gov.au/cyclone/tropical-cyclone-knowledge-centre/databases/.

Booij, N., R. C. Ris, and L. H. Holthuijsen. 1999. “A Third-generation Wave Model for Coastal Regions: 1. Model Description and Validation.” *Journal of Geophysical Research* 104 (C4): 7649–66.

Boose, Emery R., David R. Foster, and Marcheterre Fluet. 1994. “Hurricane Impacts to Tropical and Temperate Forest Landscapes.” *Ecological Monographs* 64 (4): 369–400.

Boose E.R., Serrano M.I., and Foster D.R. 2004. “Landscape and Regional Impacts of Hurricanes in Puerto Rico.pdf.” *Ecological Monographs* 74 (2): 335–52.

Bostock H, Ryan D, Brooke B, Skene D, Hancock G. 2006. “Holocene Evolution and Modern Sediment Accumulation on a Tropical Macro-Tidal Coast: Keppel Bay, Central Queensland, Australia.” 50. Indooroopilly, Australia: Cooperative Research Centre for Coastal Zone, Estuary and Waterway Management (Coastal CRC).

Boudreau, Kaitlyn, Melanie Robinson, and Zahrah Farooqi. 2022. “IPCC Sixth Assessment Report.” *Canadian Journal of Emergency Management* 2 (1). https://doi.org/10.25071/6sw6za31.

Brown, B. E. 1997. “Coral Bleaching: Causes and Consequences.” *Coral Reefs* 16 (1): S129–38.

Burke L., Reytar K., Spalding M., Perry A. 2011. *Reefs at Risk Revisited*. Washington, DC: World Resources Institute.

Busby, Posy E., Glenn Motzkin, and Emery R. Boose. 2008. “Landscape-Level Variation in Forest Response to Hurricane Disturbance across a Storm Track.” *Canadian Journal of Forest Research. Journal Canadien de La Recherche Forestiere* 38 (12): 2942–50.

Callaghan, David P., Peter J. Mumby, and Matthew S. Mason. 2020. “Near-Reef and Nearshore Tropical Cyclone Wave Climate in the Great Barrier Reef with and without Reef Structure.” *Coastal Engineering* 157 (103652): 103652.

Cardone, V. J., T. Cox, J. Greenwood, and E. F. Thompson. 1994. *Upgrade Tropical Cyclone Surface Wind Field Model. Miscellaneous Paper CERC-94-14*.

Carpenter, Kent E., Muhammad Abrar, Greta Aeby, Richard B. Aronson, Stuart Banks, Andrew Bruckner, Angel Chiriboga, et al. 2008. “One-Third of Reef-Building Corals Face Elevated Extinction Risk from Climate Change and Local Impacts.” *Science* 321 (5888): 560–63.

Castro-Sanguino, C., Y-M Bozec, D. Callaghan, J. Vercelloni, A. Rodriguez-Ramirez, S. Lopez-Marcano, Y. Gonzalez-Marrero, M. Puotinen, O. Hoegh-Guldberg, and M. Gonzalez-Rivero. 2022. “Coral Composition and Bottom-Wave Metrics Improve Understanding of the Patchiness of Cyclone Damage on Reefs.” *The Science of the Total Environment* 804 (January):150178.

Chappell, John. 1980. “Coral Morphology, Diversity and Reef Growth.” *Nature* 286 (5770): 249–52.

Cheal, A., G. Coleman, S. Delean, I. Miller, K. Osborne, and H. Sweatman. 2002. “Responses of Coral and Fish Assemblages to a Severe but Short-Lived Tropical Cyclone on the Great Barrier Reef, Australia.” *Coral Reefs* 21 (2): 131–42.

Cheal, A. J., M. Aaron MacNeil, E. Cripps, M. J. Emslie, M. Jonker, B. Schaffelke, and H.

Sweatman. 2010. “Coral–macroalgal Phase Shifts or Reef Resilience: Links with Diversity and Functional Roles of Herbivorous Fishes on the Great Barrier Reef.” *Coral Reefs* 29 (4): 1005–15.
Cheal, Alistair J., M. Aaron MacNeil, Michael J. Emslie, and Hugh Sweatman. 2017. “The Threat to Coral Reefs from More Intense Cyclones under Climate Change.” *Global Change Biology* 23 (4): 1511–24.
Christensen, J. H., K. K. Kanikicharla, E. Aldrian, S. I. Cavalcanti, I. F. De Castro, M. Dong, W. Goswami, P. Hall, and J. K. Kanyanga. 2013. “Climate Phenomena Relevance Future Regional Climate Change. : Climate Change 2013 – Physical Science Basis.” *Physical Science Basis* 9781107057999:1217–1308.
Connell, J. H. 1997. “Disturbance and Recovery of Coral Assemblages.” *Coral Reefs* 16 (0): S101–13.
Copernicus. 2024. “*ERA5 Hourly Data on Single Levels from 1940 to Present*.” Copernicus. 2024.
https://cds.climate.copernicus.eu/cdsapp#!/dataset/reanalysis-era5-single-levels?tab=overview.
Cuttler, M. V. W., J. E. Hansen, R. J. Lowe, and E. J. F. Drost. 2018. “Response of a Fringing Reef Coastline to the Direct Impact of a Tropical Cyclone.” *Limnology and Oceanography Letters* 3 (2): 31–38.
De’ath, Glenn, Katharina E. Fabricius, Hugh Sweatman, and Marji Puotinen. 2012. “The 27–year Decline of Coral Cover on the Great Barrier Reef and Its Causes.” *Proceedings of the National Academy of Sciences* 109 (44): 17995–99.
Do, Cameron, Georgia Elizabeth Saunders, and Yuriy Kuleshov. 2022. “Assessment of Tropical Cyclone Risk to Coral Reefs: Case Study for Australia.” *Remote Sensing* 14 (23): 6150.
Done, T. J. 1982. “Patterns in the Distribution of Coral Communities across the Central Great Barrier Reef.” *Coral Reefs* 1 (2): 95–107.
———. 1992. “Phase Shifts in Coral Reef Communities and Their Ecological Significance.” *Hydrobiologia* 247 (1): 121–32.
Done, T. J., L. M. DeVantier, E. Turak, D. A. Fisk, M. Wakeford, and R. van Woesik. 2010. “Coral Growth on Three Reefs: Development of Recovery Benchmarks Using a Space for Time Approach.” *Coral Reefs* 29 (4): 815–33.
Drost, Edwin J. F., Ryan J. Lowe, Greg N. Ivey, and Nicole L. Jones. 2018. “Wave-Current Interactions in the Continental Shelf Bottom Boundary Layer of the Australian North West Shelf during Tropical Cyclone Conditions.” *Continental Shelf Research* 165 (August):78–92.
Duce, S., A. Vila-Concejo, S. M. Hamylton, J. M. Webster, E. Bruce, and R. J. Beaman. 2016. “A Morphometric Assessment and Classification of Coral Reef Spur and Groove Morphology.” *Geomorphology (Amsterdam, Netherlands)* 265 (July):68–83.
Egbert, Gary D., and Svetlana Y. Erofeeva. 2002. “Efficient Inverse Modeling of Barotropic Ocean Tides.” *Journal of Atmospheric and Oceanic Technology* 19 (2): 183–204.
Emanuel, Kerry A. 2013. “Downscaling CMIP5 Climate Models Shows Increased Tropical Cyclone Activity over the 21st Century.” *Proceedings of the National Academy of Sciences of the United States of America* 110 (30): 12219–24.
Emanuel, Kerry, Ragoth Sundararajan, and John Williams. 2008. “Hurricanes and Global Warming: Results from Downscaling IPCC AR4 Simulations.” *Bulletin of the American Meteorological Society* 89 (3): 347–68.
Endean, R. 1969. *Report Investigations Made Aspects Current Acanthaster Planci (Crown-Ofthorns) Infestations Certain Reefs Great Barrier Reef. Queensland Department Primary Industries (Fisheries Branch)*. Brisbane.
Fabricius, Katharina, Glenn De’ath, Laurence McCook, Emre Turak, and David Mcb Williams. 2005. “Changes in Algal, Coral and Fish Assemblages along Water Quality Gradients on the Inshore Great Barrier Reef.” *Marine Pollution Bulletin* 51 (1-4): 384–98.
Fabricius, Katharina E., Glenn De’ath, Marji Lee Puotinen, Terry Done, Timothy F. Cooper, and Scott C. Burgess. 2008. “Disturbance Gradients on Inshore and Offshore Coral

Reefs Caused by a Severe Tropical Cyclone." *Limnology and Oceanography* 53 (2): 690–704.
Fabricius, K. E., K. Okaji, and G. De'ath. 2010. "Three Lines of Evidence to Link Outbreaks of the Crown-of-Thorns Seastar Acanthaster Planci to the Release of Larval Food Limitation." *Coral Reefs* 29 (3): 593–605.
Faxneld, Suzanne, Tove L. Jörgensen, and Michael Tedengren. 2010. "Effects of Elevated Water Temperature, Reduced Salinity and Nutrient Enrichment on the Metabolism of the Coral Turbinaria Mesenterina." *Estuarine, Coastal and Shelf Science* 88 (4): 482–87.
Fitt, William, Barbara Brown, Mark Warner, and Richard Dunne. 2001. "Coral Bleaching: Interpretation of Thermal Tolerance Limits and Thermal Thresholds in Tropical Corals." *Coral Reefs* 20 (1): 51–65.
Fox-Kemper, B., H. T. Hewitt, C. Xiao, G. Aðalgeirsdóttir, S. S. Drijfhout, T. L. Edwards, N. R. Golledge, et al. n.d. *2021: Ocean, Cryosphere Sea Level Change. Climate Change 2021: Physical Science Basis. Contribution Working Group I Sixth Assessment Report Intergovernmental Panel Climate Change*. Edited by I. Gomis, M. Huang, K. Leitzell, E. Lonnoy, J. B. R. Matthews, T. K. Maycock, T. Waterfield, O. Yelekçi, R. Yu, and B. Zhou. Cambridge, United Kingdom New York, NY, USA: Cambridge University Press.
Gallop, Shari L., Ian R. Young, Roshanka Ranasinghe, Tom H. Durrant, and Ivan D. Haigh. 2014. "The Large-Scale Influence of the Great Barrier Reef Matrix on Wave Attenuation." *Coral Reefs* 33 (4): 1167–78.
Gardner, Toby A., Isabelle M. Côté, Jennifer A. Gill, Alastair Grant, and Andrew R. Watkinson. 2005. "Hurricanes and Caribbean Coral Reefs: Impacts, Recovery Patterns, and Role in Long-Term Decline." *Ecology* 86 (1): 174–84.
Garner, G. G., T. Hermans, R. E. Kopp, A. B. A. Slangen, T. L. Edwards, A. Levermann, S. Nowicki, et al. 2021. "IPCC AR6 Sea Level Projections." Zenodo. https://doi.org/10.5281/ZENODO.5914709.
GBRMPA. 2009. *Great Barrier Reef Outlook Report 2009*. Townsville, QLD, Australia: Great Barrier Reef Marine Park Authority.
———. 2010. "Marine Shipping Incident: Great Barrier Reef Marine Park - Douglas Shoal." Great Barrier Reef Marine Park Authority. 2010. https://elibrary.gbrmpa.gov.au/jspui/retrieve/be1d646c-a013-41d1-9570-1270dfe4bd46/Shen-Neng-information-sheet-4.pdf.
———. 2011. "Impacts of Tropical Cyclone Yasi on the Great Barrier Reef: A Report on the Findings of a Rapid Ecological Impact Assessment, July 2011." https://elibrary.gbrmpa.gov.au/jspui/handle/11017/447.
Geuzaine, Christophe, and Jean-François Remacle. 2009. "Gmsh: A 3-D Finite Element Mesh Generator with Built-in Pre- and Post-processing Facilities." *International Journal for Numerical Methods in Engineering* 79 (11): 1309–31.
Grady, A. E., L. J. Moore, C. D. Storlazzi, E. Elias, and M. A. Reidenbach. 2013. "The Influence of Sea Level Rise and Changes in Fringing Reef Morphology on Gradients in Alongshore Sediment Transport." *Geophysical Research Letters* 40 (12): 3096–3101.
Graham, Nicholas A. J., Karen M. Chong-Seng, Cindy Huchery, Fraser A. Januchowski-Hartley, and Kirsty L. Nash. 2014. "Coral Reef Community Composition in the Context of Disturbance History on the Great Barrier Reef, Australia." *PloS One* 9 (7): e101204.
Greenslade D, Taylor A, Freeman J, Sims H, Schulz E, Colberg F, Divakaran P, Velic M and Kepert J. 2018. "First Generation Dynamical Tropical Cyclone Storm Surge Forecast System Part 1: Hydrodynamic Model." Australian Government Bureau of Meteorology. http://www.bom.gov.au/research/publications/researchreports/BRR-031.pdf.
Guillemot, N., P. Chabanet, and O. Le Pape. 2010. "Cyclone Effects on Coral Reef Habitats in New Caledonia (South Pacific)." *Coral Reefs* 29 (2): 445–53.
Haapkylä, J., J. Melbourne-Thomas, M. Flavell, and B. L. Willis. 2013. "Disease Outbreaks, Bleaching and a Cyclone Drive Changes in Coral Assemblages on an Inshore Reef of the Great Barrier Reef." *Coral Reefs* 32 (3): 815–24.
Ham, DA, Kelly, PHJ, Mitchell, L, Cotter, C, Kirby, RC, Sagiyama, K, Bouziani, N,

Vorderwuelbecke, S, Gregory, T, Betteridge, J, Shapero, DR, Nixon-Hill, R, Ward, C, Farrell, PE, Brubeck, PD, Marsden, I, Gibson, TH, Homolya, M, Sun, T, McRae, ATT, Luporini, F, Gregory, A, Lange, M, Funke, SW, Rathgeber, F, Bercea, G-T Markall, GR. 2023. “Firedrake User Manual.” Firedrake User Manual. https://spiral.imperial.ac.uk/handle/10044/1/104839.

Hardy, T. A., I. R. Young, R. C. Nelson, and M. R. Gourlay. 1991. “Wave Attenuation on an Offshore Coral Reef.” In *Coastal Engineering 1990*. New York, NY: American Society of Civil Engineers. https://doi.org/10.1061/9780872627765.027.

Hardy, Thomas A., Jason D. McConochie, and Luciano B. Mason. 2003. “Modeling Tropical Cyclone Wave Population of the Great Barrier Reef.” *Journal of Waterway, Port, Coastal and Ocean Engineering* 129 (3): 104–13.

Hardy, Thomas A., and Ian R. Young. 1996. “Field Study of Wave Attenuation on an Offshore Coral Reef.” *Journal of Geophysical Research* 101 (C6): 14311–26.

Harmelin-Vivien, Mireille L. 1994. “The Effects of Storms and Cyclones on Coral Reefs: A Review.” *Journal of Coastal Research*, 211–31.

Harter, Craig, and Jens Figlus. 2017. “Numerical Modeling of the Morphodynamic Response of a Low-Lying Barrier Island Beach and Foredune System Inundated during Hurricane Ike Using XBeach and CSHORE.” *Coastal Engineering* 120 (February):64–74.

Hill, J. Letter to H. Smith. 2024, 2024.

Hill, Jon. 2019. “HRDS: A Python Package for Hierarchical Raster Datasets.” *Journal of Open Source Software* 4 (37): 1112.

Hoegh-Guldberg, O., D. Jacob, M. Taylor, M. Bindi, S. Brown, I. Camilloni, R. Djalante, K. L. Ebi, and F. Engelbrecht. 2018. *Global Warming 1.5°C. IPCC Special Report Impacts Global Warming 1.5°C above Pre-Industrial Levels Related Global Greenhouse Gas Emission Pathways, Context Strengthening Global Response Threat Climate Change*. Edited by T. Waterfield. Cambridge: Cambridge University Press.

Hoegh-Guldberg, O., P. J. Mumby, A. J. Hooten, R. S. Steneck, P. Greenfield, E. Gomez, C. D. Harvell, et al. 2007. “Coral Reefs under Rapid Climate Change and Ocean Acidification.” *Science (New York, N.Y.)* 318 (5857): 1737–42.

Hoegh-Guldberg, Ove. 1999. “Climate Change, Coral Bleaching and the Future of the World’s Coral Reefs.” *Marine and Freshwater Research* 50 (8): 839–66.

———. 2011. “The Impact of Climate Change on Coral Reef Ecosystems.” In *Coral Reefs: An Ecosystem in Transition*, edited by Zvy Dubinsky and Noga Stambler, 391–403. Dordrecht: Springer Netherlands.

Hoeke, Ron, Kathleen McInnes, and Julian O’Grady. 2015. “Wind and Wave Setup Contributions to Extreme Sea Levels at a Tropical High Island: A Stochastic Cyclone Simulation Study for Apia, Samoa.” *Journal of Marine Science and Engineering* 3 (3): 1117–35.

Hoey, Andrew S., Emily Howells, Jacob L. Johansen, Jean-Paul A. Hobbs, Vanessa Messmer, Dominique M. McCowan, Shaun K. Wilson, and Morgan S. Pratchett. 2016. “Recent Advances in Understanding the Effects of Climate Change on Coral Reefs.” *Diversity* 8 (2): 12.

Holland, Greg J. 1980. “An Analytic Model of the Wind and Pressure Profiles in Hurricanes.” *Monthly Weather Review* 108 (8): 1212–18.

Hopley, D., S. G. Smithers, and K. E. Parnell. 2007. *Geomorphology Great Barrier Reef: Development, Diversity, Change*. Cambridge: Cambridge University Press.

Huang, Hui, Yi Yang, Xiubao Li, Jianhui Yang, Jiansheng Lian, Xinming Lei, Daoru Wang, and Jing Zhang. 2014. “Benthic Community Changes Following the 2010 Hainan Flood: Implications for Reef Resilience.” *Marine Biology Research* 10 (6): 601–11.

Hubbard, Dennis K., Karla M. Parsons, John C. Bythell, and N. D. Walker. 1991. “The Effects of Hurricane Hugo on the Reefs and Associated Environments of St. Croix, U.S. Virgin Islands—A Preliminary Assessment.” *Journal of Coastal Research*, 33–48.

Hughes, Terence P., and Jason E. Tanner. 2000. “Recruitment Failure, Life Histories, and Long-Term Decline of Caribbean Corals.” *Ecology* 81 (8): 2250–63.

Hughes, Terry P., James T. Kerry, Mariana Álvarez-Noriega, Jorge G. Álvarez-Romero,

Kristen D. Anderson, Andrew H. Baird, Russell C. Babcock, et al. 2017. “Global Warming and Recurrent Mass Bleaching of Corals.” *Nature* 543 (7645): 373–77.
Hughes, Terry P., James T. Kerry, Andrew H. Baird, Sean R. Connolly, Andreas Dietzel, C. Mark Eakin, Scott F. Heron, et al. 2018. “Global Warming Transforms Coral Reef Assemblages.” *Nature* 556 (7702): 492–96.
Hughes, T. P., and J. H. Connell. 1999. “Multiple Stressors on Coral Reefs: A Long -term Perspective.” *Limnology and Oceanography* 44 (3part2): 932–40.
Huston, M. A. 1985. “Patterns of Species Diversity on Coral Reefs.” *Annual Review of Ecology and Systematics* 16 (1): 149–77.
IPCC. 2023. “Summary for Policymakers.” Climate Change 2023: Synthesis Report. Contribution of Working Groups I, II and III to the Sixth Assessment Report of the Intergovernmental Panel on Climate Change. https://doi.org/10.59327/IPCC/AR6-9789291691647.001.
Jackson, J. B., M. X. Kirby, W. H. Berger, K. A. Bjorndal, L. W. Botsford, B. J. Bourque, R. H. Bradbury, et al. 2001. “Historical Overfishing and the Recent Collapse of Coastal Ecosystems.” *Science* 293 (5530): 629–37.
Johns, K. A., K. O. Osborne, and M. Logan. 2014. “Contrasting Rates of Coral Recovery and Reassembly in Coral Communities on the Great Barrier Reef.” *Coral Reefs* 33 (3): 553–63.
Jokiel, P. L., C. L. Hunter, S. Taguchi, and L. Watarai. 1993. “Ecological Impact of a Fresh-Water ‘reef Kill’ in Kaneohe Bay, Oahu, Hawaii.” *Coral Reefs* 12 (3): 177–84.
Jones, Alison M., and Ray Berkelmans. 2014. “Flood Impacts in Keppel Bay, Southern Great Barrier Reef in the Aftermath of Cyclonic Rainfall.” *PloS One* 9 (1): e84739.
Jones, R. J., J. Bowyer, O. Hoegh-Guldberg, and L. L. Blackall. 2004. “Dynamics of a Temperature-Related Coral Disease Outbreak.” *Marine Ecology Progress Series* 281:63–77.
Kalourazi, Mehdi Yaghoobi, Seyed Mostafa Siadatmousavi, Abbas Yeganeh-Bakhtiary, and Felix Jose. 2020. “Simulating Tropical Storms in the Gulf of Mexico Using Analytical Models.” *Oceanologia* 62 (2): 173–89.
Kärnä, T., S. C. Kramer, L. Mitchell, D. Ham, M. D. Piggott, and M. Baptista. 2018. “Thetis Coastal Ocean Model: Discontinuous Galerkin Discretization Three-Dimensional Hydrostatic Equations.” *Geoscientific Model Development* 11:4359–82.
Kepert, Jeff. 2001. “The Dynamics of Boundary Layer Jets within the Tropical Cyclone Core. Part I: Linear Theory.” *Journal of the Atmospheric Sciences* 58 (17): 2469–84.
Kerswell, A. P., and R. J. Jones. 2003. “Effects of Hypo-Osmosis on the Coral Stylophora Pistillata: Nature and Cause of ‘Low-Salinity Bleaching.’” *Marine Ecology Progress Series* 253:145–54.
Knutson, Thomas, Suzana J. Camargo, Johnny C. L. Chan, Kerry Emanuel, Chang-Hoi Ho, James Kossin, Mrutyunjay Mohapatra, et al. 2020. “Tropical Cyclones and Climate Change Assessment: Part II: Projected Response to Anthropogenic Warming.” *Bulletin of the American Meteorological Society* 101 (3): E303–22.
Knutson, Thomas R., John L. McBride, Johnny Chan, Kerry Emanuel, Greg Holland, Chris Landsea, Isaac Held, James P. Kossin, A. K. Srivastava, and Masato Sugi. 2010. “Tropical Cyclones and Climate Change.” *Nature Geoscience* 3 (3): 157–63.
Knutson, Thomas R., Joseph J. Sirutis, Ming Zhao, Robert E. Tuleya, Morris Bender, Gabriel A. Vecchi, Gabriele Villarini, and Daniel Chavas. 2015. “Global Projections of Intense Tropical Cyclone Activity for the Late Twenty-First Century from Dynamical Downscaling of CMIP5/RCP4.5 Scenarios.” *Journal of Climate* 28 (18): 7203–24.
Kopp, Robert E., Gregory G. Garner, Tim H. J. Hermans, Shantenu Jha, Praveen Kumar, Alexander Reedy, Aimée B. A. Slangen, et al. 2023. “The Framework for Assessing Changes To Sea-Level (FACTS) v1.0: A Platform for Characterizing Parametric and Structural Uncertainty in Future Global, Relative, and Extreme Sea-Level Change.” *Geoscientific Model Development* 16 (24): 7461–89.
Kostaschuk, Ray, James Terry, and Rishi Raj. 2001. “Tropical Cyclones and Floods in Fiji.” *Hydrological Sciences Journal* 46 (3): 435–50.

———. 2003. “Suspended Sediment Transport during Tropical‐cyclone Floods in Fiji.” *Hydrological Processes* 17 (6): 1149–64.
Lan, Yi-Ru, and Zhi-Cheng Huang. 2024. “Numerical Modeling on Wave–current Flows and Bed Shear Stresses over an Algal Reef.” *Environmental Fluid Mechanics (Dordrecht, Netherlands: 2001)*, July. https://doi.org/10.1007/s10652-024-09994-w.
Large, W. G., and S. G. Yeager. 2009. “The Global Climatology of an Interannually Varying Air–sea Flux Data Set.” *Climate Dynamics* 33 (2-3): 341–64.
Lee, J-Y, J. Marotzke, G. Bala, L. Cao, S. Corti, J. P. Dunne, F. Engelbrecht, E. Fischer, J. C. Fyfe, and C. Jones. 2021. “Future Global Climate: Scenario-Based Projections Near-Term Information.” In *Climate Change 2021: Physical Science Basis. Contribution Working Group I Sixth Assessment Report Intergovernmental Panel Climate Change*, 553–672. Cambridge: Cambridge University Press.
Lee, Katherine C., Jody M. Webster, Tristan Salles, Eleanor E. Mawson, and Jon Hill. 2022. “Tidal Dynamics Drive Ooid Formation in the Capricorn Channel since the Last Glacial Maximum.” *Marine Geology*, November, 106944.
Leijnse, Tim Willem Bart, Alessio Giardino, Kees Nederhoff, and Sofia Caires. 2022. “Generating Reliable Estimates of Tropical-Cyclone-Induced Coastal Hazards along the Bay of Bengal for Current and Future Climates Using Synthetic Tracks.” *Natural Hazards and Earth System Sciences* 22 (6): 1863–91.
Lesser, G. R., J. A. Roelvink, J. A. T. M. van Kester, and G. S. Stelling. 2004. “Development and Validation of a Three-Dimensional Morphological Model.” *Coastal Engineering* 51 (8-9): 883–915.
Lirman, Diego, and Peggy Fong. 1997. “Patterns of Damage to the Branching Coral Acropora Palmata Following Hurricane Andrew: Damage and Survivorship of Hurricane-Generated Asexual Recruits.” *Journal of Coastal Research* 13 (1): 67–72.
Longuet-Higgins, M. S., and R. W. Stewart. 1962. “Radiation Stress and Mass Transport in Gravity Waves, with Application to ‘surf Beats.’” *Journal of Fluid Mechanics* 13 (4): 481–504.
Lough, Janice M. 2008. “10th Anniversary Review: A Changing Climate for Coral Reefs.” *Journal of Environmental Monitoring: JEM* 10 (1): 21–29.
Lough, J. M. 2007. “Tropical River Flow and Rainfall Reconstructions from Coral Luminescence: Great Barrier Reef, Australia.” *Paleoceanography* 22. https://doi.org/10.1029/2006PA001377.
Lough, J. M., and D. J. Barnes. 2000. “Environmental Controls on Growth of the Massive Coral Porites.” *Journal of Experimental Marine Biology and Ecology* 245 (2): 225–43.
Lough, J. M., S. E. Lewis, and N. E. Cantin. 2015. “Freshwater Impacts in the Central Great Barrier Reef: 1648–2011.” *Coral Reefs* 34 (3): 739–51.
Lowe, Ryan J., James L. Falter, Marion D. Bandet, Geno Pawlak, Marlin J. Atkinson, Stephen G. Monismith, and Jeffrey R. Koseff. 2005. “Spectral Wave Dissipation over a Barrier Reef.” *Journal of Geophysical Research* 110 (C4). https://doi.org/10.1029/2004jc002711.
Lugo-Fernández, Alexis, Harry H. Roberts, and Joseph N. Suhayda. 1998. “Wave Transformations across a Caribbean Fringing-Barrier Coral Reef.” *Continental Shelf Research* 18 (10): 1099–1124.
Madin, Joshua S., and Sean R. Connolly. 2006. “Ecological Consequences of Major Hydrodynamic Disturbances on Coral Reefs.” *Nature* 444 (7118): 477–80.
Mallett, W. 2000. *Dynamics Atmospheric Boundary Layer Mature Tropical Cyclone: Numerical Investigation*. PhD.
Marshall, P. A., and A. H. Baird. 2000. “Bleaching of Corals on the Great Barrier Reef: Differential Susceptibilities among Taxa.” *Coral Reefs* 19 (2): 155–63.
Masson-Delmotte, V., P. Zhai, S. L. Connors, C. Péan, S. Berger, N. Caud, Y. Chen, et al. 2021. “Summary Policymakers.” In *Climate Change 2021: Physical Science Basis. Contribution Working Group I Sixth Assessment Report Intergovernmental Panel Climate Change*, 3–32. Cambridge: Cambridge University Press.
Matthews, Samuel A., David H. Williamson, Roger Beeden, Michael J. Emslie, Rickard T. M.

Abom, Daniel Beard, Mary Bonin, et al. 2024. “Protecting Great Barrier Reef Resilience through Effective Management of Crown-of-Thorns Starfish Outbreaks.” *PloS One* 19 (4): e0298073.
Mawson, Eleanor E., Katherine C. Lee, and Jon Hill. 2022. “Sea Level Rise and the Great Barrier Reef the Future Implications on Reef Tidal Dynamics.” *Journal of Geophysical Research, C: Oceans*, July. https://doi.org/10.1029/2021jc017823.
Maynard, J. A., K. R. N. Anthony, C. D. Harvell, M. A. Burgman, R. Beeden, H. Sweatman, S. F. Heron, J. B. Lamb, and B. L. Willis. 2011. “Predicting Outbreaks of a Climate-Driven Coral Disease in the Great Barrier Reef.” *Coral Reefs* 30 (2): 485–95.
McBride, J. L., and T. D. Keenan. 1982. “Climatology of Tropical Cyclone Genesis in the Australian Region.” *Journal of Climatology* 2 (1): 13–33.
McConochie, Jason D., Thomas A. Hardy, and Luciano B. Mason. 2004. “Modelling Tropical Cyclone over-Water Wind and Pressure Fields.” *Ocean Engineering* 31 (14-15): 1757–82.
Meinshausen, Malte, Zebedee R. J. Nicholls, Jared Lewis, Matthew J. Gidden, Elisabeth Vogel, Mandy Freund, Urs Beyerle, et al. 2020. “The Shared Socio-Economic Pathway (SSP) Greenhouse Gas Concentrations and Their Extensions to 2500.” *Geoscientific Model Development* 13 (8): 3571–3605.
Miller, I. 1996. “Black Band Disease on the Great Barrier Reef.” *Coral Reefs* 15 (5).
Monismith, Stephen G., Liv M. M. Herdman, Soeren Ahmerkamp, and James L. Hench. 2013. “Wave Transformation and Wave-Driven Flow across a Steep Coral Reef.” *Journal of Physical Oceanography* 43 (7): 1356–79.
Murakami, Hiroyuki, Thomas L. Delworth, William F. Cooke, Ming Zhao, Baoqiang Xiang, and Pang-Chi Hsu. 2020. “Detected Climatic Change in Global Distribution of Tropical Cyclones.” *Proceedings of the National Academy of Sciences of the United States of America* 117 (20): 10706–14.
Murray, R. J., and L. R. Ford. 1983. “Problems Analysis Data Assessment Longshore Sediment Transport: Example from North Queensland.” In *Sixth Australian Conference Coastal Ocean Engineering*, 21–26. Preprints Papers.
NASA. 2024. “Sea Level Projection Tool.” IPCC 6th Assessment Report Sea Level Projections. 2024. https://sealevel.nasa.gov/ipcc-ar6-sea-level-projection-tool.
Nyström, M., C. Folke, and F. Moberg. 2000. “Coral Reef Disturbance and Resilience in a Human-Dominated Environment.” *Trends in Ecology & Evolution* 15 (10): 413–17.
Osorio-Cano, Juan D., Juan C. Alcérreca-Huerta, Andrés F. Osorio, and Hocine Oumeraci. 2018. “CFD Modelling of Wave Damping over a Fringing Reef in the Colombian Caribbean.” *Coral Reefs* 37 (4): 1093–1108.
Page, C. A., and B. L. Willis. 2008. “Epidemiology of Skeletal Eroding Band on the Great Barrier Reef and the Role of Injury in the Initiation of This Widespread Coral Disease.” *Coral Reefs* 27 (2): 257–72.
Pain, C. C., M. D. Piggott, A. J. H. Goddard, F. Fang, G. J. Gorman, D. P. Marshall, M. D. Eaton, P. W. Power, and C. R. E. de Oliveira. 2005. “Three-Dimensional Unstructured Mesh Ocean Modelling.” *Ocean Modelling* 10 (1-2): 5–33.
Perris, Lachlan, Tristan Salles, Thomas E. Fellowes, Stephanie Duce, Jody Webster, and Ana Vila-Concejo. 2024. “The Influence of Coral Reef Spur and Groove Morphology on Wave Energy Dissipation in Contrasting Reef Environments.” *Journal of Geophysical Research. Earth Surface* 129 (8). https://doi.org/10.1029/2023jf007424.
Perry, Chris T., Gary N. Murphy, Paul S. Kench, Scott G. Smithers, Evan N. Edinger, Robert S. Steneck, and Peter J. Mumby. 2013. “Caribbean-Wide Decline in Carbonate Production Threatens Coral Reef Growth.” *Nature Communications* 4 (1): 1402.
Perry, Christopher T., and Scott G. Smithers. 2006. “Taphonomic Signatures of Turbid-Zone Reef Development: Examples from Paluma Shoals and Lugger Shoal, Inshore Central Great Barrier Reef, Australia.” *Palaeogeography, Palaeoclimatology, Palaeoecology* 242 (1): 1–20.
Pratchett, Morgan S. 2005. “Dynamics of an Outbreak Population of Acanthaster Planci at Lizard Island, Northern Great Barrier Reef (1995–1999).” *Coral Reefs* 24 (3): 453–62.

Puotinen, Marji, Edwin Drost, Ryan Lowe, Martial Depczynski, Ben Radford, Andrew Heyward, and James Gilmour. 2020. “Towards Modelling the Future Risk of Cyclone Wave Damage to the World’s Coral Reefs.” *Global Change Biology* 26 (8): 4302–15.
Puotinen, Marji, Jeffrey A. Maynard, Roger Beeden, Ben Radford, and Gareth J. Williams. 2016. “A Robust Operational Model for Predicting Where Tropical Cyclone Waves Damage Coral Reefs.” *Scientific Reports* 6 (May):26009.
Puotinen, M. L. 2004. “Tropical Cyclones in the Great Barrier Reef, Australia, 1910-1999: A First Step towards Characterising the Disturbance Regime.” *Australian Geographical Studies* 42 (3): 378–92.
———. 2007. “Modelling the Risk of Cyclone Wave Damage to Coral Reefs Using GIS: A Case Study of the Great Barrier Reef, 1969–2003.” *International Journal of Geographical Information Science: IJGIS* 21 (1): 97–120.
QGIS. 2024. *QGIS: A Free and Open Source Geographical Information System* (version 3.22). Linux. https://www.qgis.org/en/site/.
Ram, Arishma R., and James P. Terry. 2016. “Stream Turbidity Responses to Storm Events in a Pristine Rainforest Watershed on the Coral Coast of Southern Fiji.” *International Journal of Sediment Research* 31 (4): 279–90.
Roberts, T. E., J. M. Moloney, H. P. A. Sweatman, and T. C. L. Bridge. 2015. “Benthic Community Composition on Submerged Reefs in the Central Great Barrier Reef.” *Coral Reefs* 34 (2): 569–80.
Roff, George, E. Charlotte E. Kvennefors, Maoz Fine, Juan Ortiz, Joanne E. Davy, and Ove Hoegh-Guldberg. 2011. “The Ecology of ‘Acroporid White Syndrome’, a Coral Disease from the Southern Great Barrier Reef.” *PloS One* 6 (12): e26829.
Schloemer, R. W. 1954. *Analysis Synthesis Hurricane Wind Patterns Over Lake*. Okeechobee, Florida. Washington D.C.
Sheng, Y. Peter, Yanfeng Zhang, and Vladimir A. Paramygin. 2010. “Simulation of Storm Surge, Wave, and Coastal Inundation in the Northeastern Gulf of Mexico Region during Hurricane Ivan in 2004.” *Ocean Modelling* 35 (4): 314–31.
Smith, Tyler B., Peter W. Glynn, Juan L. Maté, Lauren T. Toth, and Joanna Gyory. 2014. “A Depth Refugium from Catastrophic Coral Bleaching Prevents Regional Extinction.” *Ecology* 95 (6): 1663–73.
Stephenson, W., R. Endean, and I. Bennett. 1958. “An Ecological Survey of the Marine Fauna of Low Isles, Queensland.” *Marine & Freshwater Research* 9 (2): 261.
Stoeckl, Natalie, Christina C. Hicks, Morena Mills, Katharina Fabricius, Michelle Esparon, Frederieke Kroon, Kamaljit Kaur, and Robert Costanza. 2011. “The Economic Value of Ecosystem Services in the Great Barrier Reef: Our State of Knowledge.” *Annals of the New York Academy of Sciences* 1219 (February):113–33.
Storlazzi, C. D., E. Elias, M. E. Field, and M. K. Presto. 2011. “Numerical Modeling of the Impact of Sea-Level Rise on Fringing Coral Reef Hydrodynamics and Sediment Transport.” *Coral Reefs* 30 (1): 83–96.
Stuart-Smith, Rick D., Christopher J. Brown, Daniela M. Ceccarelli, and Graham J. Edgar. 2018. “Ecosystem Restructuring along the Great Barrier Reef Following Mass Coral Bleaching.” *Nature* 560 (7716): 92–96.
Sutherland, K. P., J. W. Porter, and C. Torres. 2004. “Disease and Immunity in Caribbean and Indo-Pacific Zooxanthellate Corals.” *Marine Ecology Progress Series* 266:273–302.
Tan, James C. H., Morgan S. Pratchett, Line K. Bay, and Andrew H. Baird. 2012. “Massive Coral Mortality Following a Large Flood Event.” In , edited by D. Yellowlees and T. P. Hughes, 4. Proceedings of the 12th International Coral Reef Symposium. Townsville, QLD, Australia: James Cook University.
Terry, James P., Sitaram Garimella, and Ray A. Kostaschuk. 2002. “Rates of Floodplain Accretion in a Tropical Island River System Impacted by Cyclones and Large Floods.” *Geomorphology* 42 (3): 171–82.
Tissaoui, Y. 2024. “Numerical Techniques for Improving Simulations of Tropical Cyclones.” PhD, New Jersey Institute of Technology.
Uthicke S., Fabricius K., De’ath G., Negri A., Smith R., Warne M., Noonan S., Johansson C.,

Gorsuch H., and Anthony K. 2016. “Multiple and Cumulative Impacts on the GBR: Assessment of Current Status and Development of Improved Approaches for Management.” 1.6. National Environmental Science Programme.
Van Woesik, R., A. M. Ayling, and B. Mapstone. 1991. “Impact of Tropical cyclone’Ivor'on the Great Barrier Reef, Australia.” *Journal of Coastal Research*. https://www.jstor.org/stable/4297864.
Walsh, Kevin. 2015. “Fine Resolution Simulations of the Effect of Climate Change on Tropical Cyclones in the South Pacific.” *Climate Dynamics* 45 (9-10): 2619–31.
Walsh, Kevin J. E., John L. McBride, Philip J. Klotzbach, Sethurathinam Balachandran, Suzana J. Camargo, Greg Holland, Thomas R. Knutson, et al. 2016. “Tropical Cyclones and Climate Change.” *Wiley Interdisciplinary Reviews. Climate Change* 7 (1): 65–89.
Warder, Simon, Athanasios Angeloudis, Stephan Kramer, Colin Cotter, and Matthew Piggott. 2020. “A Comparison of Bayesian Inference and Gradient-Based Approaches for Friction Parameter Estimation.” *EarthArXiv*. https://doi.org/10.31223/osf.io/mv9qy.
Warder, Simon C., Kevin J. Horsburgh, and Matthew D. Piggott. 2021. “Adjoint-Based Sensitivity Analysis for a Numerical Storm Surge Model.” *Ocean Modelling* 160 (April):101766.
Westcott, David A., Cameron S. Fletcher, Frederieke J. Kroon, Russell C. Babcock, Eva E. Plagányi, Morgan S. Pratchett, and Mary C. Bonin. 2020. “Relative Efficacy of Three Approaches to Mitigate Crown-of-Thorns Starfish Outbreaks on Australia’s Great Barrier Reef.” *Scientific Reports* 10 (1): 12594.
Willis, Bette L., Cathie A. Page, and Elizabeth A. Dinsdale. 2004. “Coral Disease on the Great Barrier Reef.” In *Coral Health and Disease*, edited by Eugene Rosenberg and Yossi Loya, 69–104. Berlin, Heidelberg: Springer Berlin Heidelberg.
Wolanski, Eric. 1986. “An Evaporation-Driven Salinity Maximum Zone in Australian Tropical Estuaries.” *Estuarine, Coastal and Shelf Science* 22 (4): 415–24.
Wolff, Nicholas H., Aaron Wong, Renato Vitolo, Kristin Stolberg, Kenneth R. N. Anthony, and Peter J. Mumby. 2016. “Temporal Clustering of Tropical Cyclones on the Great Barrier Reef and Its Ecological Importance.” *Coral Reefs* 35 (2): 613–23.
Wong, P.P., I.J. Losada, J.-P. Gattuso, J. Hinkel, A. Khattabi, K.L. McInnes, Y. Saito, and A. Sallenger. 2014. “Coastal Systems and Low-Lying Areas.” Climate Change 2014: Impacts,Adaptation, and Vulnerability. Part A: Global and Sectoral Aspects. Contribution of Working Group II to the Fifth Assessment Report of the Intergovernmental Panel on Climate Change.
Woodley, J. D. 1980. “Hurricane Allen Destroys Jamaican Coral Reefs.” *Nature* 287 (5781): 387–387.
Wooldridge, Scott A. 2009. “Water Quality and Coral Bleaching Thresholds: Formalising the Linkage for the Inshore Reefs of the Great Barrier Reef, Australia.” *Marine Pollution Bulletin* 58 (5): 745–51.
Yan, Danchen, and Tianyu Zhang. 2022. “Research Progress on Tropical Cyclone Parametric Wind Field Models and Their Application.” *Regional Studies in Marine Science* 51 (102207): 102207.
Young, Ian. 2017. “A Review of Parametric Descriptions of Tropical Cyclone Wind-Wave Generation.” *Atmosphere* 8 (10): 194.
Young, Ian R. 1989. “Wave Transformation over Coral Reefs.” *Journal of Geophysical Research* 94 (C7): 9779–89.
Young, I. R., and G. P. Burchell. 1996. “Hurricane Generated Waves as Observed by Satellite.” *Ocean Engineering* 23 (8): 761–76.
Young, I. R., and T. A. Hardy. 1993. “Measurement and Modelling of Tropical Cyclone Waves in the Great Barrier Reef.” *Coral Reefs* 12 (2): 85–95.

Appendices

Appendix A

Tide-only model template used for models *T1_D, T2_E, T3_H, T4_I, T4I_119* and *T4I_245*.

Appendix B

Tide and Wind model template used for models *W1_D, W2_E, W3_H, W4_I, W4I_119* and *W4I_245*.

Appendix C

All the data used within this research.

Appendix D

All graphs created when analysing the Marine Monitoring Programme Data including:

- Absolute change in coral cover across Algae, Hard Coral, Soft Coral and Other Benthic vs the Maximum Bed Shear Stress, Change in Bed shear stress magnitude and the Log10 of change in bed shear stress magnitude
- Relative change in coral cover across Algae, Hard Coral, Soft Coral and Other Benthic vs the Maximum Bed Shear Stress, Change in Bed shear stress magnitude and the Log10 of change in bed shear stress magnitude
- Absolute and Relative change in coral cover across Algae, Hard Coral, Soft Coral and Other Benthic vs the Maximum Bed Shear Stress, Change in Bed shear stress magnitude and the Log10 of change in bed shear stress magnitude with added Loess Curves

Appendix E

Analysis was also conducted using the Long-Term Monitoring Programme (LTMP) data (AIMS 2021) from AIMS.

All graphs created when analysing the LTMP Data including:

- Absolute change in coral cover across Algae, Hard Coral, Soft Coral and Other Benthic vs the Maximum Bed Shear Stress, Change in Bed shear stress magnitude and the Log10 of change in bed shear stress magnitude

- Relative change in coral cover across Algae, Hard Coral, Soft Coral and Other Benthic vs the Maximum Bed Shear Stress, Change in Bed shear stress magnitude and the Log10 of change in bed shear stress magnitude
- Absolute and Relative change in coral cover across Algae, Hard Coral, Soft Coral and Other Benthic vs the Maximum Bed Shear Stress, Change in Bed shear stress magnitude and the Log10 of change in bed shear stress magnitude with added Loess Curves
- Statistical Analysis of the data including the Shapiro-Wilk Normality Test and the Kendall Tau's test

Appendix F

Analysis was also conducted combining the MMP and LTMP data.

All graphs created when analysing combined MMP and LTMP data including:

- Absolute change in coral cover across Algae, Hard Coral, Soft Coral and Other Benthic vs the Maximum Bed Shear Stress, Change in Bed shear stress magnitude and the Log10 of change in bed shear stress magnitude
- Relative change in coral cover across Algae, Hard Coral, Soft Coral and Other Benthic vs the Maximum Bed Shear Stress, Change in Bed shear stress magnitude and the Log10 of change in bed shear stress magnitude
- Absolute and Relative change in coral cover across Algae, Hard Coral, Soft Coral and Other Benthic vs the Maximum Bed Shear Stress, Change in Bed shear stress magnitude and the Log10 of change in bed shear stress magnitude with added Loess Curves
- Statistical Analysis of the data including the Shapiro-Wilk Normality Test and the Kendall Tau's test

Appendix G

A Random Forest analysis was trialled when analysing the results of the models including:

- Random forest analysis of the MMP data
- Random forest analysis of the LTMP data
- Random forest analysis of the combined MMP and LTMP data
- Random forest analysis of the MMP data with only 1 location factor

Appendix H

R-script used to extract the data needed for altering the bathymetry from the IPCC AR6 Sea Level Projection files (SSP1-1.9 and SSP2-4.5).

Appendix I

All graphs showing the elevation, velocity and bed shear stress experienced throughout the model simulation at each MMP coral reef for each tropical cyclone for both the tide-only simulations (T1_D, T2_E, T3_H, T4_I) and the tide and wind simulations (W1_D, W2_E, W3_H, W4_I).